Fully integrated modelling of surface-subsurface flow processes: quantifying in-stream and overland flow generation mechanisms.

by
Daniel Joseph Partington
BEng (Civil & Environmental) Hons, BSc (Maths and Computer Science)

Thesis submitted to The University of Adelaide
School of Civil, Environmental & Mining Engineering in
fulfilment of the requirements for the degree of
Doctor of Philosophy

Submitted December 2012

Contents

Abstract

The understanding and effective management of flood and drought issues within catchments, are critical to sustaining such systems and the environments they support. Surface water and groundwater systems within catchments exhibit important feedbacks and therefore must be considered as a single resource. Holistic consideration of these systems in catchment hydrology requires the understanding and quantification of both surface and subsurface flow processes and their interactions. This requires that the physics driving the interactions/processes are well understood. Consequently, a need has arisen for physics-based models that can aid in building intuition about these interactions/processes, and also assist in quantifying these interactions/processes. In the last decade, physics-based fully integrated surface-subsurface flow models have become an important tool in understanding and quantifying flow generation processes and surface-subsurface interactions. However, due to the relatively short history of fully integrated models, the analysis and interpretation of outputs is often incommensurate with the spatiotemporal information within the outputs. A key shortcoming of these models is the inability to use model outputs to properly analyse and interpret flow generation mechanisms and surface water-groundwater interactions with respect to the streamflow hydrograph.

In this research, a new Hydraulic Mixing-Cell (HMC) method for quantifying in-stream and overland flow generation mechanisms within physics-based models of surface-subsurface flow is developed. The HMC method is implemented and tested within the fully integrated surface-subsurface flow model code HydroGeoSphere. The HMC method is used in a series of applications to quantify the contributions to total streamflow of groundwater discharge to the stream and hillslope, and direct rainfall to the stream and hillslope.

Application of the HMC method to a hypothetical catchment is used to investigate the importance of in-stream flow travel time and losses. Results showed that it is necessary to account for in-stream travel time and stream losses in order to accurately quantify the contribution of groundwater to streamflow. The HMC method is then used with another hypothetical catchment model to investigate the potential error in 10 commonly used automated baseflow separation methods.

Simulations with a range of hydrological forcing, soil characteristics and antecedent moisture conditions showed the potential error to be significant for these automated methods; this warrants caution in overvaluing their outputs. Finally, the HMC method is employed in a case study of the Lehstenbach catchment, which included a model of a riparian wetland and catchment. Application of the HMC method in this case study was used to investigate wetland and catchment processes through separation of streamflow hydrographs and spatiotemporal analysis of flow generation mechanisms. This analysis elucidated the dynamics of overland and in-stream flow generation processes. This research has opened up a new way of analysing and interpreting flow generation mechanisms using fully integrated surface-subsurface flow models. The analysis and interpretation techniques implemented in this thesis form the basis for comprehensive analysis of outputs from physics-based modelling of catchment hydrological processes.

Statement of Originality

This work contains no material which has been accepted for the award of any other degree or diploma in any university or other tertiary institution to Daniel Partington and, to the best of my knowledge and belief, contains no material previously published or written by another person, except where due reference has been made in the text.

I give consent to this copy of my thesis when deposited in the University Library, being made available for loan and photocopying, subject to the provisions of the Copyright Act 1968.

The author acknowledges that copyright of published works contained within this thesis (as listed below) resides with the copyright holders of those works.

List of works:

Partington, D., P. Brunner, C. T. Simmons, R. Therrien, A. D. Werner, G. C. Dandy, and H. R. Maier. 2011. A hydraulic mixing-cell method to quantify the groundwater component of streamflow within spatially distributed fully integrated surface water - groundwater flow models. *Environmental Modelling and Software*, 26:886-898.

Partington, D., P. Brunner, C. T. Simmons, A. D. Werner, R. Therrien, G. C. Dandy, and H. R. Maier. 2012. Evaluation of outputs from automated baseflow separation methods against simulated baseflow from a physically based, surface water-groundwater flow model. *Journal of Hydrology*, 458-459: 28-39.

Partington, D., P. Brunner, S. Frei, C. T. Simmons, R. Therrien, A. D. Werner, H. R. Maier, G. C. Dandy, J. H. Fleckenstein. Interpreting flow generation mechanisms from integrated surface water-groundwater flow models of a riparian wetland and catchment. Submitted to *Water Resources Research* on 9 November, 2012.

I also give permission for the digital version of my thesis to be made available on the web, via the University's digital research repository, the Library catalogue, and also through web search engines, unless permission has been granted by the University to restrict access for a period of time.

Signed: . . . . . Date: . . . . . .

Acknowledgements

Firstly, I would like to thank my supervisors: Holger Maier, Graeme Dandy, Craig Simmons, Adrian Werner and Philip Brunner, for their encouragement, support, engaging exchange of ideas, and review of manuscripts over the course of my PhD. I am especially grateful to Holger Maier for the opportunity to undertake this PhD, and for his sincerity and understanding since my time as an undergraduate. I am also grateful to Graeme Dandy for the always interesting scientific discussions. I thank Craig Simmons for his untiring reassurance and uplifting enthusiasm. I am also very grateful to Adrian Werner for constantly challenging me to develop my critical thinking abilities. I am deeply indebted to Philip Brunner for his unrelenting faith in my research, and for his guidance in modelling.

I am very grateful to Rene Therrien, for the opportunity to work with the HydroGeoSphere source code, for his instrumental guidance with the code, and valuable assistance with running models. I was fortunate to collaborate with Sven Frei and Jan Fleckenstein on a case study of the Lehstenbach catchment, and I thank them for this fruitful collaboration.

I acknowledge Rob McLaren for his help in resolving modelling issues. I also acknowledge Matt Gibbs, Aaron Zecchin and Jerry Vaculik, for generously giving their time to impart their coding wizardry on me. I also thank all of the students at the University of Adelaide and Flinders University whom I have worked with and who have inspired me over the years.

I would like to thank my mother Virginia, and siblings Libby, Bill, Ben, Tom, and Lucy for their support over the years. I thank all of my friends for enduring me and my rants on hydrological modelling over the course of my study. Lastly I would like to thank my number one, Grace Lin for her amazing unwavering support on this journey; without her, I would not have come this far. I dedicate this thesis to my father, John Partington.

List of Figures

List of Tables

Chapter 1

1 Introduction

The understanding of hydrological processes and their translation to the streamflow hydrograph is critical in the management of floods and water resources, and the environments they support. A key to this is the understanding of the interactions of surface and subsurface water systems within catchments (*Winter*, 1999; *Sophocleous*, 2002). The important feedbacks exhibited by these two systems, necessitate their holistic consideration within catchment hydrology. Therefore, improving this understanding requires both the identification and quantification of surface-subsurface water interactions (e.g. losing streams) and flow generation/depletion processes (e.g. rainfall-runoff and dry-period baseflow). This means having a clear understanding of the physics of water movement within catchments. If the physics understanding is clear, and the system is well characterised, then it follows that the integrated catchment response – in the form of the streamflow hydrograph – should be able to be readily decomposed into the constituent flow generation processes, i.e. groundwater discharge and direct rainfall to the stream, and groundwater discharge and direct rainfall to the hillslope (see Figure 1.1).

It was highlighted by *Hewlett and Troendle* (1975) that accurate prediction of the streamflow hydrograph implies adequate modelling of the sources, flowpaths and residence time of water. This "adequate" modelling suggests the use of spatially and temporally distributed hydrological models, of which many have been developed (see *Singh and Woolhiser* (2002) for a comprehensive review). It follows from *Hewlett and Troendle's* statement that adequate modelling of the sources, flowpaths and residence times requires adequate representation of the physics of water flow, i.e. deterministic-conceptual modelling (see *Kampf and Burges*, 2007).

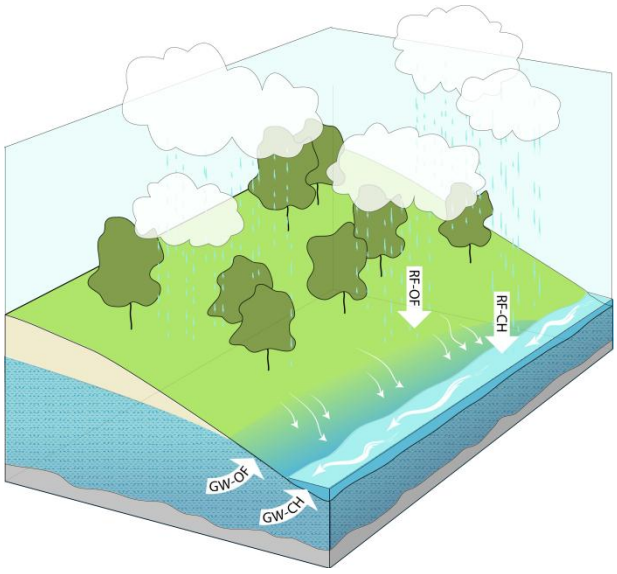

Figure 1.1: Streamflow generation at the plot scale by both in-stream (groundwater discharge and rainfall to the stream channel) and overland (groundwater discharge and rainfall to the hillslope) flow generation processes.

Freeze and Harlan (1969) provided a blueprint for what is often considered "adequate" physics-based modelling of water flow within catchments. The inevitably complex models that arise from this blueprint can aid in building intuition about the catchment-scale hydrological processes responsible for streamflow, but subject to the assumptions in the physical equations (e.g. that a representative elementary volume exists in the subsurface).

In the last decade, the blueprint of *Freeze and Harlan* (1969) has been realised with the advent of physics-based fully Integrated Surface-Subsurface Hydrological Models (ISSHM) (*Gaukroger and Werner*, 2011). Examples of ISSHMs include InHM (*VanderKwaak and Loague*, 2001), MODHMS (*HydroGeoLogic*, 2006), HydroGeoSphere (HGS) (*Therrien et al.*, 2009), and ParFlow (*Kollet and Maxwell*, 2006). ISSHMs are used within this thesis to describe models which solve simultaneously the surface and subsurface flow equations. Within ISSHMs, 2D surface flow is usually represented using an approximation to the St Venant equations (e.g. diffusion wave), and 3D variably saturated subsurface flow is usually represented using Richard's equation. ISSHMs can be used to analyse and interpret hydrological processes and in developing conceptual understanding of catchment processes (*Ebel and Loague*, 2006). A particularly important attribute of these models is that rainfall is partitioned into infiltration, ponding, and overland flow in a realistic manner

(*Therrien et al.*, 2009) without any *a priori* assumption of these processes (*Mirus et al*., 2011a). This partitioning is dependent on the rate of rainfall, antecedent moisture conditions and catchment physical characteristics. However, this means that the hydrological processes (e.g. groundwater discharge to a stream or infiltration excess overland flow) need to be identified and interpreted after simulations.

Studies utilising ISSHMs are becoming increasingly widespread (e.g., *Frei et al.*, 2010; *Maxwell and Kollet*, 2008; *Park et al.*, 2011; *Brunner et al.*, 2009). These examples focused on processes in small-scale synthetic systems, which enabled insight to be gained into the controls on flow generation (*Frei et al.*, 2010; *Maxwell and Kollet*, 2008; *Park et al.*, 2011) and depletion (*Brunner et al.*, 2009). In larger-scale (e.g. catchment scale) systems it is difficult to resolve how the hydrological drivers affect the hydrological outputs (e.g. the outlet streamflow hydrograph). This is because hydrological outputs at a given point in space and time are only affected by hydrological drivers that occur at the same location and at the same time (i.e. by 'active' processes (*Ambroise*, 2004)). In larger-scale systems, hydrological drivers that occur at a particular point in time (active processes) do not necessarily end up contributing to the hydrological output at that or a later time. This is because of the influence of travel times, flow impediments (e.g. riparian wetlands or weirs), and losses (e.g. infiltration or evaporation). Consequently, where such influences are significant, there is a need to distinguish between 'active' and 'contributing' streamflow generation processes (*Ambroise*, 2004), where contributing processes are those that contribute to flow at a particular location at a particular time, and potentially include active processes. These influences will be important in catchments that exhibit significant travel times for water and/or where flow depletion processes are significant relative to flow generation processes (e.g. strong losing streams). The differences between active and contributing flow generation processes are driven by active flow depletion mechanisms (surface water losses) and the lag-time between active flow generation mechanisms taking place and the time that the resultant flow reaches the point of interest (e.g. the point where the streamflow hydrograph is measured).

A key shortcoming of ISSHMs is in linking the distributed hydrologic response to the point response (e.g. where the streamflow hydrograph is measured), i.e.

capturing the contributing processes. Active processes are readily obtained from ISSHMs that output the nodal fluid mass balance components, i.e. surface-subsurface exchange fluxes, rainfall input, evaporation output, surface inflows and outflow and changes in storage. However, attaining the contributing processes requires the ability to use these outputs of active processes to properly analyse and interpret streamflow generation mechanisms with respect to the streamflow hydrograph.

The advent of ISSHMs has been critical in being able to improve our conceptual understanding of hydrological processes, but the benefits of analysing internal processes and meaningfully separating flow hydrographs are still to be realised. This is a major shortcoming as it prevents development in building the intuition of hydrologic response to various hydrological drivers (i.e. rainfall and evapotranspiration). A clear need has arisen for research into the identification and quantification of contributing in-stream and overland flow generation mechanisms at larger (e.g. catchment) scales, particularly given that there are still difficulties in the ability to conduct or scale up the measurements that are required in order to gain this understanding at/to the catchment scale (*Fleckenstein et al.*, 2010).

1.1. Research Objectives

This research aims to improve the understanding of streamflow generation and surface water-groundwater interaction through quantifying in-stream and overland flow generation mechanisms within physics-based models of surface-subsurface flow. In such models, this requires the development of a new method for interpreting in-stream and overland flow generation mechanisms. This development will provide a platform for investigation into hydrological systems that exhibit complex spatiotemporal patterns of in-stream and overland flow generation mechanisms. To achieve the overall aims of this research, four main research objectives are developed with three sub-objectives, which are listed below. The linking of each of these objectives is shown in Figure 1.2.

Objective 1: To develop a method to quantify the contribution of flow generation mechanisms to streamflow, allowing separation of the streamflow hydrograph into its constituent flow generation components (i.e. groundwater discharge and direct

rainfall to the stream, and groundwater discharge and direct rainfall to overland areas).

> *Objective 1.1*: To improve model based investigation into groundwater discharge to total streamflow within streams exhibiting complex stream-aquifer interactions.
>
> *Objective 1.2*: To improve model-based investigation into the contribution to total streamflow of rainfall and groundwater discharge from overland areas.

Objective 2: To develop a benchmark against which baseflow separation methods can be tested against.

> *Objective 2.1*: To determine the potential error in commonly used automated methods for estimation of in-stream groundwater contributions to streamflow.

Objective 3: To investigate the spatiotemporal variability in both overland and in-stream flow generation mechanisms within a modelling framework.

Objective 4: To investigate the dichotomy that exists between 'active' and 'contributing' streamflow generation mechanisms within a modelling framework.

Objective 5: To incorporate the method developed in Objective 1 into an ISSHM code to provide a platform for other researchers to utilise the method developed within this research.

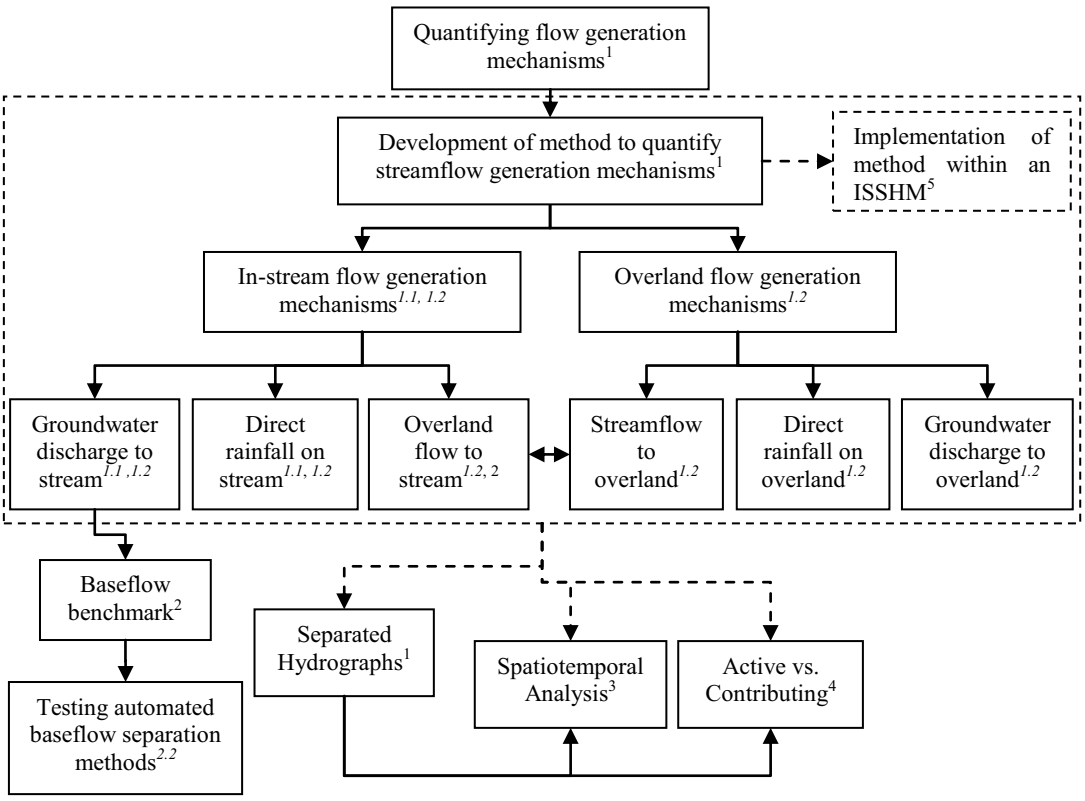

Figure 1.2: Research objectives and their hierarchy. Objectives are denoted by the superscript numbers in each of the flowchart boxes.

1.2. Thesis Overview

This thesis is organised into five chapters. The main body of this thesis consists of **Chapters 2** to **4**, which correspond to three journal papers (*Partington et al.*, 2011; *Partington et al.*, 2012a; *Partington et al.*, 2012b). In **Chapter 2** (*Partington et al.*, 2011) a new method is developed for accurately quantifying groundwater contributions to streamflow (**Objective 1**) with respect to the streamflow hydrograph, and this method is used to investigate the complexity of groundwater contributions to streamflow (*Objective 1.1*). In **Chapter 3** (*Partington et al.*, 2012a) the work in **Chapter 2** is extended, and a baseflow model benchmark is developed (**Objective 2**) against which potential error is investigated in commonly used automated methods for the separation of baseflow from streamflow hydrographs (*Objective 2.1*). In **Chapter 4 (***Partington et al.*, 2012b) the work of **Chapter 2** is extended to investigate overland flow generation mechanisms (*Objective 1.2*), and the new method is applied to a case study of a real catchment. Within the case study, all surface flow generation mechanisms are quantified (*Objective 1.2*), spatiotemporal variability in flow generation mechanisms is analysed (**Objective 3**), and the difference between active and

contributing processes is analysed (**Objective 4**). The linking of each of the papers to the objectives is depicted below in Figure 1.3. Although the manuscript has been reformatted in accordance with University guidelines, and sections renumbered for inclusion within this thesis, the material within this paper is otherwise presented herein as published. Copies of the publications "as published" are provided in the Appendix A and B.

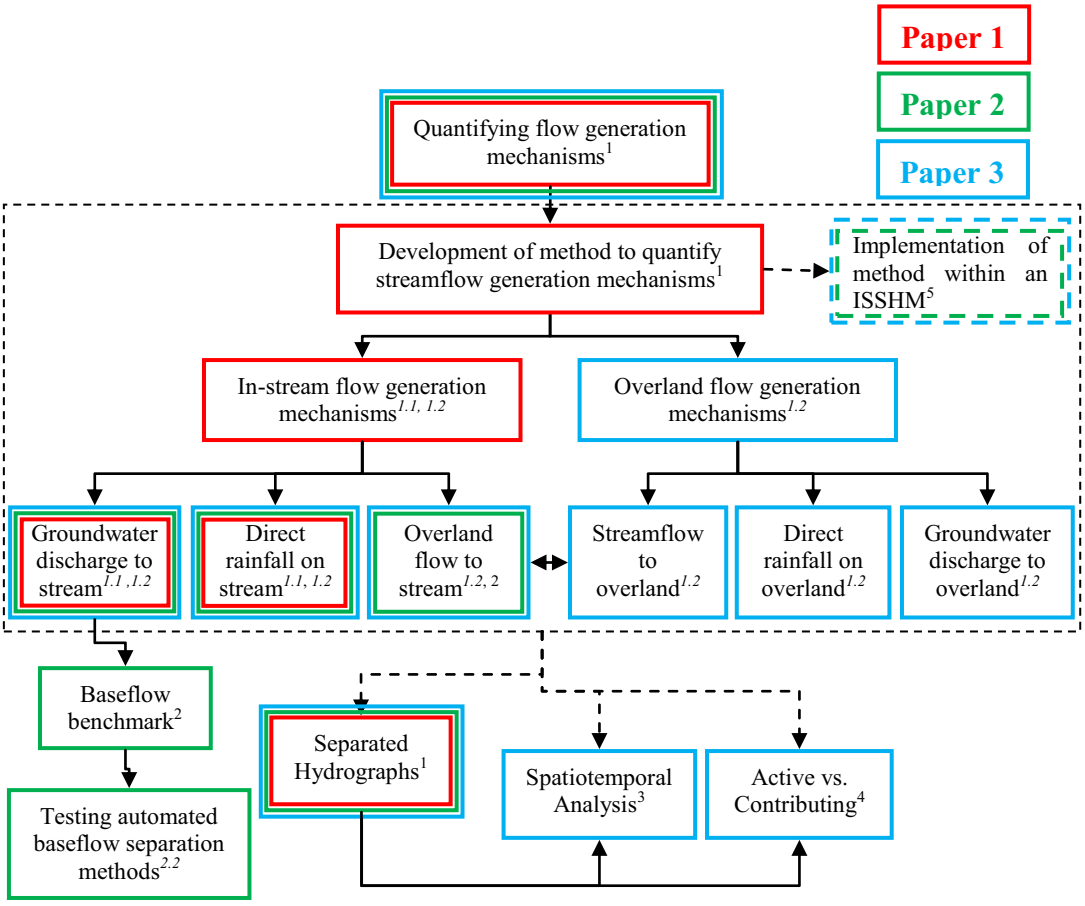

Figure 1.3: Linkage of research objectives and publications.

Conclusions of the research within this thesis are provided in **Chapter 5**, which summarises: 1) the research contributions, 2) limitations and 3) future directions for further research.

Chapter 2

2 A hydraulic mixing-cell method to quantify the groundwater component of streamflow within spatially distributed fully integrated surface water - groundwater flow models (Paper 1)

Statement of Authorship

Title of Paper	Evaluation of outputs from automated baseflow separation methods against simulated baseflow from a physically based, surface water-groundwater flow model
Publication Status	(•) Published ( ) Accepted for Publication ( ) Submitted for Publication ( ) Publication Style
Publication Details	Partington, D., P. Brunner, C. T. Simmons, A. D. Werner, R. Therrien, G. C. Dandy, and H. R. Maier. 2012. Evaluation of outputs from automated baseflow separation methods against simulated baseflow from a physically based, surface water-groundwater flow model. *Journal of Hydrology*, 458-459: 28-39.

Author Contributions

By signing the Statement of Authorship, each author certifies that their stated contribution to the publication is accurate and that permission is granted for the publication to be included in the candidate's thesis.

Name of Principal Author (Candidate)	Daniel Partington		
Contribution to the Paper	Designed and conducted numerical experiments, coded baseflow analysis tool and wrote manuscript.		
Signature		Date	23/11/2012

Name of Co-Author	Philip Brunner		
Contribution to the Paper	Supervised manuscript preparation and reviewed draft.		
Signature		Date	3.12.2012

Name of Co-Author	Craig Simmons		
Contribution to the Paper	Supervised manuscript preparation and reviewed draft.		
Signature		Date	23/11/12

Name of Co-Author	Adrian Werner		
Contribution to the Paper	Supervised manuscript preparation and reviewed draft.		
Signature		Date	23/11/12

Name of Co-Author	Rene Therrien		
Contribution to the Paper	Supervised manuscript preparation and reviewed draft.		
Signature		Date	Nov 24, 2012

Name of Co-Author	Holger Maier		
Contribution to the Paper	Supervised manuscript preparation and reviewed draft.		
Signature		Date	5/12/12

Name of Co-Author	Graeme Dandy		
Contribution to the Paper	Supervised manuscript preparation and reviewed draft.		
Signature		Date	3/12/12

Please cut and paste additional co-author panels here.

Abstract

The complexity of available hydrological models continues to increase, with fully integrated surface water-groundwater flow and transport models now available. Nevertheless, an accurate quantification of streamflow generation mechanisms within these models is not yet possible. For example, such models do not report the groundwater component of streamflow at a particular point along the stream. Instead, the groundwater component of streamflow is approximated either from tracer transport simulations or by the sum of exchange fluxes between the surface and the subsurface along the river. In this study, a hydraulic mixing-cell (HMC) method is developed and tested that allows to accurately determine the groundwater component of streamflow by using only the flow solution from fully integrated surface water - groundwater flow models. By using the HMC method, the groundwater component of streamflow can be extracted accurately at any point along a stream provided the subsurface/surface exchanges along the stream are calculated by the model. A key advantage of the HMC method is that only hydraulic information is used, thus the simulation of tracer transport is not required. Two numerical experiments are presented, the first to test the HMC method and the second to demonstrate that it quantifies the groundwater component of streamflow accurately.

2.1. Introduction

A quantitative understanding of stream flow hydrographs is an important precondition to the understanding and effective management of any catchment (*VanderKwaak and Loague*, 2001; *Jones et al.*, 2006; *Mirus et al.*, 2009). The streamflow hydrograph is generated by different mechanisms such as groundwater discharge to the stream, discharge from the unsaturated zone, overland flow, preferential flow through macropores and/or fractures, and direct precipitation to the stream. These streamflow generation components can exhibit complex spatial and temporal behaviour. This complexity makes it difficult to easily decompose stream flow hydrographs in terms of stream flow generation mechanisms if one or several components of the hydrograph are unknown. Groundwater discharge is a critical streamflow generation component that is difficult to quantify. The quantitative assessment of the groundwater component of streamflow (which

represents the quantity of streamflow at a given point in space and time consisting of groundwater discharging directly to the stream) is of great importance in understanding catchment hydrology and informing water resources management, as highlighted by *Sophocleous* (2002) and *Winter* (1999). Accurate simulation of the groundwater component of streamflow is therefore important in hydrological modelling exercises (e.g. *Gilfedder et al.*, 2009; *Croton and Barry*, 2001; *Facchi et al.*, 2004) in order to inform water resources management.

The groundwater component of stream flow cannot be measured easily in the field (*Hatterman et al.*, 2004) and therefore is usually quantified using indirect methods. Indirect methods can involve the use of environmental and conservative tracers for separation of the hydrograph (*McGlynn and McDonnell*, 2003; *McGuire and McDonnell*, 2006), and recession analysis based on conceptual storage-discharge relationships for the catchment (*Chapman*, 2003; *Eckhardt*, 2008). However, as pointed out by *Hewlett and Troendle* (1975), 'the accurate prediction of the hydrograph implies adequate modelling of the sources, flowpaths and residence time of water'. In particular, capturing the flowpaths requires a spatially distributed model. Unless the assumptions of the indirect methods can be resolved or justified, the adequate modelling of sources and flowpaths of water would be insufficient. If the modelling is insufficient, then it follows that the separation of the hydrograph may be meaningless. Given the difficulty faced in accurately measuring sources and flowpaths within hillslopes, let alone entire catchments, some benefit can be found in examining hypotheses which can be adequately 'measured' in the 'virtual laboratory' (*Weiler and McDonnell*, 2006).

One could expect that the tools for quantifying the groundwater component of streamflow are now readily available in the latest generation of fully integrated spatially distributed models such as InHM (*VanderKwaak and Loague*, 2001), MODHMS (*HydroGeoLogic*, 2006), HydroGeoSphere (HGS) (*Therrien et al.*, 2009), Wash123D (*Cheng et al.*, 2005) and ParFlow (*Kollet and Maxwell*, 2006). However, this is not the case. Even within spatially distributed numerical models quantifying source components remains a challenge (*Sayama and McDonnell*, 2009). The same applies to the ultimate delivery mechanisms as defined in *Sklash and Farvolden* (1979). Because the currently available numerical models do not

report the groundwater component of streamflow at a given location, it is often approximated by introducing tracers or by setting it equal to the summed exfiltration along a section or entire length of the stream. The summed exfiltration is defined in this paper as the sum of all fluxes from the subsurface to the stream at a specific point in time upstream of the point at which the hydrograph is measured.

However, these approaches are problematic. For example, the summed exfiltration during a simulation is not equal to the groundwater component of streamflow at the same simulation time. This can be attributed to the fact that portions of the summed exfiltration exhibit a time lag from the point of entering the stream to the point of streamflow measurement, as a result of potentially significant transit times within stream networks (*McGuire and McDonnell*, 2006). This time lag cannot be captured if the groundwater component of streamflow is approximated by the summed exfiltration. Furthermore, if the stream loses water to the subsurface between a point of groundwater discharging into the stream and the point where the hydrograph is measured, only a portion of the groundwater entering the stream will contribute to the groundwater component of streamflow at the point of hydrograph measurement. In that case, the summed exfiltration will overestimate the groundwater component of streamflow at the point of hydrograph measurement.

In this study, a mixing-cell method for quantifying the groundwater component of streamflow in fully integrated spatially distributed models is described. Mixing-cell models have often been used in hydrogeology to model solute transport (*Adar et al.*, 1988; *Campana and Simpson*, 1984). Mixing-cell models rely only on conservation of mass. The hydraulic mixing-cell (HMC) method described in this study relies on hydraulic information only (i.e. fluxes). Moreover, the method allows tracking streamflow generation mechanisms at every cell or element within the stream of the model domain. Therefore, complex spatial and temporal effects are captured and can be accounted for. The method is developed and tested using a particular numerical model (HydroGeoShpere, *Therrien et al.*, 2009), but it can be implemented to any code that reports the exchange between the subsurface and surface in a spatially distributed manner. The paper also aims to explore the

suitability of traditional methods (e.g. equilibrating the groundwater component of streamflow to the summed exfiltration) for quantifying the groundwater component of streamflow within numerical models.

2.2. Existing methods for extracting streamflow generation components

The hypothetical catchment shown in Figure 2.1 is used to illustrate the challenges of extracting the groundwater component of streamflow from numerical models using existing methods. In the catchment shown, the stream, which is flowing from A to B to C, is gaining in sections A and C, but losing in section B.

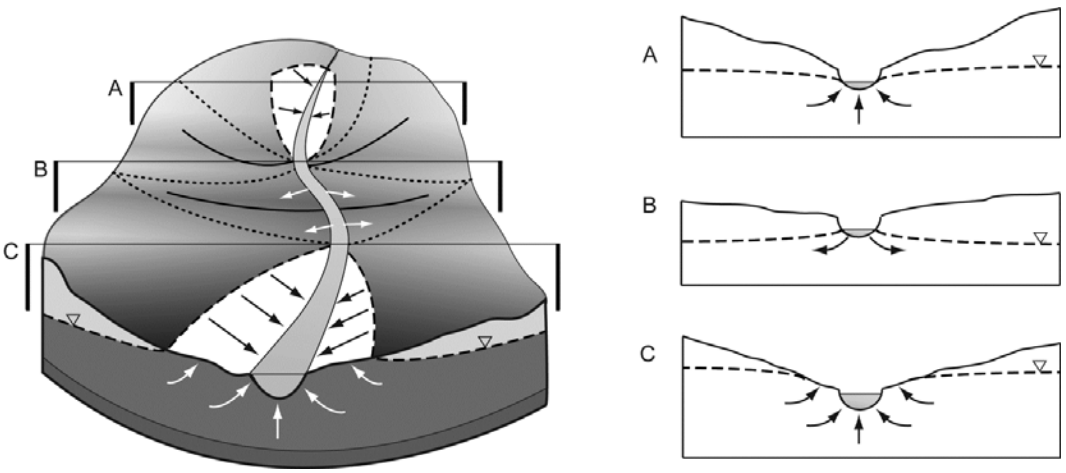

Figure 2.1: Conceptual diagram of a surface water-groundwater catchment (left hand side) featuring different flow regimes (as illustrated in the right part of the figure). The white sections of the catchment adjacent to the stream represent the groundwater discharge upslope of the stream (return flow). The dashed lines on the right part of the figure represent the water table. The flow direction is towards the reader.

2.2.1. Summed exfiltration along the length of the stream

For each of cross sections A, B and C of the hypothetical catchment shown in Figure 2.1, the expected streamflow hydrograph is shown in Figure 2.2, along with the groundwater component of streamflow and the summed exfiltration. The streamflow in Figure 2.2 A, B and C refers to the point measurement at each of cross sections A, B and C. Although the results shown in Figure 2.2 are hypothetical, they illustrate the following two problems that arise by

approximating the groundwater component of the streamflow using the summed exfiltration:

1) the summed exfiltration does not account for the time lag between the upstream points of groundwater discharging from the aquifer to the stream and the point where the hydrograph is measured, as illustrated by the time lag between the summed exfiltration and the groundwater component of streamflow curves. The streamflow travel times for the summed exfiltration upstream of cross sections A, B and C actually correspond to the time lag between the peaks of the summed exfiltration and the streamflow hydrograph in Figure 2.2.

2) changing flow regimes cannot be considered correctly. When a part of the stream is losing and other parts are gaining, the summed exfiltration is not equal to the groundwater component of streamflow at a particular location, even if the aforementioned time lag is negligible.

The effect of ignoring time lags and discounting losses along the stream becomes clear when moving downstream from cross sections A to B to C. For example, the course of the groundwater component of streamflow at cross section A features a flatter and broader distribution through time compared to the summed exfiltration upstream of A. When considering the streamflow hydrograph at cross section C in Figure 2.2, the significance of time lags, particularly from the most upstream sub-catchments, becomes apparent.

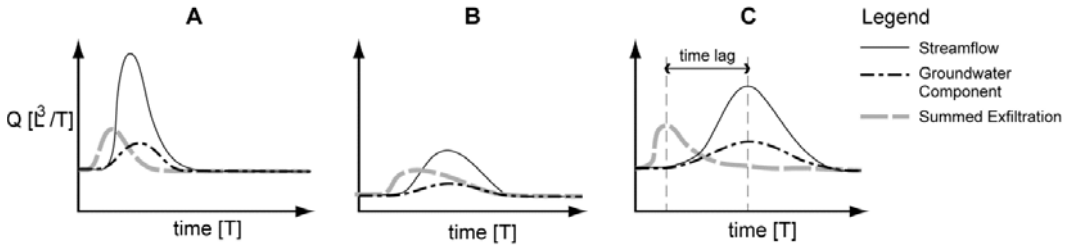

Figure 2.2: Hydrograph at cross sections A, B and C of the catchment shown in Figure 2.1. The streamflow and corresponding component of groundwater flowing through cross sections A, B and C are shown. Also, the summed exfiltration upstream of cross sections A, B and C, respectively, are shown.

2.2.2. Tracer based hydrograph separation

The use of conservative tracers within models provides temporal information on the original source of water (i.e. groundwater, soil water, rainfall). Whilst the

application of solutes is extremely useful in identifying the source of streamflow, it gives no real indication of the mechanism of streamflow generation (*McGuire and McDonnell*, 2006). Even with temporal information on the source of water, the parameters associated with tracer transport (i.e. diffusion, tortuosity and dispersivity) often affect the interpretation of the source as demonstrated in *Jones et al.* (2006). *Jones et al.* (2006) found that the value of dispersivity used in simulating the transport of tracers could lead to large overestimation of the pre-event water's contribution to streamflow. In their model using InHM of the Borden rainfall-runoff experiment, the pre-event contributions to streamflow using longitudinal dispersion α_L = 0.5 m and 0.005 m were found to be 41.6% and 33.9%, respectively, with the hydraulically based subsurface contribution close to 0%. These results would suggest that in the streamflow hydrograph in Figure 2.1 at cross section C of the catchment, the groundwater component of streamflow could be easily overestimated using tracers as illustrated in Figure 2.3.

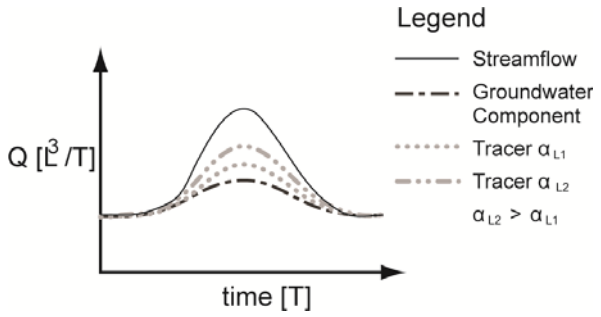

Figure 2.3: The theoretical hydrograph at cross section C of the catchment shown in Figure 2.1. The streamflow, groundwater discharge component and tracer based separation (for dispersivity values of α_{L1} and α_{L2}) are shown.

Given such large variation in the tracer based interpretations of groundwater contributions to streamflow, it seems quite clear that inherent accuracy relies on reliability and certainty of the transport parameters. Any uncertainty in the dispersivity directly relates to uncertainty in quantifying the groundwater component of streamflow. Therefore quantifying the groundwater component of the streamflow hydrograph within models using tracers may be undermined by large uncertainty.

2.3. A hydraulic balance using a hydraulic mixing-cell method

The hydraulic mixing-cell (HMC) method introduced in this paper allows the streamflow generation mechanisms to be deconvoluted from the streamflow hydrograph at any point along the stream. The method relies on standard hydraulic output from numerical models only. It is based on the modified mixing cell of *Campana and Simpson* (1984). Furthermore, it is assumed for the simplicity of coding that the width of the stream does not change during the simulation and additionally that the flow direction in the stream does not change. This mass balance of the HMC method is verified by application to two numerical test cases using HydroGeoSphere. The method can be generalised to any spatially distributed surface water - groundwater code, as mentioned previously.

2.3.1. Theory

The numerical modelling of streamflow requires discretisation over space and time of the relevant governing flow equation using a finite difference (FD), finite volume (FV) or finite element (FE) scheme. The method developed herein is designed to fit in accordingly with existing numerical models.

Consider the continuity of flow for a stream cell *i* of arbitrary shape. This can be expressed in terms of the streamflow generation/depletion as:

$$Q_{Up} \pm Q_{GW} \pm Q_{OF} \pm Q_{UF} \pm Q_{PF} + Q_{Rain} - Q_{Down} - Q_{Evap} = \frac{dV}{dt} \qquad \textbf{(2.1)}$$

Where Q_{Up} [L^3/T] is the upstream flow (generated from groundwater, overland flow, unsaturated flow and rainfall) into the stream cell; Q_{GW}, Q_{OF}, Q_{UF} and Q_{PF} [L^3/T] are the groundwater, overland flow, unsaturated flow and preferential flow, respectively, flowing into or out of the cell; Q_{Rain} [L^3/T] is the rainfall contribution to the stream cell, Q_{Down} is the flow downstream (generated from groundwater, overland flow, unsaturated flow and rainfall) flowing out of the cell [L^3/T]; Q_{Evap} [L^3/T] is the loss of water from storage (composed of groundwater, overland flow, unsaturated flow and rainfall) due to evaporation; dV/dt [L^3/T] is the rate of change of storage within the cell.

More concisely the fluid mass balance for a particular cell *i* with neighbouring cells *j* in the surface domain can be written as:

$$\sum_{j=1}^{n} Q_{ji} - \sum_{j=1}^{m} Q_{ij} = \frac{dV_i}{dt} \tag{2.2}$$

Where Q_{ji} [L^3/T] is the j^{th} flux into the cell *i*; Q_{ij} [L^3/T] is the j^{th} flux out of the cell *i*; V_i [L^3] is the volume in cell *i*; *t* [T] is time; and *n* and *m* denote *n* sources and *m* sinks.

By multiplying Eq. 2.2 by *dt* and integrating both sides over the interval t_1 to t_2, (t_2>t_1) we obtain the following:

$$V_{t_2} - V_{t_1} = \int_{t_1}^{t_2} \sum_{j=1}^{n} Q_{ji} dt - \int_{t_1}^{t_2} \sum_{j=1}^{m} Q_{ij} dt \tag{2.3}$$

$$V_{t_2} = V_{t_1} + \sum_{j=1}^{n} V_{ji}\Big|_{t_1}^{t_2} - \sum_{j=1}^{m} V_{ij}\Big|_{t_1}^{t_2} \tag{2.4}$$

For each cell the discrete volumetric balance over each time step *dt* can be written:

$$V_i^N = \sum_{k=1}^{K} V_{i(k)}^N \tag{2.5}$$

for *K* streamflow components, where V_i^N [L^3] is the total volume of water in cell *i* at time *N*; $V_{i(k)}{}^N$ [L^3] are the volumes of groundwater flow, unsaturated flow, overland flow, preferential flow and direct rainfall water, respectively, in cell *i* at time *N*. These constituent balances are defined as:

$$V_{i(k)}^N = V_{i(k)}^{N-1} + \sum_{j=1}^{n} V_{ji(k)}\Big|_{N-1}^{N} - \sum_{j=1}^{m} V_{ij(k)}\Big|_{N-1}^{N} \tag{2.6}$$

Where $V_{ji(k)}$ and $V_{ij(k)}$ [L^3] are the volumes of the k^{th} component of streamflow generation into and out of cell *i* from neighbouring cell *j*, from time *N*-1 to *N* respectively.

In order to calculate the volumetric balance, initial conditions of each streamflow component of the stream water must be known in each cell. The components of flow are defined as a fraction of the total volume (V_i) such that:

$$\sum_{k=1}^{K} f_{i(k)}^{N} = \frac{\sum_{k=1}^{K} V_{i(k)}^{N}}{V_i^{N}} = 1 \qquad \textbf{(2.7)}$$

Where $f_{i(k)}{}^{N}$ [L^3/L^3] is defined as the k^{th} fraction of each streamflow component.

If the form of the function of fluxes can be reconstructed from the flow solution then, using the modified mixing cell approach of *Campana and Simpson* (1984), each component of streamflow can be determined by substituting Eq. 2.6 into Eq. 2.7 and rearranging giving:

$$\sum_{k=1}^{K} f_{i(k)}^{N} = \frac{\sum_{k=1}^{K}\left(V_{i(k)}^{N-1} + \sum_{j=1}^{n} V_{ji(k)}\Big|_{N-1}^{N} - \sum_{j=1}^{m} V_{ij(k)}\Big|_{N-1}^{N} \right)}{V_i^{N}} \qquad \textbf{(2.8)}$$

Considering only the k^{th} fraction and expanding out the volumetric terms to explicitly represent the fractions, then rearranging yields:

$$f_{i(k)}^{N} = \left(\frac{V_i^{N-1}}{V_i^{N}} - \frac{\sum_{j=1}^{m} V_{ij}\Big|_{N-1}^{N}}{V_i^{N}} \right) f_{i(k)}^{N-1} + \frac{\sum_{j=1}^{n} V_{ji}\Big|_{N-1}^{N} f_{j(k)}^{N-1}}{V_i^{N}} \qquad \textbf{(2.9)}$$

Where there are n sources and m sinks for cell i; $f_{j(k)}{}^{N-1}$ denotes fraction k at time N-1 in neighbouring cell j. The terms on the right hand side of Eq. 2.9 relate to the stability of this approach. They can be considered from left to right as a.) the ratio of storage in the previous timestep to the current storage less the ratio of outflow volume to storage and b.) the ratio of inflow volume to storage. The stability of this method requires that the volume of water entering or leaving the stream cell over a time step is not greater than the storage at the end of the time step. This is fairly intuitive as it is not possible to remove more mass than existed at the start of the timestep (N-1) or insert more mass than exists at the end of the timestep (N).

For each component of streamflow the fraction is determined using the modified mixing cell which approaches a perfectly mixed cell as the time step approaches zero. A perfectly mixed cell will completely mix all contents across the entire cell instantaneously and takes the form:

$$f_{i(k)}^{N} = \frac{V_i^{N-1}}{V_i^{N}} f_{i(k)}^{N-1} - \frac{\sum_{j=1}^{m} V_{ij}\Big|_{N-1}^{N} \left(f_{i(k)}^{N-1} + \sum_{j=1}^{n} V_{ji}\Big|_{N-1}^{N} f_{j(k)}^{N-1} \right)}{V_i^{N} + \sum_{j=1}^{n} V_{ji}\Big|_{N-1}^{N}} + \frac{\sum_{j=1}^{n} V_{ji}\Big|_{N-1}^{N} f_{j(k)}^{N-1}}{V_i^{N}} \qquad \textbf{(2.10)}$$

It can be readily seen that Eq. 2.9 approaches Eq. 2.10 as the time step approaches zero, as only the first term on the right hand side in both equations will remain.

In applying this method, volumes in and out need to be determined at the start and end of each timestep. This requires reconstruction of the functions describing flux in and out of each cell. The approach used in calculating volumes needs to be consistent with the manner in which the fluid mass balance is calculated in the particular model used. In this study, the HydroGeoSphere (HGS) (*Therrien et al.*, 2009) code is used in which the flux Q between two adjacent nodes is back calculated at the end of the time step, giving rise to the following equation for evaluating the volume in or out over each time step:

$$V_{ij}^{N} = Q_{ij}^{N} \times \Delta t^{N} \quad \text{where} \quad \Delta t^{N} = (t^{N} - t^{N-1}) \qquad \textbf{(2.11)}$$

Where Q_{ij}^{N} denotes the calculated flux from HGS from node *i* to *j* over Δt.

The form of Eq. 2.11 will vary from code to code depending on how the fluid mass balance is calculated. Furthermore, the choice of numerical approach, be it finite difference, finite volume or finite element, is irrelevant as long as the volumetric balance for each cell is formulated correctly and is mass conservative. The latter requirement is due to the error in the mass balance at each time step being cumulative in the HMC method. Stability of the HMC method is not guaranteed for any flow solution as highlighted above. The use of suitable convergence criteria within the flow solution is imperative in successful application of the HMC method. A strict convergence criterion that is applied at

the nodal level is required. The nodal flow check tolerance in HGS, which is derived in *McLaren et al.* (2000), was utilised to ensure the nodal volumetric balances calculated in the HMC method were sufficient in preventing large cumulative errors. The choice of timestep and cell size also plays an important role in the stability of the HMC method because the volumetric balance at each HMC cell over each timestep is directly related to timestep and cell size. The proportion of volumes of water entering or leaving each cell over each time step compared to the storage volume in the cell has a direct impact on the HMC method's stability. The use of small HMC cells and large timesteps can lead to the volume entering or leaving a cell being greater than the storage and as such the method will become unstable causing spurious oscillations. Hence it is necessary to use suitable time steps for a fixed grid (i.e. fixed cell size) to ensure stability.

2.3.2. Implementation of the HMC method in HydroGeoSphere

The testing of the HMC method outlined in this paper was carried out by considering two conceptual test cases using the HGS model. HGS solves the diffusion wave approximation to the 2D St Venant equations in the surface domain and solves a modified form of the 3D Richards equation for variably saturated flow in the subsurface domain using a control volume finite element approach (details of the model can be found in *Therrien et al.* (2009)). The surface and subsurface are coupled using either continuity of head or (as in this study) a conductance concept, with exchanges between the two domains given by:

$$q_{exch} = \frac{k_r K_{zz}}{l_{exch}} (h_o - h_{pm}) \qquad \textbf{(2.12)}$$

Where q_{exch} [L/T] is the exchange flux between the surface and subsurface domain; k_r [dimensionless] is the relative permeability; K_{zz} [L/T] is the saturated hydraulic conductivity of the porous medium; l_{exch} [L] is the coupling length, h_o [L] and h_{pm} [L] are the heads of the surface and subsurface, respectively. HGS has been verified for both gaining (*Therrien et al.*, 2009) and losing streams (*Brunner et al.*, 2009a, 2009b). The model solves the governing flow equations using the finite element (FE) method, finite volume (FV) method or, alternatively, the finite difference (FD) method applied on a node centred grid (*Therrien et al.*, 2009).

Application of the HMC method requires specific HGS model outputs in order to accurately construct the volumetric balances in each HMC cell. As HGS utilises a node centred approach, the following HGS outputs are required for the volumetric balance at any given node:

1.) Computed surface water depth at the node – for the storage at each time step.

2.) Contributing area, *CA* [L^2] for the node determined from finite element basis functions (1/4 of the area of each element adjacent to the node for both FD and FE on a structured rectangular grid) – for the *Storage* (= *depth* x *CA*) [L^3] at each time step.

3.) Exchange flux between the subsurface and surface node – for the volume (Eq. 2.11) exchanged between the subsurface and surface over each time step.

4.) Flux from upstream contributing nodes – for the upstream volume (Eq. 2.11).

5.) Flux to downstream nodes – for the downstream volume (Eq. 2.11).

1.) and 2.) are used to calculate V_i, 3.) used to calculate V_{ji} for the exchange, 4.) used to calculate V_{ji} for upstream flow, 5.) used to calculate V_{ij} for downstream flow. The initial values for the fractions of stream flow are subjective and so a dummy (or undefined) fraction can be used until the streamwater is turned over at which point the dummy fraction will be zero.

This output data provides all the information required to apply the HMC method and determine the groundwater component of streamflow at each time step in each cell of the stream. The partitioning of groundwater, overland flow and rainfall entering the HMC cell is calculated from the upstream cell in the previous time step. The fractions of streamflow components leaving a given cell over a given time step are given by the cells' fractions at the previous time step. In doing so, water entering over a given time step remains in the given cell until the next time step. The HMC method was coded in Visual Basic for Excel and is used as a post processing tool on HGS outputs.

2.3.3. Verification of mass conservation in the HMC method

2.3.3.1. Test case 1

This test case is used to check that the flow components can be tracked accurately and to explore the significance of grid discretisation. The surface domain of the model is subjected to groundwater discharge (gaining conditions) across half of the model surface. This groundwater discharge in the gaining region is equal to the summed exfiltration obtained from the overall water balance, providing a benchmark against which the method can be tested.

The model domain is 2 m x 1 m x 1 m, split into two evenly sized rectangular cells (Figure 2.4). Two regions are highlighted in Figure 2.4, a gaining region in one half and a non-gaining region in the other. The non-gaining region has negligible interaction with the subsurface. With the soil fully saturated and an initial surface water depth of 0.01 m across the surface domain, a square pulse of groundwater (1.0 m^3/day for 0.1 days) is injected into the subsurface cell underlying the gaining region. No-flow boundaries are applied to all edges of the model domain allowing the groundwater (GW) pulse to be the only forcing function within the model. This simulation is run over a period of half a day with the groundwater pulse applied at 0.1 days. The grid spacing is 1 m along the x, y and z axes. For this HGS simulation, a control volume finite difference formulation is used to solve the coupled surface and subsurface flow equations. The nodal properties give rise to three 'cells' for the HMC method (see Figure 2.4). Note that rather than considering six nodes individually, the HMC 'cells' each consist of 2 adjacent nodes perpendicular to the flow direction. The HMC cells are given the initial conditions of containing 'surface water' (SW) only and hence $f_{SW} = 1$ and $f_{GW} = 0$ for all HMC cells at $t = 0$.

In the surface domain, a high value of Manning's n (1.5 x 10-5 day/$m^{1/3}$) is used in order to make the transient part of the simulation apparent. The aquifer parameters are defined such that surface/subsurface interactions other than the groundwater pulse are negligible. The porosity is 0.45 and a low value of hydraulic conductivity (1 x 10^{-4} m/day) is used to effectively render the subsurface inactive with regard to infiltration.

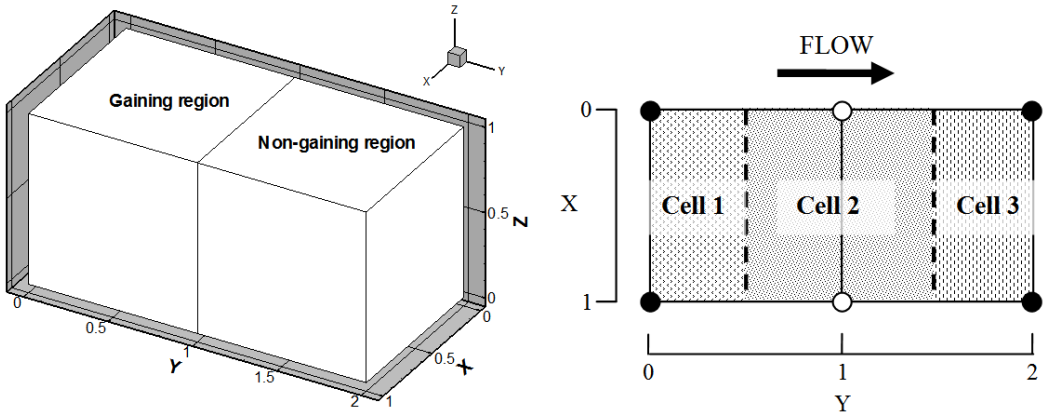

Figure 2.4: Test case 1: "two-region" model grid, and HMC cells for HGS nodes in "two-region" model grid. In the right part of the figure the two nodes at y = 0 belong to HMC cell 1, the two nodes at y = 1 belong to HMC cell 2 and the nodes at y = 3 belong to HMC cell 3.

As the subsurface is fully saturated, infiltration is negligible, and the groundwater injected to the system will directly result in a fluid flux from the subsurface to the surface domain. The coupling length chosen (1 x 10^{-5} m) is sufficiently small to achieve continuity of head between the surface and subsurface. A maximum timestep of 1 x 10^{-3} days was used for the first simulations. As the diffusion wave approximation to the Saint Venant Equations is used in HGS, inertial effects are ignored and therefore water entering the gaining region will move to the non-gaining region and not flow back as it would if inertial effects were included.

Figure 2.5 shows the volumetric balances of surface water and groundwater calculated for each of the three HMC cells in the model, highlighting the subtle complexities that can easily be overlooked when considering the dynamics of such a system. It can be seen in cell 1 of Figure 2.5 that whilst the groundwater pulse is applied to the subsurface, groundwater is entering the gaining region, causing an increase in volume (and hence head) and a resultant flux from the gaining to the non-gaining region. Moreover, the volume of surface water in the gaining region decreases as the groundwater enters, which is due to the water in the gaining region flowing to the non-gaining region. The volumes of groundwater and surface water in cell 2 are collectively larger than those in cells 1 or 3 because the contributing area of cell 2 is twice that of cells 1 and 3 (see Figure 2.4). The small lag between the surface water and groundwater curves in the volumetric balance for cell 3 (Figure 2.5) indicates that surface water initially

contributes more to the flow from the gaining region to the non-gaining region, as the surface water is displaced by the groundwater. The SW and GW balances for each of the HMC cells in the top panel of Figure 2.5 are also shown with the total cell volume. Clearly, the SW and GW balances sum to the total volume, indicating that that the HMC method conserves mass. The SW and GW fractions for each of the HMC cells in the bottom panel of Figure 2.5 are seen from the average of the two fractions to be inversely proportional to each other, as expected. As the balances are calculated independently, this further highlights the accuracy within the HMC method.

The relative error (ε) in the balances is based on Eq. 2.7 and is determined using the following equation:

$$\varepsilon = \left| 1 - \sum_{j=1}^{k} f_{i(k)}^{N} \right| \qquad \textbf{(2.13)}$$

The relative error relates to the accuracy of the numerical methods for solving the flow equations, which is determined by the convergence criteria used in the numerical scheme. This error grows slightly due to round-off errors and imperfect balances in the numerical scheme used to solve the flow equations (finite difference in this case). Such imperfect balances will always exist due to error in the numerical scheme adopted, however they can be minimised by use of a small value for the convergence criterion. In this test case the maximum relative error in the HMC method was 1.5 x 10^{-3}% in cell 1.

To investigate the effect of discretisation, the grid spacing *dy* in the flow direction (y axis) is reduced in HGS from 1 m to 10 cm. As a result, the number of corresponding cells in the HMC method increases to 21 (see Figure 2.6). Three different simulations are then run to test the impact of time discretisation, with constant time steps equal to 10^{-2}, 10^{-3} and 10^{-4} days, respectively.

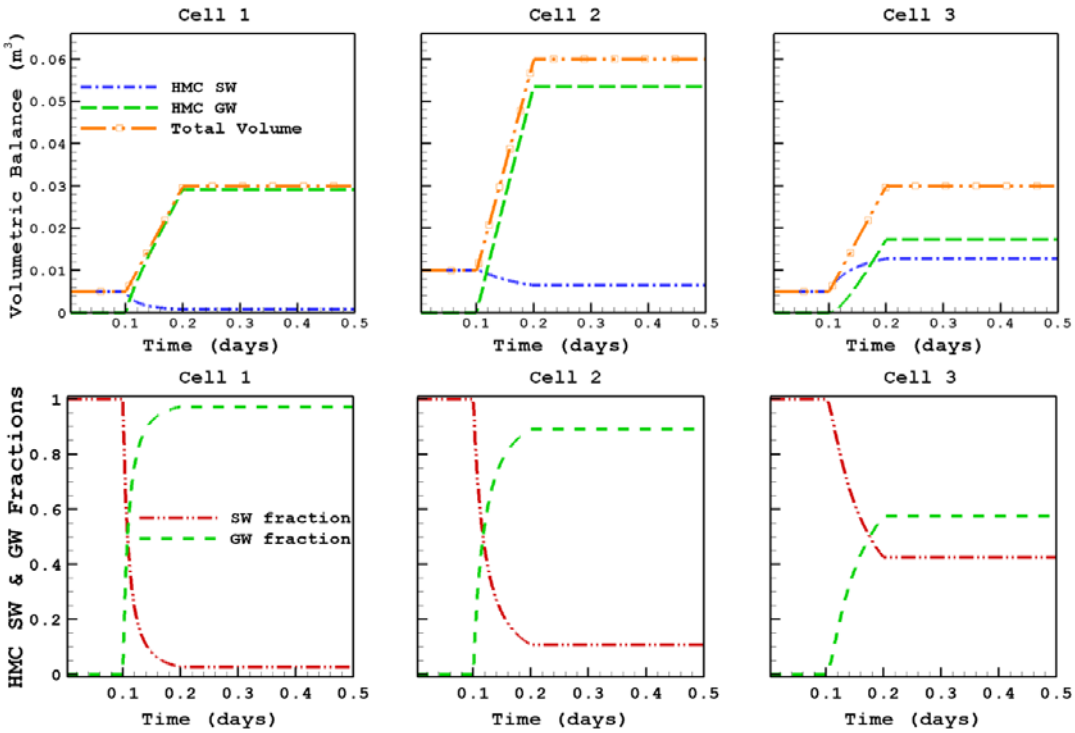

Figure 2.5: HMC cell, SW and GW balances (top panel) and fractions (bottom panel) for test case 1. The volumetric balance in the top row shows the HMC calculated balances for SW and GW in the HMC cells as well as the total volume in the cell which is calculated directly from the model outputs. The HMC cell SW and GW fractions in the bottom panel are calculated independently of each other.

The effects of temporal discretisation on the SW and GW fractions for the case of *dy* = 10 cm are shown in Figure 2.7. In Figure 2.7, only the two end cells (1 and 21) and the middle cell (11) are shown. It can be seen that the finer timesteps make little difference to the SW and GW fractions in cells 1 and 11, but that a distinctly different solution of the SW and GW fractions arises in cell 21 for the three timesteps used, with convergence at $t = 10^{-3}$ and 10^{-4} days. It follows that it is important to note that the timestep used in the model will dictate the SW and GW fraction profiles in the HMC method. As highlighted in the theory, as *dt* approaches zero, a perfectly mixed cell solution is approached. Variation in grid size changes the representative area of the HMC cells. For example, halving the grid size would result in the HMC cell area for the larger grid size being represented by two HMC cells for the halved grid size. As the HMC cells are representative of an area and not a point, results based on different grid discretisations are not directly comparable. However, finer grids will give greater spatial resolution of the SW and GW fractions along the surface. It follows that

smaller cell sizes in the model grid and hence in the HMC method, result in greater spatial clarity of the solution, converging towards a point solution as *dy* approaches zero. As *dy* approaches zero, the area of the cell approaches zero and hence the volume in the cell approaches zero. Given that stability requires that the volume in or out of the cell cannot be greater than the storage, the time step *dt* will also have to decrease as *dy* decreases to ensure numerical stability.

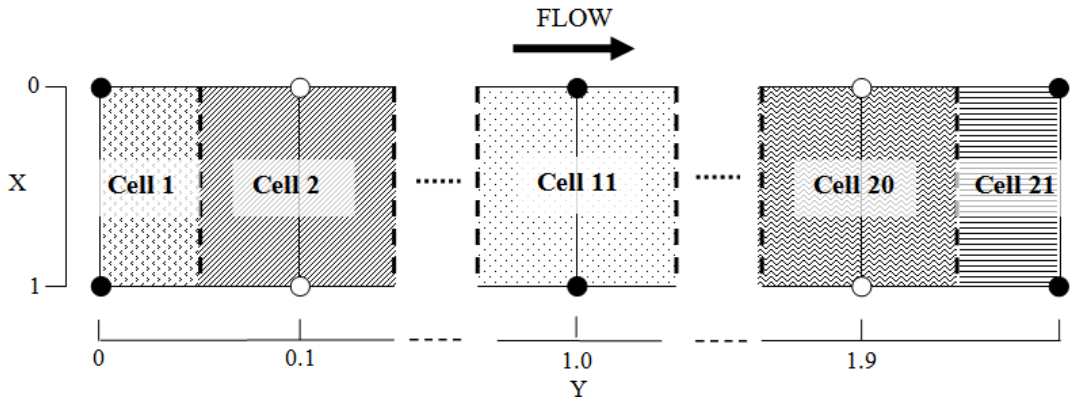

Figure 2.6: The 21 HMC cells for the "two-region" model with *dy* = 10 cm.

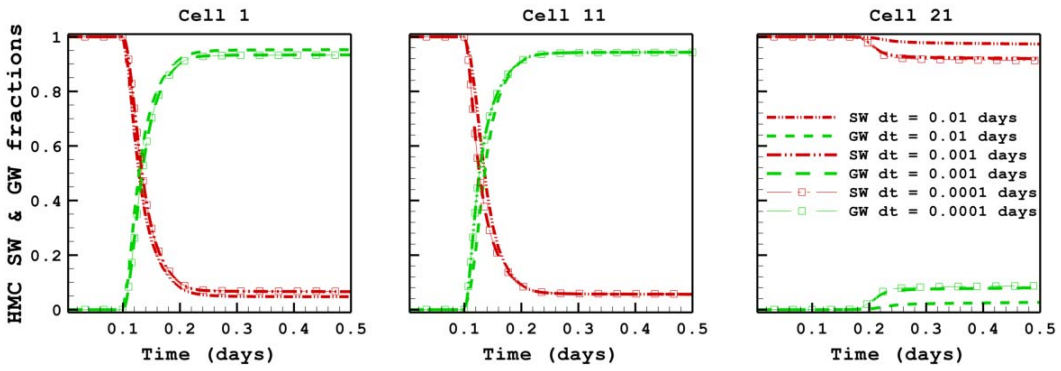

Figure 2.7: Effect of temporal discretisation on the SW and GW fractions in HMC cells 1, 11 and 21.

A second approach to testing the accuracy of the HMC method is to compare the total volumes of surface water and groundwater resulting from summing these components in each HMC cell at the end of the simulation with the overall water balance in the model. By summing the final volumes of groundwater in each HMC cell, and comparing these to the total volume that was exchanged from the subsurface to the surface domain during the simulation, a global volume error (*GVE*) can be defined as follows:

$$GVE(\%) = \left| 1 - \frac{\sum_{\forall i} f_{i(GW)}^{N} V_i^{N}}{\sum_{\forall N} Q_{SE}^{N} \Delta t^{N}} \right| \times 100 \qquad \textbf{(2.14)}$$

Where Q_{SE}^{N} [L^3/T] is the summed exfiltration (*SE*) across the model domain at time *N* from the overall water balance of HGS.

This measure gives the error of the HMC method relative to the summed exfiltration from the overall water balance. The cumulative error of the HMC method (as opposed to the instantaneous nodal fluid mass balance error in HGS) will grow according to the convergence criteria, number of time steps and number of stream cells. As the GVE is based on the summed exfiltration from the overall water balance, it can only be used along completely gaining sections. It also requires that all water is retained in the model domain (i.e. no losses). The maximum relative error and GVE are given in Table 2.1 for the different spatial and temporal discretisation tested, highlighting both the reduced maximum relative error and GVE as the spatial and temporal resolution is increased.

Table 2.1: Maximum relative error in the HMC method, and the global volume error (GVE) for the HMC method.

	HMC max. relative error	**GVE**	**Timesteps**
dy = 1m, t = 0.001 days	1.5 x 10^{-3}%	1.97 x 10^{-4}%	500
dy = 10cm, t = 0.01 days	1.8 x 10^{-4}%	5.23 x 10^{-10}%	50
dy = 10cm, t = 0.001 days	3.6 x 10^{-5}%	1.17 x 10^{-10}%	500
dy = 10cm, t = 0.0001 days	3.9 x 10^{-7}%	2.81 x 10^{-11}%	5000

In the HMC cells of Test case 1, the relative and absolute errors are relatively small and consequently the HMC method can be used in larger and more complex model scenarios provided that fluid mass conservation is fulfilled.

2.3.3.2. Test case 2

The model setup for Test case 2 mirrors the physical processes of the catchment shown in Figure 2.1. This test case is used to test not only the theoretical effects of time lags (seen in the hydrographs of Figure 2.2) and accurate attribution and tracking of streamflow generation mechanisms, but also to test the HMC method

in a highly transient model scenario whilst comparing the HMC method's groundwater component of streamflow with the summed exfiltration from the overall water balance of the model.

Test case 2 is loosely based on the tilted V-catchment by *Panday and Huyakorn* (2004), which has been used in verification of surface/subsurface interaction in fully integrated models such as MOD-HMS and HGS. A number of modifications are carried out to the V-catchment to mirror the spatial and temporal distribution of the catchment shown in Figure 2.1. In order to distribute the subsurface to surface exchange to the stream over its entire length, the slopes are reduced, resulting in a significantly flatter catchment. The model domain shown in Figure 2.8 is 1000 m along the *y* axis by 810 m along the x axis (catchment area of 810,000 m^2), with a homogeneous soil layer thickness of 20 m at (x = 800 – 810 m, y = 0 m) increasing in thickness with a gentle surface slope of 5 x 10^{-4} m/m along the y axis (from y = 0 m to y = 1000 m) and 0.02 m/m along the x axis (from x = 800 m to x = 0 m). With the use of the gentle slopes, the head gradient required in order to produce an exchange from the subsurface to the surface along the entire stream is achieved by raising the adjacent plane 2 m over a 5 m length above the streambed as shown in the cross section of Figure 2.9.

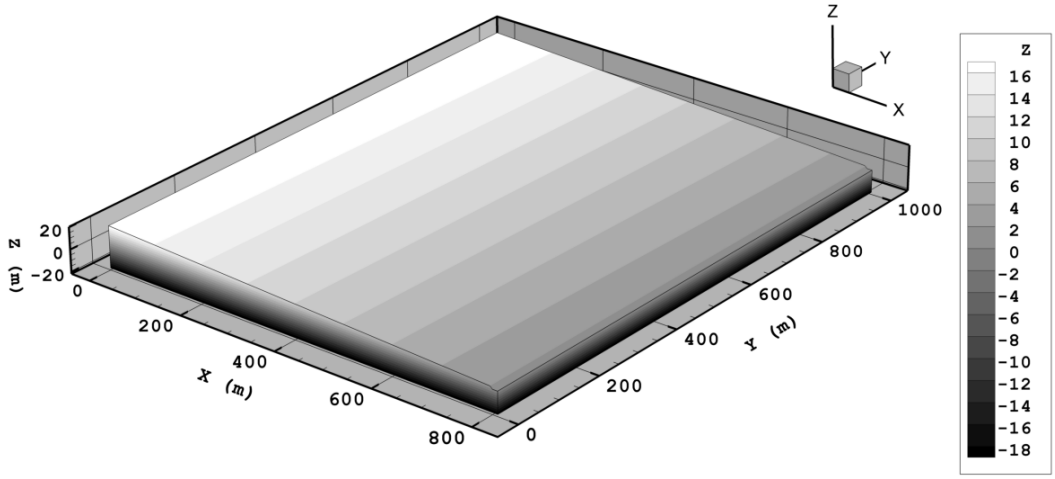

Figure 2.8: Test case 2 catchment model (modified version of the V-catchment in Panday and Huyakorn (2004)). The contours correspond to the elevation.

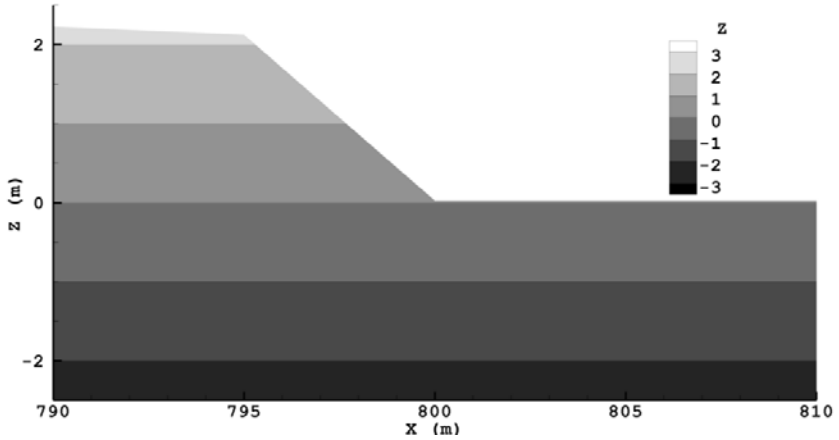

Figure 2.9: Part cross section of hypothetical catchment highlighting the raised plane which is used to create a greater hydraulic gradient next to the stream leading to constant subsurface to surface exchange along the entire length (from x = 790 – 810 m, at y = 0 m and z = -4 to 2 m). The plane (left), bank (middle) and streambed (right) are seen in the division of top cells.

Grid spacing along the x axis is 50 m from x = 0 – 750 m, 25 m from x = 750 – 775 m, 15 m from x = 775 – 790 m, 5 m from x = 790 - 800 and 10 m from x = 800 – 810 m. The grid spacing is 50 m along the y axis and 1 m along the z axis for the first 10 m below the surface with a thickness of 10 m to 26.5 m, varying with the slopes of the catchment for the bottom layer. Streamflow at the downstream boundary is governed by a critical depth boundary condition at the end of the stream, which acts at nodes (800,0,0) and (810,0,0). The critical depth boundary in HGS specifies the surface head to be at critical depth at the nodes which are set with this boundary condition.

Saturation-relative permeability and saturation-pressure relationships are described by the *van Genuchten* (1980) equations. The soil is a homogeneous sand with the soil parameters derived from *Carsel and Parrish* (1988). The surface friction is described using Manning's n, with a value representing a straight uniform channel (*Chow*, 1959), and a rill storage height and obstruction height (as defined in *Panday and Huyakorn* (2004)) of 1 mm and 0 mm, respectively. The rill storage height provides a threshold to surface flow whilst the obstruction height provides retardation to flow. The surface and subsurface parameters are detailed in Table 2.2. The coupling length (Eq. 2.12) is chosen such that continuity of pressure at the surface/subsurface interface is maintained, without jeopardising the accuracy of the flow solution. The solution of continuous

pressure at the surface/subsurface interface leads to much larger run times for the simulations in this study (see *Ebel et al.*, 2009), however for small coupling lengths, the solution approaches that of continuous pressure at the surface/subsurface interface.

Table 2.2: Surface and subsurface parameters for test case 2.

Parameter	Value
Surface	
Manning's roughness	0.015 s/m$^{1/3}$
Rill storage height	0.001 m
Obstruction storage height	0.0 m
Subsurface	
Porosity	0.1
Saturated hydraulic conductivity	8.25 x 10^{-5} m/s
Van Genuchten α	14.5 m^{-1}
Van Genuchten β	2.68
Residual saturation θ_r	0.045
Surface/Subsurface coupling	
Coupling length	0.5 m

The simulations for the hypothetical catchment are carried out in two phases:

1. Firstly, initial conditions are generated by running the model with a fully saturated subsurface with only the critical depth forcing function in the surface domain for approximately 40 days. This first simulation provides quasi steady-state initial conditions for phase 2.

2. Based on these initial conditions the model is run for another 40 days with 3 rainfall events and constant groundwater pumping throughout the entire simulation. The drawdown around the pump results in a losing section along a part of the stream. Rainfall is applied across the entire catchment, starting at time t = 0 seconds at a rate of 5.88 x 10^{-7} m/s (2.12 mm/hr) for a day at a time with three recovery periods after each rainfall period of 10, 5 and 22 days, respectively for each rainfall event. Pumping is applied at node (750,500,0) at a rate of -0.02 m^3/s throughout the simulation time. This extraction rate is sufficient to produce losses over part of the stream. Over the length of the simulation there is a rainfall input of 1.75 x 10^5 m^3 and a loss through pumping of 6.84 x 10^4 m^3. The maximum time

step used in the second phase of the simulation is 100 seconds. The rainfall and pumping in the second phase create highly transient conditions. The length of the stream that is losing is changing throughout the simulation. The nature of this transience in the streamflow conditions allows for rigorous stability testing of the HMC method because the stream cells are switching between gaining and losing and are subject to sharp changes in volume and rate of change of volume in the cell.

The rainfall events in the simulations provide recharge to the groundwater system, sustaining flow to the stream. However, the gentle rainfall events and gentle slopes in the catchment result in pure recharge with no overland flow on the planes and hence no direct overland flow to the stream itself. Figure 2.10 highlights the changes in the subsurface to surface exchange, as well as the depth and velocity along the stream at time = 1 second, 12 days and 40 days. At t =1 second in Figure 2.10, the initial stream is gaining along its entire length, before groundwater abstraction has taken effect. At t = 12 days, there is an increased discharge of groundwater at the top and bottom areas of the stream, which can be attributed to the recharge resulting from rainfall as well as stream losses in the middle section due to near stream groundwater extraction. The proportion of the stream that is gaining and losing is varying throughout the entire simulation.

At t = 40 days, the subsurface to surface exchange to the stream has decreased along the length of the stream due to the last rainfall event finishing 20 days earlier. It also shows an increased loss from the stream over the middle losing section due to reduced recharge in response to the groundwater extraction. This loss rate from the stream in the middle causes the stream depth to drop over the losing region, however streamflow is maintained through the entire simulation. This qualitative analysis provides a reasonable understanding of the governing processes in the system. For quantifying the groundwater component of streamflow, the HMC method is required.

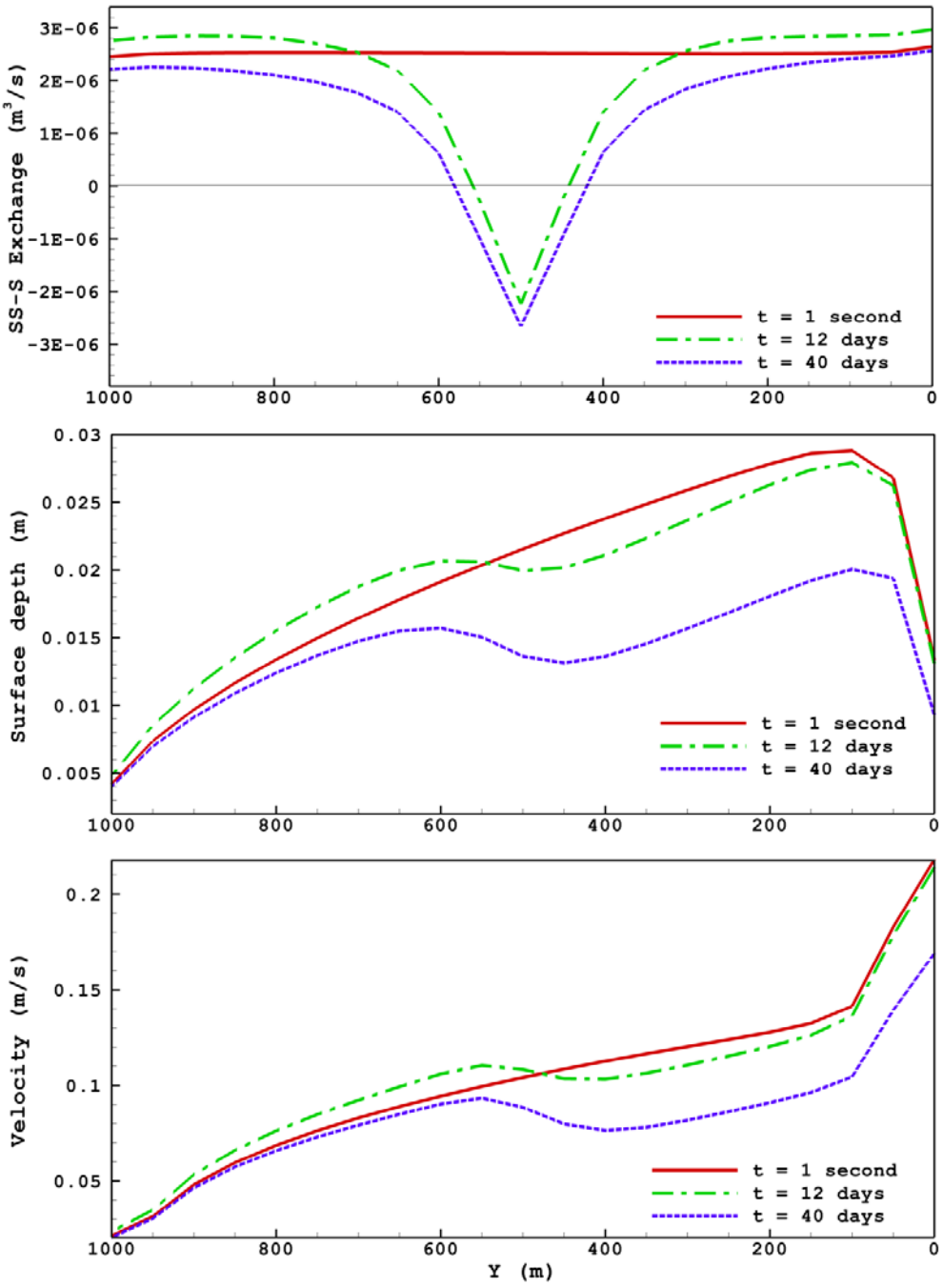

Figure 2.10: Evolution of the losing section of the stream in the hypothetical catchment. A positive exchange in the top panel of plots denotes subsurface to the surface exchange and vice versa for a negative exchange. The depth and velocity profile along the stream are shown below. At *t* = 1 second, the stream is gaining along the full length. At b.) *t* = 12 days, the pumping has reduced the positive exchange section of the stream adjacent to the pumping location. At c.) *t* = 40 days, the stream is partially losing along a small section whilst maintaining flow along the losing section.

The HMC method is applied to each pair of adjacent nodes that are located at x = 800 m and x = 810 m and that lie in the stream perpendicular to the direction of flow. HMC cells are numbered from upstream (y = 1000m) to downstream (y = 0m) and correspond perfectly to the HGS cells. This gives rise to 21 HMC cells, with 20 surface cells (x = 800 – 810 m and y = 0 – 1000 m) defined as the stream. As a node based approach is used, the contributing area of nodes lying along x = 800 m takes into account the surface cells lying between x = 795 – 800 m. The HMC maximum relative error in the simulation was 8.7 x 10^{-3}% in HMC cell 13 at around t = 12 days.

The use of the HMC method allows the quantification of the groundwater component of streamflow at any cell along the stream. Since the simulation set up does not produce overland flow, the streamflow in each HMC cell consists of the groundwater component and the direct rainfall component of streamflow. The resultant groundwater component and direct rainfall fractions before and after the first rainfall event for the HMC cells located at y = 0, 600 and 1000 m are shown in Figure 2.11. In Figure 2.11, the rise and fall of the direct rainfall fraction is sharp and fast in cell 1 and slower and longer in cells 13 and 21. This can be attributed to the time lags of upstream flow that are evident at the downstream cells and to the streamflow velocity in each cell. In Figure 2.10, the stream flow velocity is seen to increase from the top of the stream (y = 1000 m) to the bottom of the stream (y = 0 m) as water keeps entering the stream, although this is only seen in the gaining regions. At t = 12 and 40 days, the stream is losing over the middle section which is clearly evident in Figure 2.10 at around y = 400 m where the velocity drops off only to start increasing again at y = 500 m. As surface flow velocity is faster at the bottom sections of the catchment, storage effects alone can be ruled out as causing the slower recession of the rainfall fraction in cells 13 and 21. The rainfall fraction after the first rainfall event (t = 1 day) in cells 13 and 21 must be due to rainfall from upstream cells in which there is a significant time lag of approximately 0.2 days. It is also apparent that the rainfall fraction in cell 13 is greater than the fraction in cell 21, which can be attributed to the increase in the groundwater entering when moving downstream of cell 13. As there are only two streamflow generation mechanisms in this simulation, the same explanation leads to the groundwater component of streamflow results shown in Figure 2.11.

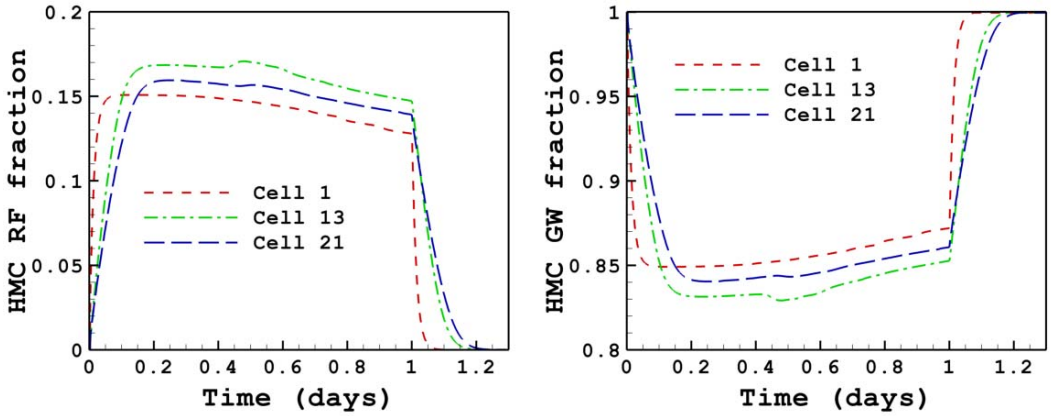

Figure 2.11: HMC direct rainfall (RF) and groundwater (GW) component fractions before and after the first rainfall event for cells 1, 13, and 21. Note the time lags of rainfall in the downstream cells 13 and 21 (~3.5hrs).

The resulting partition of the groundwater component of streamflow is shown in Figure 2.12. The HMC groundwater component of streamflow and direct rainfall to the stream are calculated using the HMC fractions in HMC cell 21. It is highlighted that the summed exfiltration from the overall water balance cannot be used as a measure of the groundwater component of streamflow as it clearly leads to an overestimation as the summed exfiltration is greater than the streamflow. This is due to the losses occurring in the middle section of the stream, which is not captured by the summed exfiltration upstream of this section where flows are partially lost through the losing section of the stream. The infiltration in the overall water balance cannot be utilised to account for the net change either, due to the very large amount of infiltration over the planes resulting from the rainfall events. Whilst the error in the groundwater component of streamflow as estimated using the summed exfiltration along the stream may appear small, the volumetric differences found by integrating the summed exfiltration and HMC groundwater component of streamflow over the recession periods (t = 1 – 11 days, t = 12 – 17 days and t = 18 - 40 days) were found to be 1,620 m^3 (1.62 Ml), 858 m^3 (0.85 Ml) and 5,420 m^3 (5.42 Ml), respectively. This is a total of 7,340 m^3 (7.34 Ml) during the recession periods, a significant difference in response to a single hydrograph event in a small catchment. Given the area of this catchment (0.81 km^2), the impacts on the difference/error that would be seen in a larger catchment are significantly greater. However, it is not only the area of the catchment that will

make use of the HMC method critical in determining the groundwater component of streamflow generation. The travel time within the streams also undermines the application of the summed exfiltration as seen in Figure 2.11. As the streams become longer, the streamflow travel time from upstream to downstream increases, and as such the summed exfiltration can be much sharper and completely out of phase with the total streamflow as hypothesised in Figure 2.2. The proportion and distribution of both gaining and losing sections also have a clear effect of leading to overestimation of the groundwater component of streamflow at the outlet.

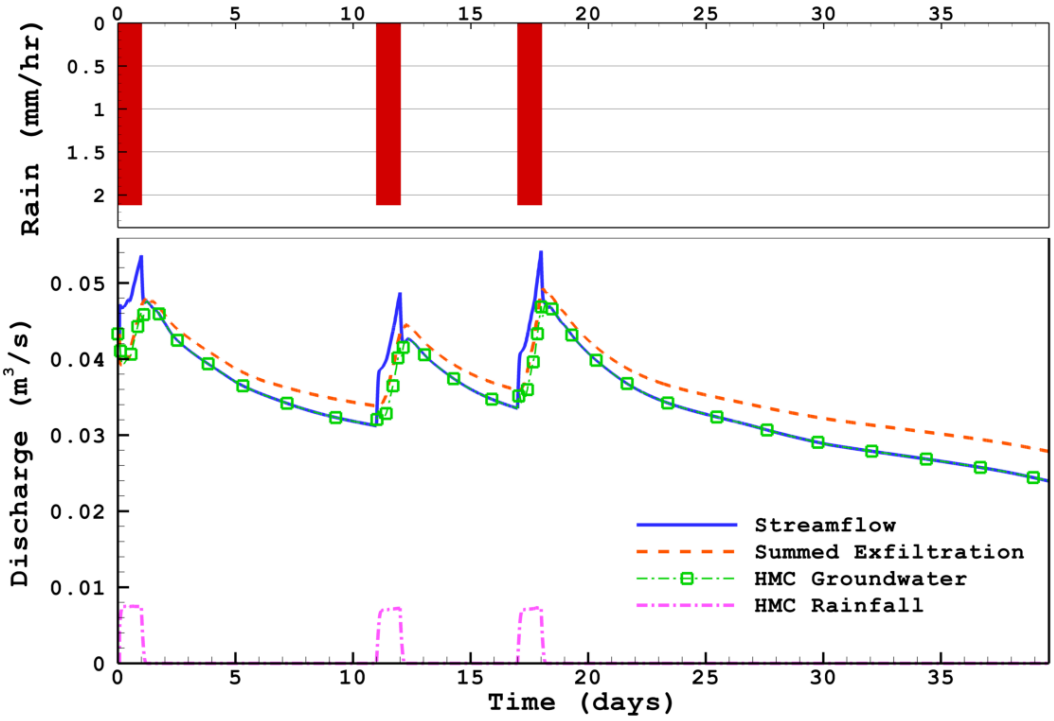

Figure 2.12: Hyetograph for catchment and Hydrograph at the catchment outlet, showing separation of direct rainfall and groundwater components of streamflow, as well as the summed exfiltration from the overall water balance. The summed exfiltration (SE) from the water balance is clearly seen to exceed the outflow in this hypothetical catchment. The HMC direct rainfall and groundwater components of streamflow are calculated using the HMC fractions in HMC cell 21.

2.4. Discussion and Conclusions

The hydraulic mixing-cell (HMC) method developed in this paper overcomes many of the limitations that exist in current methods of quantifying streamflow generation mechanisms based on fully integrated spatially distributed SW-GW

interaction models. The HMC method accurately extracts streamflow generation mechanisms using only hydraulic information. Streamflow generation mechanisms at every HMC defined cell along the stream are extracted by post-processing of the flow solution obtained from the numerical flow model. Because the HMC method tracks the streamflow generation mechanisms along the stream, temporal and spatial components that affect these mechanisms can be accounted for. The HMC method correctly handles changing flow regimes (e.g. if a stream changes from gaining to losing within the catchment), accounts for storage effects within the channel and the time lags that occur within a catchment. These attributes give the HMC method the ability to deal with the dynamic nature of varying flow regimes in large and complex systems, such as the catchment described in Figure 2.1. The only data requirements for the HMC method are the fluxes at each cell and surface water depths, which are part of the flow solution. By using this method, one does not have to make the commonly made assumptions of negligible time lags in streamflow and exchanges being always positive to the stream, in order to determine the streamflow generation mechanisms.

In the current formulation, the HMC method is based on the modified mixing cell (*Campana and Simpson*, 1984). Unless the mixing processes in the river are explicitly simulated, the modified mixing rule has to be used. As highlighted in the theory section, the HMC method is stable as long as the ratio of the volume of water entering or leaving a HMC cell to the storage volume of the HMC cell is less than unity. The assumption of constant river width and flow direction are used in the coding of the HMC algorithm in this study. The initial formulation of the HMC method presented here is based on the assumption of a constant river width. In models such as HGS, the width of the stream can change in response to a changing flowrate. In order to capture a changing river, the definition of the river in the HMC algorithm must match the changes in the river. Further development of the method is required to quantify streamflow generation mechanisms in such systems. The HMC method presented is applicable (in principle) to any spatially distributed flow modelling code, however the coding requires generalisation to time varying river widths and lengths. The HMC

method should be routinely employed as either a subroutine within the model code or a standard post processing tool in the new versions of the available codes.

Acknowledgements

This work is supported by the Australian Research Council through its Linkage scheme and the South Australian Department of Water, Land and Biodiversity Conservation as industry partners under grant number LP0668808. Parts of this research were funded by the Swiss National Foundation, Ambizione grant PZ00P2_126415. The views expressed in this paper are solely those of the authors.

Chapter 3

3 Evaluation of outputs from automated baseflow separation methods against simulated baseflow from a physically based, surface water-groundwater flow model. (Paper 2)

Statement of Authorship

Title of Paper	A hydraulic mixing-cell method to quantify the groundwater component of streamflow within spatially distributed fully integrated surface water - groundwater flow models
Publication Status	(•) Published ( ) Accepted for Publication ( ) Submitted for Publication ( ) Publication Style
Publication Details	Partington, D., P. Brunner, C. T. Simmons, R. Therrien, A. D. Werner, G. C. Dandy, and H. R. Maier. 2011. A hydraulic mixing-cell method to quantify the groundwater component of streamflow within spatially distributed fully integrated surface water - groundwater flow models. *Environmental Modelling and Software*, 26:886-898.

Author Contributions

By signing the Statement of Authorship, each author certifies that their stated contribution to the publication is accurate and that permission is granted for the publication to be included in the candidate's thesis.

Name of Principal Author (Candidate)	Daniel Partington		
Contribution to the Paper	Development of HMC method, testing and implementation of method, wrote manuscript.		
Signature		Date	23/11/2012

Name of Co-Author	Philip Brunner		
Contribution to the Paper	Supervised manuscript preparation and reviewed draft.		
Signature		Date	3.12.2012

Name of Co-Author	Craig Simmons		
Contribution to the Paper	Supervised manuscript preparation and reviewed draft.		
Signature		Date	23/11/12

Name of Co-Author	Rene Therrien		
Contribution to the Paper	Supervised manuscript preparation and reviewed draft.		
Signature		Date	Nov 24, 2012

Name of Co-Author	Adrian Werner		
Contribution to the Paper	Supervised manuscript preparation and reviewed draft.		
Signature		Date	23/11/12

Name of Co-Author	Holger Maier		
Contribution to the Paper	Supervised manuscript preparation and reviewed draft.		
Signature		Date	5/12/12

Name of Co-Author	Graeme Dandy		
Contribution to the Paper	Supervised manuscript preparation and reviewed draft.		
Signature		Date	3/12/12

Please cut and paste additional co-author panels here.

Abstract

Baseflow is often considered to be the groundwater discharge component of streamflow. It is commonly estimated using conceptual models, recursive filters or a combination of the two. However, it is difficult to validate these methods due to the current challenges of measuring baseflow in the field. In this study, simulation of a synthetic catchment's response to rainfall is carried out using a fully integrated surface water-groundwater flow model. A series of rainfall events with differing recovery periods and varied antecedent moisture conditions is considered to span a range of different streamflow generation dynamics. Baseflow is estimated for the outlet hydrograph of the synthetic catchment using a selection of commonly used automated baseflow separation methods. These estimates are compared to the baseflow signal obtained from the numerical model, which serves as the control experiment. Results from these comparisons show that depending on the method used, automated baseflow separation underestimates the simulated baseflow by as much as 28%, or overestimates it by up to 74%, during rainfall events. No separation method is found to be clearly superior to the others, as the performance of the various methods varies with different soil types, antecedent moisture conditions and rainfall events. The differences between the various approaches clearly demonstrate that the baseflow separation methods investigated are not universally applicable.

3.1. Introduction

Quantifying baseflow contributions to streamflow is of great interest in the understanding, identification and quantification of streamflow generation processes, in particular where baseflow supports important ecosystems and/or provides critical dry season water supply (e.g. *Smakhtin*, 2001; *Werner et al.*, 2006). The term baseflow is often referred to as the groundwater contribution to streamflow (e.g. *Freeze*, 1972; *Brutsaert and Nieber*, 1977; *Eckhardt*, 2005), although it is also referred to as the release from both groundwater and other natural storages of water that sustain streamflow between rainfall events (e.g. *Hall*, 1968; *Smakhtin*, 2001; *Piggott et al.*, 2005). In this paper, the term baseflow is used to describe groundwater discharge that reaches the stream, not including interflow through the vadose zone.

Baseflow can be inferred through field measurements of temperature, artificial and natural tracer concentrations, and flow in seepage meters installed in stream beds (*Becker et al.*, 2004; *Cook et al.*, 2003; *Cook et al.*, 2008). However, for practical reasons, it is very difficult to apply these techniques over an entire catchment. Furthermore, the required end members in chemical mass balance approaches are difficult to characterise (*McCallum et al.*, 2010), which complicates baseflow estimates using measurement of tracers. Consequently, the available field methods do not currently allow accurate determination of spatially and temporally distributed baseflow. In the absence of detailed field data, but where a streamflow hydrograph is available, baseflow is therefore often estimated using simple baseflow separation methods.

Since the early twentieth century, a variety of methods has been developed to estimate baseflow. The earliest methods and some of the more recent ones are based on a linear storage-discharge relationship between aquifer and stream (e.g. *Maillet*, 1905; *Barnes*, 1939; *Hall*, 1968; *Boughton*, 1993). More recently, non-linear storage-discharge relationships have also been applied to baseflow separation (e.g. *Wittenberg*, 1994; *Wittenberg and Sivapalan*, 1999; *Wittenberg*, 2003) following theoretical studies suggesting that non-linear recessions are appropriate for some catchments. Also, other methods that use some form of hydrological reasoning have been developed without a physically based mathematical framework. Currently, the separation of baseflow from the streamflow hydrograph can be carried out utilising methods that can be grouped into the following four categories: 1) graphical separation (*Sloto and Crouse*, 1996), 2) recession analysis (*Tallaksen*, 1995), 3) conceptual models (*Barnes*, 1939; *Singh and Stall*, 1971; *Furey and Gupta*, 2001; *Eckhardt*, 2005; *Huyck et al.*, 2005) and 4) recursive digital filters (*Nathan and McMahon*, 1990; *Arnold and Allen*, 1999).

The different categories of separation approaches as noted above have been compared and reviewed in several previous studies (*Hall*, 1968; *Nathan and McMahon*, 1990; *Arnold et al.*, 1995; *Chapman*, 1999; *Smakhtin*, 2001; *Schwartz*, 2007; *Eckhardt*, 2008). The reviews of *Hall* (1968), *Smakhtin* (2001) and *Schwartz* (2007) provide a history of methods for baseflow separation, and discuss

the problems related to the definition of baseflow, as well as the underlying assumptions of the different separation methods. In the context of identifying groundwater recharge from streamflow records, the underlying assumptions that underpin many methods were examined by *Halford and Mayer* (2000). They concluded that identifying the groundwater contribution from streamflow records can be ambiguous due to drainage exponentially decreasing from other sources, such as bank storage, wetlands and the unsaturated zone. Furthermore, they noted that simple automated methods are highly subjective with respect to their algorithmic structure, and affected by the same underlying assumptions as other more complex methods.

The analyses used in comparative studies to evaluate baseflow separation methods (e.g. *Nathan and McMahon*, 1990; *Arnold et al.*, 1995; *Mau and Winter*, 1997; *Chapman*, 1999; *Halford and Mayer*, 2000; *Schwartz*, 2007; *Eckhardt*, 2008) are often based on subjective measures, such as the plausibility of hydrological behaviour, rather than a quantitative comparison to a known and well-quantified baseflow hydrograph. This point was emphasised by *Mau and Winter* (1997) who highlighted the need to validate baseflow estimates to avoid issues related to subjective measures and other shortcomings of simplified methods. Unfortunately, to date, no measured baseflow hydrograph at the catchment scale is available. Until comprehensive data and better observation techniques come into existence, numerical models, although theoretical, provide the best independent conceptualisation of baseflow dynamics in catchments under different forcing functions and hydrological conditions.

Some studies (e.g. *Szilagyi*, 2004; *Fenicia et al.*, 2006; *Ferket et al.*, 2010) have compared baseflow estimated by separation methods with simulated baseflow from lumped and semi-distributed catchment models. However, a critical analysis of separation methods is inhibited by the lack of a reliable estimate of baseflow, as well as some simplifications in the lumped and semi-distributed models, such as the aquifer storage-discharge relationship (linear reservoir in *Fenicia et al.* (2006), the sum of multiple linear reservoirs in *Szilagyi* (2004), and the Boussinesq-equation in *Ferket et al.* (2010)).

More recently, physically based separation methods have been developed based on process-based formulations of fluid mass balance equations of an aquifer (e.g. *Furey and Gupta*, 2001; *Furey and Gupta*, 2003; *Huyck et al.*, 2005). They constitute an important step in overcoming the subjective elements of earlier simpler methods, and attempt to alleviate some of their simplifying assumptions. As well as the development of two physically based baseflow separation methods, *Furey and Gupta* (2003) evaluated their methods against a complex physically based numerical model of a hill-slope. Their study appears to be the first to critically compare baseflow separation methods with a physically based numerical model. However, by considering only the discharge from a single 2D synthetic hill-slope (rather than a catchment), *Furey and Gupta* (2003) neglected important catchment-scale processes, such as channel routing (e.g. streamflow attenuation and translation) and channel losses (through losing sections, abstraction and evaporation).

Fully integrated surface and subsurface flow models, some examples of which are HydroGeoSphere (HGS) (*Therrien et al.*, 2009), MODHMS (*Hydrogeologic Inc.*, 2006) and Parflow (*Kollet and Maxwell*, 2006), are useful for evaluating simpler models because they do not need to assume a functional relationship between baseflow and streamflow, or simple empirical relations. These models typically represent 3D variably saturated subsurface flow with Richard's equation, and 1D and 2D surface flow with the diffusion wave approximation to the St. Venant equations. A unique feature of fully integrated models is that water that is derived from rainfall is allowed to partition into overland flow, streamflow, evaporation, infiltration and recharge, whilst subsurface discharge to surface water features, such as lakes and streams, occurs in a physically based fashion (*Therrien et al.*, 2009). Therefore, physically based numerical models provide an excellent means for comparison of baseflow separation methods if the modelled baseflow component of streamflow can be extracted.

Using physically based numerical models of 3D systems to evaluate baseflow separation methods is difficult because the baseflow component of streamflow is not a standard output. For a 2D hill-slope model, the baseflow component of outflow is simply groundwater discharge. However, in the extension beyond 2D

hill-slopes, the baseflow component of simulated streamflow must be calculated in some other way. As highlighted by *Partington et al.* (2011), the available integrated models do not explicitly report the groundwater contribution to streamflow. This problem is of particular importance for catchments where the flow regime between surface water and groundwater is changing (e.g. gaining to losing sections of a stream and vice versa). To overcome these difficulties, *Partington et al.* (2011) developed a hydraulic mixing-cell (HMC) approach that allows extraction of the groundwater contribution to streamflow within integrated surface and subsurface flow models. Combining the HMC approach with the HydroGeoSphere model, they demonstrated that spatiotemporal fluxes into and out of a stream can be translated to a point along the stream allowing for meaningful hydrograph separation. The HMC method allows for theoretical examination of baseflow dynamics within a 3D catchment model, thus providing a platform for comparison to automated baseflow separation methods.

In the current study, the HMC method is used in conjunction with HGS in order to compare the outputs from a series of commonly used automated baseflow separation methods. A numerical control experiment is developed using the integrated model to simulate hydrological processes within a synthetic catchment. Multiple simulations are carried out using differing initial, hydrologic and forcing conditions in order to generate a series of outflow and baseflow hydrographs. Baseflow separation methods are then applied to the outflow hydrographs from the simulations. This allows comparison of the baseflow obtained from the separation methods to the simulated baseflow. The commonly used separation methods are based on graphical, conceptual and digital filter methods. The analysis is limited to automated methods that are readily available and that only rely on streamflow discharge data and catchment area. This analysis does not include an assessment of more complex physically based methods. However, it is noteworthy that this approach could also be used to test physically based methods, e.g. those developed by *Furey and Gupta* (2001).

3.2. Methodology

The HydroGeoSphere (HGS) model used here is a fully integrated, physically based model that simultaneously simulates 3D variably saturated subsurface flow

and 2D surface flow (*Therrien et al.*, 2009). Water is exchanged between the surface and subsurface domains through a first-order leakage relation based on the head difference between the domains. The model also accounts for evapotranspiration as a function of the leaf area index, soil moisture and root depth. For further details on the numerical formulation and a review of the code, the reader is referred to *Park et al.* (2009), *Therrien et al.* (2009) and *Brunner and Simmons* (2011).

3.2.1. The synthetic catchment

The geometry of the catchment is loosely based on the tilted V-catchment employed by *Panday and Huyakorn* (2004). As in *Panday and Huyakorn* (2004), the catchment is symmetrical and therefore only half of the catchment is modelled (shown in Figure 3.1). This particular geometry is an ideal synthetic framework for generating hydrographs, because a range of hydrological processes control the catchment's behaviour. These processes include 3D saturated/unsaturated groundwater flow, infiltration/exfiltration, overland flow and streamflow. An analysis of the *Panday and Huyakorn* (2004) synthetic catchment highlighting some of the issues associated with their model setup was undertaken by *Gaukroger and Werner* (2011), and in response to these, several modifications to the original setup are adopted here. The steep slopes and initially horizontal water table in the *Panday and Huyakorn* (2004) case cause all groundwater discharge to be concentrated around the outlet. Reducing the slope of the catchment (particularly along the stream) creates a greater spatial distribution of the surface-subsurface exchanges throughout the catchment. Therefore, the slopes perpendicular and parallel to the stream are decreased from 0.05 m/m and 0.02 m/m to 0.002 m/m and 0.0005 m/m, respectively. Furthermore, the horizontal water table represents an unrealistic (overly dry) initial condition. To start the model from more realistic initial conditions, the catchment is saturated and allowed to drain for between 7 and 9 months without any precipitation events. The original roughness coefficients used for the hill-slope and stream domains cause overland flow to be dominant parallel and adjacent to the stream, rather than in the stream (*Gaukroger and Werner*, 2011). In order to allow overland flow to discharge into the stream as it reaches the banks (rather than flowing alongside the

stream), the same roughness (0.015 $s/m^{1/3}$) is used in both the overland flow and stream domains. Also, the plane adjacent to the stream is raised by 0.6 m over a 5 m length to promote direct discharge of groundwater to the stream as opposed to upslope exfiltration or return flow. Finally, the areal extent of the catchment is increased from 810,000 m^2 to 3,220,000 m^2 by doubling the original length and width of the catchment (keeping the stream width at 10 m). This reduces boundary effects and increases aquifer storage capacity, which promotes sustained baseflow contributions to the stream. Given the modifications outlined above, a wide range of hydrographs can be generated by changing the forcing functions (e.g. rainfall, groundwater pumping and evapotranspiration).

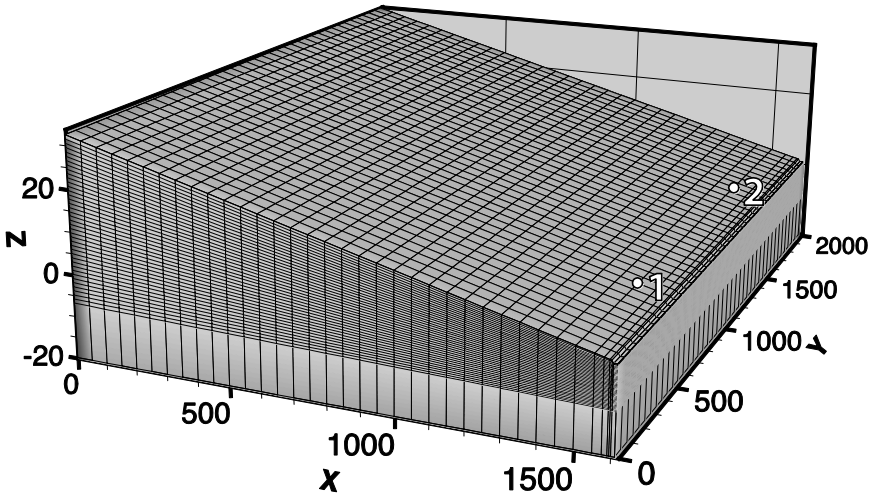

Figure 3.1: Modified tilted V-catchment used for simulation of the synthetic catchment's rainfall response. Points 1 and 2 denote locations of groundwater pumps. Note that due to the symmetry of the catchment, only half of it is shown.

The bottom elevation of the model domain is set at -20 m relative to the 0 m elevation of the streambed at the outlet. The aquifer properties are homogeneous and isotropic. In separate model scenarios, two different sets of properties of the aquifer material are considered (Table 3.1). Properties for evaporation and transpiration are also included in Table 3.1.

The spatial discretisation in the catchment model is as follows: grid spacing along the x axis is 50 m from x = 0 - 1550 m, 25 m from x = 1550 - 1575 m, 15 m from x = 1575 - 1590 m, 5 m from x = 1590 - 1600 m and 10 m from x = 1600 - 1610 m. The grid spacing along the y axis is 50 m. The vertical grid discretisation

Table 3.1: Surface and subsurface parameters for the synthetic catchment model. For a detailed description of these model parameters see *Therrien et al.* (2009).

increases in thickness according to the slopes perpendicular and parallel to the stream. Vertical discretisation along the z axis ranges from 0.25 m to 1 m for the first 10 m below the surface. The time steps used in the model vary in accordance with an adaptive time-stepping approach with a maximum step of 1000 seconds. A no flow boundary is applied at the bottom and sides of the model domain. A critical depth boundary is used at (x, y, z) = (1600 m, 0 m, 0 m) and (1610 m, 0 m, 0 m) to control the outflow at the stream outlet.

3.2.2. Baseflow calculation using the HMC method

The tracking of the streamflow generation mechanisms within a model simulation requires the tracking of the spatiotemporal fluxes into, out of, and along the stream. Parcels of groundwater discharging directly to the stream are "tracked" using the HMC method (*Partington et al.*, 2011) to allow determination of when (and if) groundwater contributes to streamflow, as measured at the outlet (or at any other location along the stream). The HMC method accounts for the travel time along the stream and the spatiotemporal variation in the surface-subsurface exchange fluxes, thereby separating the simulated streamflow hydrograph into baseflow, overland flow and direct rainfall to the stream. A version of HGS that has the HMC method incorporated into it is used to simulate the outlet hydrograph of the synthetic catchment in response to a series of rainfall events, and considering groundwater pumping and evapotranspiration. The calculated HMC baseflow is used as the control experiment with which baseflow separations of the simulated hydrograph are compared.

3.2.3. Baseflow separation using automated methods

The automated methods for baseflow separation used in this study are implemented using the programs HYSEP (*Sloto and Crouse*, 1996), PART (*Rutledge*, 1998) and BFLOW (*Arnold and Allen*, 1999). The Eckhardt filter (*Eckhardt*, 2005) is also used. All of these approaches are well established methods, are readily available, and were previously compared in the study of *Eckhardt* (2008). However, they were judged subjectively based on hydrological plausibility. Detailed descriptions of all approaches can be found in the above

cited literature, hence only a very brief overview of these methods is provided below.

The HYSEP program allows the use of three curve fitting methods of hydrograph separation; sliding interval (HYSEP1), fixed interval (HYSEP2) and local minimum (HYSEP 3), as detailed in *Pettyjohn and Henning* (1979). For these three methods, an empirical relationship is used, which relates the catchment area to the number of days until baseflow makes up all streamflow, after a streamflow peak.

PART uses a form of streamflow partitioning based on antecedent streamflow recession (similar to the local minimum method of HYSEP), details of which are given in *Rutledge* (1998). The determination of the antecedent recession requirement in PART is done in three ways (see *Rutledge*, 1998) and thereby provides three baseflow estimates: PART1, PART2 and PART3.

The BFLOW program uses the *Lyne and Hollick* (1979) filter, which is a low-pass filter. This separation method uses signal processing theory, and is based on the hydrological reasoning that baseflow is the low frequency component of streamflow. The filter equation for baseflow is expressed as (*Eckhardt*, 2005):

$$b_t = \alpha b_{t-1} + \frac{1-\alpha}{2}(Q_t + Q_{t-1}) \text{ subject to } b_t \leq Q_t \qquad \textbf{(3.1)}$$

Where b_t [L^3/T] is the baseflow at time step t [T], α [dimensionless] is the filter parameter and Q_t [L^3/T] is the streamflow at time step t. It is worth noting the constraint $b_t \leq Q_t$, which is required in applying (1) to avoid predictions of baseflow greater than streamflow (*Chapman*, 1991; *Eckhardt*, 2005). This constraint is discussed further in Section 3.4.3. The BFLOW program carries out three passes of the filter: forwards (BFLOW1), backwards (BFLOW2) and forwards again (BFLOW3) and uses a filter parameter $\alpha = 0.925$ as suggested by *Nathan and McMahon* (1990). Each pass of the filter acts to attenuate the baseflow signal. Despite having no physical basis, the baseflow separation of BFLOW has been found to agree well with manual separation techniques (*Arnold and Allen*, 1999).

The Eckhardt filter is a two-parameter filter based on the assumption that aquifer outflow is linearly proportional to storage. This filter limits the maximum ratio of baseflow to streamflow. *Eckhardt* (2005) describes this as potentially beneficial following the demonstration of *Spongberg* (2000) that runoff has a non-negligible low-frequency component. The equation for this filter is given by (*Eckhardt*, 2005):

$$b_t = \frac{(1-BFI_{\max})ab_{t-1} + (1-a)BFI_{\max}Q_t}{1-aBFI_{\max}} \text{ subject to } b_t \le Q_t \qquad \textbf{(3.2)}$$

Where a [dimensionless] is the baseflow recession constant and $BFI_{\max}$ [dimensionless] is the maximum value of the baseflow index.

As the $BFI_{\max}$ cannot be identified prior to separation, *Eckhardt* (2005) suggests using a value of 0.80 for perennial streams with porous aquifers, 0.50 for ephemeral streams with porous aquifers, and 0.25 for perennial streams with hard rock aquifers. The use of $BFI_{\max} = 0.50$ yields an equivalent filter to that proposed by *Chapman* (1991). In the formulation of *Chapman* (1991), a filter is developed to overcome baseflow being constant in the absence of direct runoff (similar to the *Lyne and Hollick* (1979) filter; *Nathan and McMahon* (1990)). This gives the filter parameter physical meaning in the form of the baseflow recession constant *a*. The recession constant for the *Eckhardt* (2005) filter is determined using the method outlined in *Eckhardt* (2008). This method involves plotting the flow Q_t against Q_{t-1} for periods where streamflow is decreasing for five consecutive days. A linear regression that passes through the origin is then calculated for these data points. The slope of this regression gives the recession constant *a*.

All streamflow data generated from the numerical model are translated to daily time-steps before being processed by HYSEP, PART, BFLOW and the Eckhardt filter. This translation is done in order to be compatible with the automated methods. The translation is carried out by calculating the average flow for each day. The influence of this constraint is discussed in Section 3.5.

3.3. Model Simulations

To provide varied catchment responses and streamflow regimes, the synthetic catchment is subjected to varied rainfall and antecedent moisture conditions. These different conditions are used to examine the extent to which the HYSEP, BFLOW, PART and the Eckhardt separation methods reproduce and capture the HMC calculated baseflow signal. Two of the simulations are also subject to near-stream groundwater pumping. The simulations with groundwater pumping allow investigation into the common scenario of a modified catchment. Although some separation methods are specified for use in undisturbed catchments, they are still applied in this study to simulations with pumping. However, for this reason, the simulations with pumping are considered separately from the simulations without pumping. The baseflow separation methods are evaluated quantitatively and qualitatively against the simulated baseflow using measures that account for total baseflow volume, as well as baseflow dynamics.

Initially, eight model scenarios are simulated (Table 3.2). The first three scenarios (1, 2 and 3) consider the influence of pumping for the sandy catchment. Scenarios 4 and 5 consider different initial conditions as the starting points for scenarios 4 and 5, respectively. Scenarios 6, 7 and 8 consider a change in soil properties of the sand to loamy sand. As well as providing the controlled baseflow signal for evaluation of baseflow separation methods, the variation of aquifer properties provides insight into their influence on streamflow generation mechanisms.

Table 3.2: Scenarios for simulating catchment response. Scenarios with an asterisk denote scenarios where groundwater pumping is applied in the catchment.

Scenario	Soil	Initial Water table	Pumping
1	Sand	WT3	-
2*	Sand	WT3	pump 1
3*	Sand	WT3	pump 1and 2
4	Sand	WT2	-
5	Sand	WT1	-
6	Loamy sand	WT3	-
7	Loamy sand	WT2	-
8	Loamy sand	WT1	-

The initial hydraulic heads and water table elevations are obtained by draining the fully saturated catchment for a period of 7, 8 and 9 months without applying any rainfall forcing or subsurface boundary recharge. The initial conditions used are: water table 1 (WT1) = 7 months drainage, water table 2 (WT2) = 8 months drainage and water table 3 (WT3) = 9 months drainage. For each of these initial conditions the stream is still flowing at the end of the drainage period, whilst providing significantly different initial conditions.

The catchment's response is controlled by modifying the forcing functions (e.g. rainfall, pumping and ET) to scenarios with a series of different initial conditions. The rainfall varies in intensity and duration over three rain events throughout each of the simulations. The same rainfall boundary is applied in each of the eight scenarios as follows:

1) 10 days without rainfall, then rainfall at a rate of 2 mm/h for 24 h followed by 10 days without rainfall; and

2) rainfall at a rate of 4 mm/h for 48 h followed by 5 days without rainfall; and

3) rainfall at a rate of 40 mm/h for 3 h followed by 30 days without rainfall (58 days and 3 h total)

The idealised rainfall events are uniform and constant with sufficiently large recovery periods such that the streamflow generation processes resulting from individual events can be clearly identified. The rainfall rates and durations are chosen to represent a range of streamflow generation mechanisms.

Pumping is applied in scenarios 2 and 3 at two locations (shown in Figure 3.1): Pump 1 located at (x, y, z) = (1550 m, 500 m, 0 m), and pump 2 located at (x, y, z) = (1550 m, 1500 m, 0 m). The pumping rate is increased linearly from 0.00 to 0.01 m^3/s for pump 1 over the first day of simulation in scenario 2, with pump 2 inactive. In scenario 3, the pumping rate is increased linearly from 0.00 to 0.015 m^3/s for both pumps 1 and 2 over the first day of simulation. For scenarios 2 and 3, pumping is applied over the entire simulation. This pumping rate induces losing conditions locally along the stream near the pumping location. Pumping therefore

allows the effect of varied flow regimes (i.e. gaining and losing sections) on streamflow generation to be explored with respect to baseflow.

Based on the initial simulations, evapotranspiration (ET) is applied to 5 additional scenarios (denoted as 9, 10, 11, 12 and 13; not listed in Table 3.2). The setup and forcing functions of scenarios 9, 10, 11, 12 are the same as for scenario 1, except that constant specified evaporation rates of 2, 5, 10 and 26 mm/day are applied, respectively. Some high evaporation rates (10 and 26 mm/day) are chosen to explore the influence that high ET in the catchment has on the baseflow separation methods. ET is also applied to scenario 13 with the same setup and forcing functions as for scenario 6, but with a constant specified evaporation rate of 5 mm/day. The simulations with ET are performed in order to examine the influence of ET on baseflow dynamics, baseflow recession and performance of separation methods against the simulated baseflow.

3.4. Results

3.4.1. Fully integrated model simulations

The simulated streamflow hydrograph at the outlet and the corresponding streamflow generation components (calculated from the HMC method) are shown for scenarios 1 (Figure 3.2) and 2 (Figure 3.3). The streamflow generation mechanisms varied in response to different rainfall events. In all scenarios that were based on sandy material properties, streamflow was dominated by baseflow because the high infiltration capacity of the sand allowed for quick recharge. Consequently, there was only a small overland flow component due to saturation excess runoff. The almost horizontal slope of the catchment limited the vertical extent of the unsaturated zone to less than 1 m, resulting in a short delay between infiltration and recharge. As the timing between infiltration and recharge was short, there was a rapid response in the baseflow component of streamflow. As illustrated in Figure 3.2, after a short and rapid initial increase, baseflow did not change significantly during the first two rainfall events and reached an apparent steady-state. As opposed to baseflow, streamflow changed during this apparent steady-state. Therefore, the ratio of streamflow to baseflow changes as a function of time, but not consistently across events.

The apparent steady-state baseflow was only observed during the first two events. However, in the third event no apparent steady-state was reached. In this event, an initial rapid increase in head in the subsurface quickly increased the hydraulic gradient from the aquifer to the stream. During this rainfall event, the time delay from rainfall starting to the onset of overland flow is much slower than the time delay to the increase in groundwater discharge caused by the rapid aquifer response. After 1 hour, the overland flow and accumulating direct rainfall to the stream increased the stream stage, thus reducing the hydraulic gradient between the aquifer and stream. This is a clear demonstration of the forcing functions controlling the baseflow dynamics.

The baseflow response from all three rainfall events did not follow the typical pattern of baseflow response as presented in standard textbooks, e.g. *McCuen* (2005) and *Linsley et al.* (1958). This is an important observation because these patterns are the basis for graphical approaches of baseflow separation. The pattern of baseflow during rainfall events obtained from the HGS model demonstrated a fast and transient response in stream-aquifer interaction. This was apparent at the beginning and cessation of the rainfall events, where an abrupt change in baseflow occurs, rather than a smooth and delayed response. The high transience of the stream aquifer interaction was also apparent in scenarios 2 and 3. The drawdown around the pump induced a loss in the adjacent stream, creating a variable flow regime with dynamic losing and gaining sections. The drawdown also increased the time between infiltration and recharge, further affecting the system dynamics.

The effect of ET (at a rate of 5 mm/day) is shown in Figure 3.4 for the example of scenario 10. In comparison to scenario 1, the inclusion of ET in scenarios 9, 10, 11 and 12 slightly reduced event peaks and the baseflow component. These changes are due to the reduction in storage through losses from ET. However, it can be seen by comparison of Figure 3.2 and Figure 3.4, that the baseflow dynamics were very similar; the reduced overland flow component lead to a slightly higher proportion of baseflow with respect to streamflow.

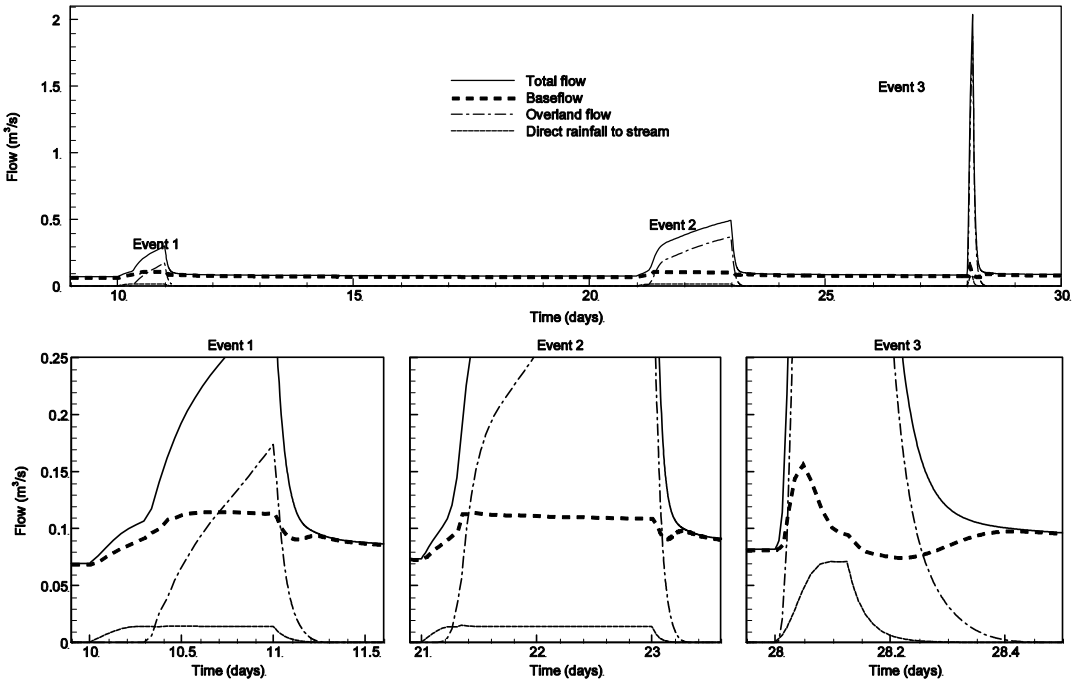

Figure 3.2: Streamflow hydrograph at the outlet and HMC flow components for scenario 1 (without pumping), with highlighted events. An apparent steady-state baseflow rate was observed in the first event (10.5-11 days) and second event (21.4-23 days).

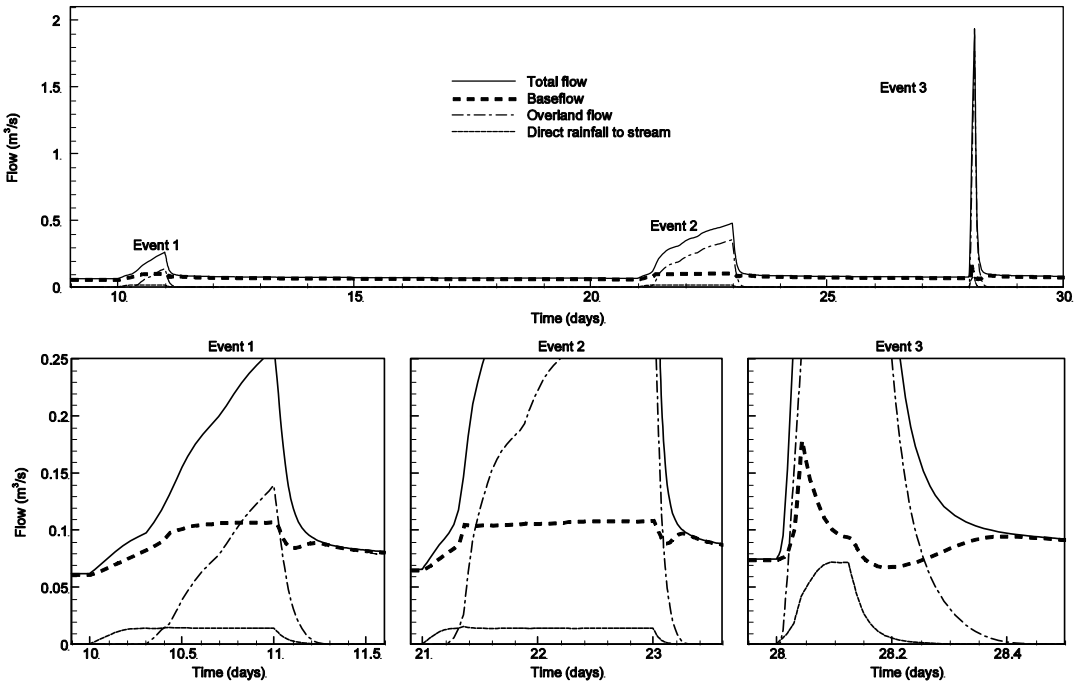

Figure 3.3: Streamflow hydrograph at the outlet and HMC flow components for scenario 2 (with pumping), with highlighted events. An apparent steady-state baseflow rate was observed in the first two rainfall events.

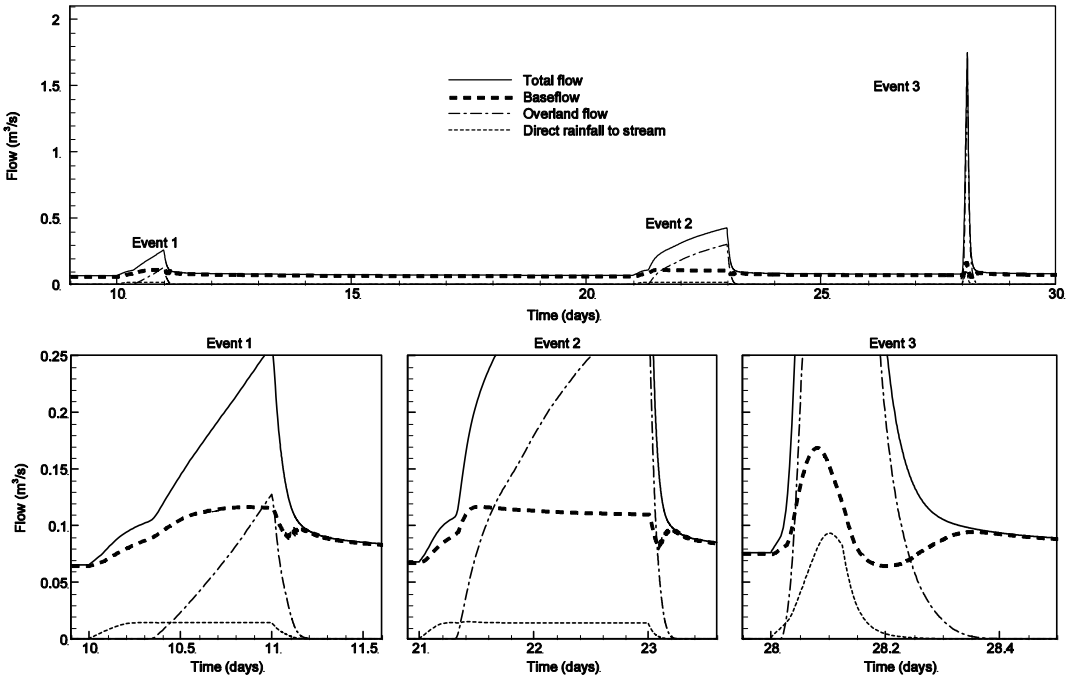

Figure 3.4: Streamflow hydrograph at the outlet and HMC flow components for modified scenario 1 (with 5mm/day ET), with highlighted events. An apparent steady-state baseflow rate was still observed in the first event (10.5-11 days) and second event (21.4-23 days).

3.4.2. Recession analysis

Following the approach of *Eckhardt* (2008), the recession periods were identified as periods in which streamflow was decreasing for 5 consecutive days. These periods were used to calculate the recession constant a (as defined in section 3.2.3). The slope for each linear regression of Q_{t+1} vs. Q_t passing through the origin was used as the recession constant a, which was then applied using the Eckhardt separation method. Figure 3.5 shows the resulting recession constant a, and R^2 value obtained from the linear regression for each scenario. It can be seen in Figure 3.5 that the R^2 for each regression was very close to 1. For all scenarios, this high R^2 value supports the assumption of a linear reservoir during recession periods, which is inherent in the Eckhardt method.

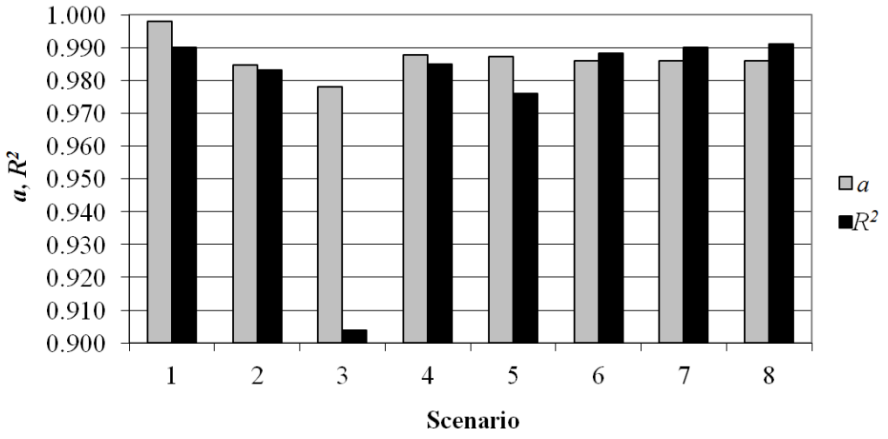

Figure 3.5: Values of recession constant a and R^2 value for the linear regression of Q_t vs Q_{t+1}, for sand and initial conditions WT1, WT2, WT3 and without/with pumps 1 and 2 active. The high value of R^2 suggests a linear storage-discharge relationship at the outlet during recession periods.

Adding ET in scenarios 9 to 13 reduced slightly the recession constant a, by less than 2% and it also slightly reduced the linearity of the storage-discharge relationship ($R^2 > 0.96$) of the catchment during recession periods. The linearity assumption for the storage-discharge relationship for this synthetic catchment was therefore still deemed reasonable.

3.4.3. Comparison of baseflow separation methods

All of the automated separation methods used are subject to the condition that baseflow cannot exceed streamflow. This is imposed because without this constraint, all of these methods can yield baseflow estimates above streamflow. By contrast, *Furey and Gupta* (2001) suggested that such a condition should not be imposed on physically-based methods. This way it is possible to identify time periods where estimated baseflow exceeds streamflow and diagnose these estimation errors. Steps can then be taken to modify the method while honouring physical processes so that these errors are reduced or fully removed. This constraint has repercussions for our analysis. In recession periods, the baseflow calculated from the automated separation methods is perfectly matched to the HMC calculated baseflow, because streamflow is entirely composed of baseflow. Therefore, an assessment of the differences between the simulated and approximated baseflow hydrographs is only meaningful during rainfall events. Consequently, this comparison is carried out during the rainfall events (i.e. 10-13

days, 21-25 days and 28-30 days) with the commonly used ratio of baseflow to streamflow, and two statistical measures, as follows:

a) the baseflow index (*BFI*), which is the ratio of the total baseflow volume to the total streamflow volume over a given period:

$$BFI = \frac{V_{baseflow}}{V_{streamflow}} \tag{3.3}$$

Where $V_{baseflow}$ [L^3] and $V_{streamflow}$ [L^3] are the total volume of baseflow and streamflow, respectively, over the simulation period.

b) the Nash-Sutcliffe model efficiency (*NSE*) coefficient:

$$NSE = 1 - \frac{\sum_{t=1}^{T}(b_o^t - b_m^t)^2}{\sum_{t=1}^{T}(b_o^t - \bar{b}_o)^2} \tag{3.4}$$

Where b_o^t [L^3/T] is the HMC calculated baseflow at time step t [T], b_m^t [L^3/T] is the baseflow from automated separation at time step t [T], and $\bar{b}_o$ [L^3/T] is the mean HMC calculated baseflow. The *NSE* provides a measure with values ranging from -∞ to 1 (where 1 indicates a perfect match), of how well the separation methods compare to the HMC calculated baseflow. *Moriasi et al*. (2007) suggest that a $NSE > 0.5$ is satisfactory.

And c) the percent bias (*PBIAS*) (*Gupta et al*., 1999):

$$PBIAS = \frac{\sum_{t=1}^{T}(b_o^t - b_m^t) \times 100}{\sum_{t=1}^{T}(b_o^t)} \tag{3.5}$$

The *PBIAS* provides a measure of over or underestimation for each event, with an optimal value of 0%. Positive values of *PBIAS* indicate an underestimation, whereas negative values indicate overestimation of baseflow. *Moriasi et al.* (2007) suggest that a *PBIAS* of up to ±25% for streamflow is satisfactory, and this is used to guide acceptable *PBIAS* results in this study.

The baseflow index (*BFI*), Nash-Sutcliffe efficiency (*NSE*) and percent bias (*PBIAS*) are given for each of the three rainfall events in Table 3.3,Table 3.4, and Table 3.5, respectively, for scenarios 1-8. The values for $NSE < 0.5$ and $|PBIAS| > 25\%$ are highlighted. The *BFI*s calculated across the entire simulation for each scenario are ranked for each separation method in Figure 3.6. Ranking is in order of best to worst *BFI* relative to the *BFI* observed from the HGS model (based on the HMC calculated baseflow). The results for the testing of the inclusion of ET for scenario 1 are shown in Table 3.6.

For event 1, the *NSE*s were satisfactory over all scenarios for HYSEP2, PART1, PART2, PART3, BFLOW1, BFLOW2 and the Eckhardt separation methods. However, in scenario 3, HYSEP1, HYSEP3 and BFLOW3 had a *NSE* less than 0.5, with BFLOW3 showing a very unsatisfactory performance indicated by a negative *NSE*. The BFLOW1 separation had a single instance of *NSE* less than 0.5 and the Eckhardt separation had two instances of *NSE* less than 0.5. However, these were only slightly below this value, indicating that the performance of these methods was almost satisfactory. The *PBIAS* was at a maximum of 33.8% for event 1 of scenario 3 for the BFLOW3 separation method, showing a large underestimation of the HMC calculated baseflow. All separation methods for event 1 tended to underestimate baseflow. Only BFLOW1 overestimated baseflow, which occurred for the sandy loam in scenarios 6-8.

For event 2, the *NSE*s were below 0.5 for each separation method in at least one of the eight scenarios. The BFLOW3 separation showed very poor performance with negative *NSE*s in scenarios 2-5. In each of these scenarios, BFLOW3 had a *PBIAS* showing underestimation of baseflow by more than 25%. The HYSEP1, HYSEP2, BFLOW1 and Eckhardt methods showed poor performance for sandy loam (scenarios 6-8) with negative *NSE*s in each scenario. The *PBIAS* for HYSEP1 and BFLOW1 separation showed overestimation of baseflow ranging from 40%-73% in the sandy loam scenarios. It is interesting to note that the scenarios in which HYSEP1, HYSEP2 and BFLOW1 performed well, HYSEP3, PART1, PART2, PART3, BFLOW2 and BFLOW3 performed poorly and vice versa.

Table 3.3: *BFI*, *NSE* and *PBIAS* for simulated baseflow and estimated baseflow during event 1 using HYSEP, PART, BFLOW and the Eckhardt separation methods. Lightly shaded cells highlight a *NSE* < 0.5 and darkly shaded cells highlight $|PBIAS| > 25\%$. Scenarios with an asterisk denote where groundwater pumping is applied in the catchment.

Scenario		Simulated	HYSEP1	HYSEP2	HYSEP3	PART1	PART2	PART3	BFLOW1	BFLOW2	BFLOW3	ECKHARDT
1	BFI	0.789	0.659	0.691	0.643	0.772	0.694	0.673	0.692	0.675	0.640	0.630
	NSE		0.607	0.698	0.591	0.872	0.742	0.692	0.751	0.722	0.577	0.567
	PBIAS		16.47%	12.40%	18.48%	2.12%	11.96%	14.66%	12.20%	14.36%	18.90%	20.15%
2*	BFI	0.815	0.666	0.706	0.646	0.798	0.711	0.683	0.693	0.679	0.623	0.653
	NSE		0.547	0.677	0.519	0.878	0.724	0.655	0.693	0.660	0.423	0.584
	PBIAS		18.30%	13.35%	20.68%	2.00%	12.74%	16.15%	14.93%	16.71%	23.52%	19.89%
3*	BFI	0.832	0.651	0.705	0.627	0.811	0.713	0.674	0.676	0.659	0.551	0.667
	NSE		0.426	0.635	0.372	0.890	0.686	0.574	0.591	0.537	-0.014	0.604
	PBIAS		21.73%	15.25%	24.62%	2.54%	14.25%	19.01%	18.73%	20.73%	33.81%	19.84%
4	BFI	0.878	0.717	0.763	0.699	0.850	0.770	0.737	0.735	0.731	0.694	0.675
	NSE		0.561	0.701	0.538	0.899	0.748	0.669	0.668	0.660	0.513	0.461
	PBIAS		18.34%	13.07%	20.32%	3.17%	12.23%	16.06%	16.26%	16.75%	21.00%	23.14%
5	BFI	0.929	0.753	0.803	0.735	0.902	0.814	0.772	0.762	0.762	0.727	0.703
	NSE		0.546	0.735	0.526	0.947	0.761	0.660	0.629	0.629	0.491	0.414
	PBIAS		18.87%	13.54%	20.82%	2.86%	12.40%	16.83%	17.91%	17.91%	21.71%	24.32%
6	BFI	0.286	0.255	0.265	0.250	0.267	0.267	0.260	0.333	0.270	0.250	0.286
	NSE		0.817	0.871	0.804	0.903	0.903	0.873	0.335	0.963	0.802	0.984
	PBIAS		10.86%	7.13%	12.63%	6.76%	6.76%	9.21%	-16.42%	5.42%	12.70%	-0.09%
7	BFI	0.310	0.272	0.283	0.266	0.285	0.285	0.277	0.348	0.288	0.266	0.302
	NSE		0.765	0.829	0.753	0.864	0.864	0.829	0.561	0.933	0.752	0.977
	PBIAS		12.35%	8.60%	14.14%	8.23%	8.23%	10.70%	-12.25%	7.11%	14.16%	2.60%
8	BFI	0.341	0.295	0.308	0.289	0.310	0.310	0.301	0.369	0.312	0.289	0.324
	NSE		0.732	0.803	0.720	0.839	0.839	0.800	0.721	0.906	0.716	0.955
	PBIAS		13.32%	9.53%	15.08%	9.11%	9.11%	11.64%	-8.37%	8.47%	15.23%	4.90%

Table 3.4: *BFI*, *NSE* and *PBIAS* for simulated baseflow and estimated baseflow during event 2 using HYSEP, PART, BFLOW and the Eckhardt separation methods. Lightly shaded cells highlight a *NSE* < 0.5 and darkly shaded cells highlight $|PBIAS| > 25\%$. Scenarios with an asterisk denote where groundwater pumping is applied in the catchment.

Scenario		Simulated	HYSEP1	HYSEP2	HYSEP3	PART1	PART2	PART3	BFLOW1	BFLOW2	BFLOW3	ECKHARDT
1	BFI	0.486	0.531	0.453	0.394	0.415	0.415	0.404	0.470	0.418	0.379	0.409
	NSE		0.741	0.707	0.337	0.501	0.501	0.422	0.693	0.616	0.177	0.504
	PBIAS		-9.45%	6.64%	18.83%	14.51%	14.51%	16.82%	3.09%	13.93%	21.93%	15.85%
2*	BFI	0.499	0.549	0.459	0.386	0.415	0.415	0.398	0.463	0.410	0.365	0.434
	NSE		0.702	0.696	0.140	0.399	0.399	0.268	0.677	0.461	-0.106	0.635
	PBIAS		-10.07%	8.03%	22.68%	16.75%	16.75%	20.12%	7.13%	17.71%	26.89%	12.94%
3*	BFI	0.527	0.588	0.474	0.373	0.419	0.419	0.393	0.452	0.400	0.336	0.474
	NSE		0.621	0.683	-0.186	0.244	0.244	0.035	0.532	0.202	-0.645	0.764
	PBIAS		-11.62%	9.97%	29.22%	20.52%	20.52%	25.36%	14.20%	23.97%	36.16%	9.98%
4	BFI	0.559	0.586	0.506	0.442	0.467	0.467	0.454	0.510	0.467	0.419	0.437
	NSE		0.877	0.692	0.222	0.402	0.402	0.314	0.622	0.488	-0.002	0.228
	PBIAS		-4.86%	9.38%	20.88%	16.33%	16.33%	18.80%	8.76%	16.37%	25.03%	21.77%
5	BFI	0.635	0.650	0.566	0.492	0.524	0.524	0.507	0.552	0.519	0.458	0.461
	NSE		0.907	0.687	0.137	0.342	0.342	0.246	0.508	0.397	-0.162	-0.077
	PBIAS		-2.40%	10.94%	22.54%	17.54%	17.54%	20.15%	13.14%	18.23%	27.84%	27.45%
6	BFI	0.163	0.282	0.197	0.148	0.155	0.155	0.152	0.248	0.170	0.144	0.200
	NSE		-12.697	-3.793	0.835	0.922	0.922	0.890	-7.843	0.916	0.767	-0.718
	PBIAS		-73.36%	-21.35%	8.99%	4.59%	4.59%	6.81%	-52.42%	-4.42%	11.23%	-23.21%
7	BFI	0.174	0.285	0.203	0.155	0.163	0.163	0.159	0.253	0.177	0.151	0.208
	NSE		-9.248	-2.599	0.763	0.868	0.868	0.826	-5.774	0.973	0.678	-0.315
	PBIAS		-64.03%	-17.11%	10.77%	6.27%	6.27%	8.56%	-45.59%	-2.02%	13.16%	-19.75%
8	BFI	0.186	0.289	0.211	0.163	0.171	0.171	0.167	0.259	0.186	0.158	0.217
	NSE		-6.686	-1.690	0.700	0.820	0.820	0.770	-4.173	0.994	0.605	-0.012
	PBIAS		-55.91%	-13.52%	12.14%	7.57%	7.57%	9.92%	-39.58%	-0.04%	14.60%	-16.77%

Table 3.5: *BFI*, *NSE* and *PBIAS* for simulated baseflow and estimated baseflow during event 3 using HYSEP, PART, BFLOW and the Eckhardt separation methods. Lightly shaded cells highlight a *NSE* < 0.5 and darkly shaded cells highlight $|PBIAS| > 25\%$. Scenarios with an asterisk denote where groundwater pumping is applied in the catchment.

Scenario		Simulated	HYSEP1	HYSEP2	HYSEP3	PART1	PART2	PART3	BFLOW1	BFLOW2	BFLOW3	ECKHARDT
1	BFI	0.567	0.530	0.537	0.530	0.548	0.537	0.533	0.559	0.519	0.492	0.557
	NSE		0.972	0.976	0.972	0.987	0.979	0.975	0.998	0.959	0.920	0.996
	PBIAS		6.46%	5.24%	6.46%	3.35%	5.25%	5.96%	1.37%	8.53%	13.24%	1.80%
2*	BFI	0.581	0.530	0.539	0.530	0.556	0.539	0.534	0.565	0.513	0.481	0.572
	NSE		0.949	0.957	0.949	0.977	0.962	0.954	0.990	0.925	0.863	0.997
	PBIAS		8.81%	7.27%	8.81%	4.42%	7.28%	8.24%	2.89%	11.70%	17.31%	1.69%
3*	BFI	0.596	0.527	0.539	0.527	0.561	0.539	0.531	0.567	0.492	0.446	0.592
	NSE		0.912	0.926	0.912	0.960	0.934	0.920	0.971	0.844	0.721	0.999
	PBIAS		11.68%	9.64%	11.68%	5.90%	9.68%	11.02%	5.02%	17.53%	25.24%	0.70%
4	BFI	0.620	0.577	0.584	0.577	0.596	0.584	0.580	0.605	0.562	0.524	0.571
	NSE		0.967	0.971	0.967	0.982	0.974	0.970	0.993	0.950	0.892	0.970
	PBIAS		6.87%	5.78%	6.87%	3.85%	5.79%	6.44%	2.40%	9.42%	15.51%	7.93%
5	BFI	0.684	0.636	0.644	0.636	0.657	0.644	0.639	0.663	0.612	0.562	0.583
	NSE		0.966	0.970	0.966	0.981	0.973	0.969	0.989	0.942	0.863	0.907
	PBIAS		6.98%	5.85%	6.98%	3.97%	5.86%	6.50%	2.99%	10.42%	17.72%	14.73%
6	BFI	0.257	0.251	0.254	0.251	0.258	0.254	0.252	0.283	0.247	0.236	0.275
	NSE		0.996	0.999	0.996	1.000	0.999	0.998	0.877	0.989	0.974	0.941
	PBIAS		2.32%	1.05%	2.32%	-0.51%	1.07%	1.71%	-10.46%	3.78%	7.82%	-7.39%
7	BFI	0.267	0.259	0.262	0.259	0.267	0.262	0.260	0.292	0.255	0.243	0.284
	NSE		0.994	0.997	0.994	1.000	0.998	0.996	0.904	0.987	0.967	0.954
	PBIAS		3.08%	1.76%	3.08%	0.12%	1.77%	2.43%	-9.27%	4.44%	8.82%	-6.49%
8	BFI	0.278	0.267	0.271	0.267	0.276	0.271	0.269	0.300	0.264	0.251	0.294
	NSE		0.991	0.995	0.991	0.999	0.996	0.994	0.925	0.984	0.960	0.964
	PBIAS		3.77%	2.41%	3.77%	0.65%	2.42%	3.10%	-8.16%	5.02%	9.65%	-5.70%

Table 3.6: Comparison of *BFI*, *NSE* and *PBIAS* for (scenario 1 with and without ET) simulated baseflow and estimated baseflow during event 2 using HYSEP, PART, BFLOW and the Eckhardt separation methods. Lightly shaded cells highlight a *NSE* < 0.5 and darkly shaded cells highlight | *PBIAS* | > 25%.

ET (mm/day)		Simulated	HYSEP1	HYSEP2	HYSEP3	PART1	PART2	PART3	BFLOW1	BFLOW2	BFLOW3	ECKHARDT
0	BFI	0.486	0.531	0.453	0.394	0.415	0.415	0.404	0.470	0.418	0.379	0.373
	N-S		0.741	0.707	0.337	0.501	0.501	0.422	0.693	0.616	0.177	0.130
	PBIAS		-9.45%	6.64%	18.83%	14.51%	14.51%	16.82%	3.09%	13.93%	21.93%	23.19%
2	BFI	0.513	0.539	0.465	0.408	0.428	0.428	0.417	0.482	0.429	0.393	0.436
	N-S		0.868	0.673	0.235	0.390	0.390	0.313	0.629	0.494	0.094	0.509
	PBIAS		-5.13%	9.40%	20.49%	16.48%	16.48%	18.67%	6.04%	16.28%	23.28%	14.94%
5	BFI	0.553	0.568	0.490	0.430	0.453	0.453	0.440	0.500	0.448	0.414	0.458
	N-S		0.896	0.642	0.144	0.305	0.305	0.224	0.560	0.366	-0.007	0.404
	PBIAS		-2.79%	11.24%	22.18%	18.07%	18.07%	20.31%	9.53%	18.85%	25.11%	17.19%
10	BFI	0.703	0.699	0.606	0.508	0.562	0.562	0.533	0.575	0.523	0.491	0.529
	N-S		0.817	0.722	-0.117	0.225	0.225	0.061	0.315	0.050	-0.253	0.133
	PBIAS		0.52%	13.74%	27.68%	20.02%	20.02%	24.19%	18.08%	25.54%	30.08%	24.67%
26	BFI	0.852	0.790	0.696	0.591	0.654	0.654	0.618	0.633	0.597	0.563	0.597
	N-S		0.705	0.602	-0.202	0.113	0.113	-0.054	0.035	-0.117	-0.387	-0.088
	PBIAS		7.34%	18.27%	30.60%	23.28%	23.28%	27.54%	25.75%	29.91%	33.97%	29.96%

More interestingly, where the HYSEP1, HYSEP2 and BFLOW1 methods performed poorly, these methods largely overestimated baseflow whereas where the HYSEP3, PART1, PART2, PART3, BFLOW2 and BFLOW3 methods performed poorly, these particular methods largely underestimated baseflow.

For event 3, the *NSE* was greater than 0.5 for every method in each scenario, with values close to 1. The largest *PBIAS* was for BFLOW3 in scenario 3, showing underestimation of baseflow by just over 25%.

The inclusion of ET in scenarios 9-13 showed that as the ET rate was increased, the *BFI* increased. ET also lead to a reduction in performance (both *NSE* and *PBIAS*) for every separation method, except HYSEP1.

The rankings of separation methods (shown in Figure 3.6) based on *BFI* over the entire simulation provide a summary of the performance of each of the separation methods. The best replication of *BFI* resulted from the HYSEP1 method in scenarios 1-5, from PART1 in scenario 6, and from HYSEP2 in scenarios 7-8. The BFLOW3 method was worst in scenarios 1-3 and 8. The Eckhardt method performed worst in scenarios 4 and 5.

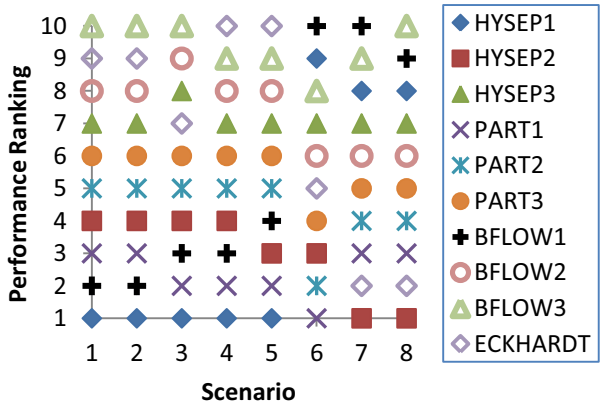

Figure 3.6: Performance based ranking using BFI over the whole simulation for HYSEP, PART, BFLOW and the Eckhardt separation methods. 1 indicates best performance, 10 indicates worst performance.

The baseflow separations from the streamflow hydrograph in scenario 1 obtained using HYSEP, PART, BFLOW and the Eckhardt separation methods are shown in Figure 3.7. Visual inspection of baseflow curves in Figure 3.7 shows that the ability of these separation methods to match the simulated baseflow was poor in

almost all cases, despite the fact that they had satisfactory *NSE* and *PBIAS* values. It is clear that despite reasonable estimates of the *BFI* for each scenario, the dynamics of baseflow during rainfall were missed.

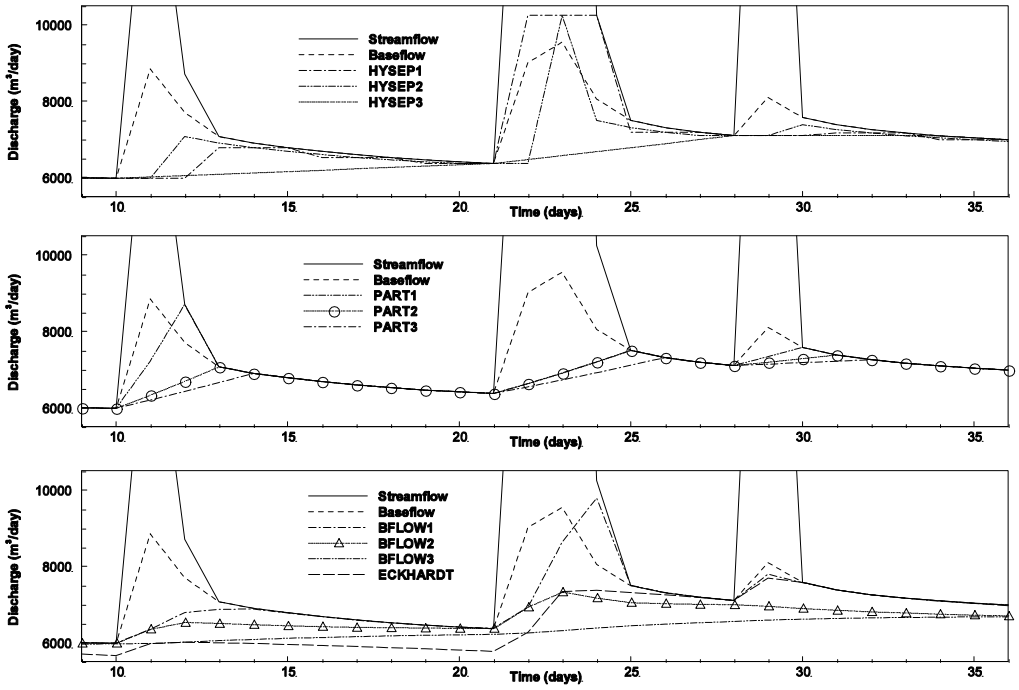

Figure 3.7: Comparison of simulated daily baseflow and baseflow estimated using HYSEP, PART, BFLOW and the Eckhardt separation methods for scenario 1.

3.5. Discussion

The baseflow hydrographs obtained using HGS (with the HMC method) were used as a control experiment to test the performance of a series of automated baseflow separation methods. The initial conditions (antecedent moisture), forcing functions (rainfall patterns, pumping and ET) as well as the physical properties (soil properties) of the catchment were varied across simulation scenarios. The varied conditions across the different model scenarios allowed the generation of unique baseflow behaviour, controlled by a range of hydrological processes. The application of the HMC method allowed quantification of the relative importance of hydrological processes to the streamflow hydrograph. While the structure and geology of the synthetic model used in this study were simple, the hydrological processes considered were simulated in a physically based way. Despite the simplified nature of the catchment, the baseflow separation methods consistently

failed to perform satisfactorily. This is easily attributed the variability of the baseflow dynamics as observed across all simulation scenarios. Increasing the complexity of the catchment (e.g. heterogeneous geology, more realistic topography and rainfall patterns), is likely to lead to an even more complex baseflow response. With increased complexity, it is expected that the variability seen in baseflow dynamics will remain and hence that the simple automated baseflow separation methods examined will not perform any better in estimating baseflow.

An initial analysis of the hydrographs revealed that the behaviour of baseflow was fundamentally different between rainfall events. For the first two events, baseflow remained constant and reached an apparent steady-state despite the changing forcing functions. In contrast, baseflow dynamics during the third event were highly transient. This illustrates that the controlling processes of baseflow are not always static, but instead change in response to different forcing functions. It also challenges the common assumption (based on hydrological reasoning) of the simple automated baseflow separation methods, that a simple fixed relation between baseflow and streamflow exists, for all rainfall events and antecedent moisture conditions. It is observed that this is not necessarily the case.

In the synthetic catchment used in this study, an apparent steady-state of baseflow discharge was reached for certain rain events. Once this apparent steady-state was reached, streamflow only increased with increasing overland flow. This led to a baseflow response that is dependent upon the rate and duration of rainfall. For all three events, the relationship between baseflow and streamflow was not consistent, as assumed by the BFLOW1, BFLOW2, BFLOW3 and Eckhardt separation methods. The variation of the ratio of baseflow to streamflow was observed in response to different rainfall events, as well as for the different initial antecedent moisture conditions. The variation observed in these simulations highlights an inability to accurately capture the average baseflow with the various baseflow separation methods examined. Moreover, it demonstrates the often acknowledged, but seldom addressed ambiguity of the separation methods used. The results from this numerical experiment suggest that quantifying baseflow in catchments with non-stationary processes, such as varied climatic conditions that

are outside of seasonality, will alter the streamflow generation mechanisms and hence the *BFI*.

The *NSE*s for rainfall events 1 and 3 for each of the scenarios indicated satisfactory results for the baseflow separations. The agreement between the simulated baseflow method and separation methods for event 3 was significantly better than for the other two events. For rainfall event 2, the *NSE*s showed a poor match between the automated separation methods and HMC calculated baseflow for different methods in each scenario, with both large overestimation and underestimation of the HMC calculated baseflow in some cases. This variability in each of the methods' ability to match the HMC calculated baseflow across scenarios and corresponding rainfall events highlights that no single separation method performed consistently well in the control experiment. The *BFI* based rankings of the separation methods show that, on average, PART1 and HYSEP2 performed best overall in capturing the baseflow volume across the eight scenarios.

One of the limitations found in the use of the automated separation methods was the constraint of using daily streamflow data. It can be seen from the results in Figure 3.2 and Figure 3.3 that the behaviour of the baseflow varied on at least an hourly time scale, much smaller than could be captured in a daily time step. However, this is only a limitation when it is essential to accurately capture baseflow behaviour at finer timescales (e.g. flood modelling). In the context of low flow hydrology, where estimates of annual baseflow contributions are required, the nuances seen in the baseflow behaviour during rainfall events is not important as long as the average baseflow is captured. However, it is possible that the nuances seen in the hourly time step of this catchment present themselves in a larger catchment at the daily time step, in which case use of these filters would be problematic and would fail to capture even the average behaviour.

The automated separation methods result in the largest difference during rainfall events in which recharge is also occurring. This means that any perennial streams that are subject to significant and extended rainfall periods will be the most difficult to accurately determine the *BFI* for. This is because the proportion of

time that streamflow is not driven purely by baseflow affects the relative magnitude of the potential baseflow error.

3.6. Conclusions

Whilst commonly used automated baseflow separation methods are known to be somewhat ambiguous and arbitrary, the potential errors have not been quantified previously using a 3D fully integrated physically based flow model. The numerical experiments in this study strongly suggested that baseflow dynamics are complex, even in a simple catchment. The complexity of baseflow dynamics was seen to affect the performance of the simple automated separation methods. The frequently used automated baseflow separation methods could not perform satisfactorily across all events and scenarios considered. This suggests that caution should be used when applying these methods, depending on the flow dynamics of the catchment being studied. Unfortunately, there are no clear indicators as to which separation methods are most and least appropriate under particular conditions, which is not surprising given the absence of a true physical basis in the simple methods examined. This is cause for concern because baseflow separation is an important tool influencing decisions and outcomes of the various applications it is used for, such as the analysis of event runoff; recharge estimation; low flow forecasting; hydrogeologic parameter estimation; hydrologic model calibration; and the identification of source areas; and dominant processes producing runoff (*Schwartz* (2007)). Large errors will undermine the many applications baseflow separation is used for.

Further work is required to understand the appropriate use of baseflow separation methods. More complex baseflow separation methods than those considered in this study should be tested in future studies. Physically based filters (e.g. *Furey and Gupta*, 2001, 2003; *Huyck et al.*, 2005) could prove to be more robust. This is because they provide a physically based relation of rainfall and ET (and other physical parameters) to baseflow. However, such methods clearly require more data (e.g. rainfall time series) which may not be readily available. It is perhaps the case that the uncertainty associated with simple automated methods precludes their use for providing anything more than very rough estimates of baseflow.

An improved understanding of baseflow dynamics is required for a broader range of catchments. With respect to baseflow dynamics, future studies should aim to elucidate: (a) scale dependence of baseflow generation to test if the baseflow response seen in the hourly time step of this small synthetic catchment occurs at the daily time step for larger catchments (e.g. > 20 km^2); (b) testing how the *BFI* varies as a result of non-stationary processes; (c) testing of the impact of variations in geology, topography and vegetation, by incrementally adding layers of complexity to similar models in order to try and understand baseflow dynamics. Further investigation within numerical models should play a role in establishing physically based recommendations as to the appropriateness of commonly used automated baseflow separation methods in different catchment types and settings. Given the reality of the physical interpretations and subsequent calculations that such simple automated separation methods are used to support, there is a need to establish either stricter guidelines for such methods, develop improved methods (e.g. physically based methods) or at least provide error bounds on such estimates.

Acknowledgements

The authors gratefully acknowledge the reviewers' comments, which greatly improved the final manuscript. This work is supported by the Australian Research Council through its Linkage grant scheme and the South Australian Department for Water as industry partners under grant number LP0668808. Part of this research was funded by the Swiss National Foundation, Ambizione grant PZ00P2_126415.

Chapter 4

4 Interpreting streamflow generation mechanisms from integrated surface-subsurface flow models of a riparian wetland and catchment. (Paper 3)

Statement of Authorship

Title of Paper	Interpreting streamflow generation mechanisms from integrated surface-subsurface flow models of a riparian wetland and catchment
Publication Status	○ Published ○ Accepted for Publication ◉ Submitted for Publication ○ Publication Style
Publication Details	Partington, D., P. Brunner, S. Frei, C. T. Simmons, R. Therrien, A. D. Werner, H. R. Maier, G. C. Dandy, and J. H. Fleckenstein, 2012. Interpreting streamflow generation mechanisms from integrated surface-subsurface flow models of a riparian wetland and catchment. Submitted to *Water Resources Research*.

Author Contributions

By signing the Statement of Authorship, each author certifies that their stated contribution to the publication is accurate and that permission is granted for the publication to be included in the candidate's thesis.

Name of Principal Author (Candidate)	Daniel Partington		
Contribution to the Paper	Conceptualisation and development of improved HMC algorithm, implementation of HMC algorithm in HGS code, modelling, wrote manuscript except for description of Lehstenbach catchment.		
Signature		Date	23/11/2012

Name of Co-Author	Philip Brunner		
Contribution to the Paper	Supervised manuscript preparation and reviewed draft.		
Signature		Date	3.12.2012

Name of Co-Author	Sven Frei		
Contribution to the Paper	Development of models, wrote description of Lehstenbach catchment, reviewed draft.		
Signature		Date	11/22/2012

Name of Co-Author	Craig Simmons		
Contribution to the Paper	Supervised manuscript preparation and reviewed draft.		
Signature		Date	23/11/12

Name of Co-Author	Rene Therrien		
Contribution to the Paper	Supervised manuscript preparation and reviewed draft. Provided guidance in implementing the HMC algorithm in the HGS code.		
Signature		Date	Nov 24, 2012

Name of Co-Author	Adrian Werner		
Contribution to the Paper	Supervised manuscript preparation and reviewed draft.		
Signature		Date	23/11/12

Name of Co-Author	Holger Maier		
Contribution to the Paper	Supervised manuscript preparation and reviewed draft.		
Signature		Date	5/12/12

Name of Co-Author	Graeme Dandy		
Contribution to the Paper	Supervised manuscript preparation and reviewed draft.		
Signature		Date	3/12/12

Name of Co-Author	Jan Fleckenstein		
Contribution to the Paper	Supervised manuscript preparation and reviewed draft.		
Signature		Date	December 4th, 2012

Please cut and paste additional co-author panels here.

Abstract

The understanding of streamflow generation processes is vitally important in the management of water resources. In the absence of the data required to achieve this, Integrated Surface-Subsurface Hydrological Models (ISSHM) can be used to assist with the development of this understanding. However, the standard outputs from these models only enable elicitation of information about hydrological drivers and hydrological responses that occur at the same time. This generally limits the applicability of ISSHMs for the purposes of obtaining an improved understanding of streamflow generation processes to catchment areas that do not exhibit significant storage, travel times or flow depletion mechanisms. In order to overcome this limitation, a previously published Hydraulic Mixing-Cell (HMC) method is improved so that it can be used to follow surface water derived from direct rainfall and groundwater discharge to the stream and adjacent overland flow areas. The developed approach was applied to virtual experiments (based on the Lehstenbach catchment in south-eastern Germany), which are composed of two ISSHMs of contrasting scales: (1) a riparian wetland of area 210 m^2, and (2) a catchment of area 4.2 km^2. For the two models, analysis of modelling results for a large storm event showed complex spatiotemporal variability in streamflow generation and surface water-groundwater interaction. Further analysis with the HMC method elucidated in-stream and overland flow generation mechanisms. This study showed within a modelling framework, that identification and quantification of in-stream and overland flow generation better informed understanding of catchment functioning through decomposition of streamflow hydrographs, and analysis of spatiotemporal variability of flow generation mechanisms.

4.1. Introduction

Understanding streamflow generation and surface water-groundwater interaction is of great importance for the management of water resources, as highlighted in reviews by *Winter* (1999), Sophocleous (2002), and more recently *Fleckenstein et al*. (2010). In the absence of relevant data, distributed physics-based Integrated Surface-Subsurface Hydrological Models (ISSHM) (see *Gaukroger and Werner*, 2011; *Sebben et al*., 2012) represent a useful alternative for providing insight into

hydrological processes at detailed spatiotemporal resolutions (e.g. *Mirus et al*., 2011b). This is because ISSHMs are capable of simulating feedbacks between the surface and subsurface, including all forms of overland flow generation and re-infiltration (*Kampf and Burges*, 2007). In addition, ISSHMs can assist with analysing and interpreting hydrological processes and in developing conceptual understanding of catchment processes (*Ebel and Loague*, 2006). ISSHM examples include HydroGeoSphere (*Therrien et al*., 2009), InHM (*Vanderkwaak*, 1999), ParFLOW (*Kollet and Maxwell*, 2006), CATHY (*Camporese et al*., 2010) and MODHMS (*HydroGeoLogic Inc*., 2006). In recent years, studies related to understanding streamflow generation and surface water-groundwater interaction using numerical models have become increasingly widespread (e.g., *Brunner et al*., 2009; *Frei et al*., 2010; *Maxwell and Kollet*, 2008; *Park et al*., 2011).

The aforementioned studies focused on processes in small-scale synthetic systems, enabling insight to be gained into the controls on flow generation (*Frei et al*., 2010; *Maxwell and Kollet*, 2008; *Park et al*., 2011) and depletion (*Brunner et al*., 2009). However, difficulties arise when attempting to gain the same level of insight for larger, catchment-scale systems. This is because in small-scale systems, hydrological outputs at a particular place and time are generally only affected by hydrological drivers that occur at the same location and at the same time (i.e. by 'active' processes (*Ambroise*, 2004)). However, this is not the case for larger-scale systems, where local hydrologic response is not only affected by local processes but largely by processes taking place in other locations and at other times. This is a result of the influence of surface and groundwater flow travel times, flow impediments (e.g. riparian wetlands or weirs), and losses (e.g. infiltration or evaporation). Consequently, hydrological drivers that occur at a particular point in time (active processes) do not necessarily end up contributing to the hydrological output at that or a later time. As a result, when considering streamflow generation processes at the catchment scale, there is a need to distinguish between 'active' and 'contributing' processes (*Ambroise*, 2004), where contributing processes are those that contribute to flow at a particular location at a particular time, and necessarily include active processes upstream of the point of interest. It follows therefore, that all contributing processes are derived from active processes, occurring both upstream and at the point of interest; however,

not all active processes will become contributing processes downstream of where they occur, due to flow depletion processes such as evapotranspiration, and infiltration to the subsurface. This distinction is particularly important in catchments with relatively long travel times for water and/or where flow depletion processes are significant.

While information on active processes is provided as standard output from ISSHMs, the same is not the case for information on contributing processes. For example, the lag-times between individual recharge events and resulting stream flow increases are not reported. As a result, previous studies that have used ISSHMs at the catchment scale (e.g. *Goderniaux et al*., 2009; *Goderniaux et al*., 2011; *Loague and Vanderkwaak*, 2002; *Ebel et al*., 2008; *Li et al*., 2008; *Shen and Phanikumar*, 2010; *Mirus et al*., 2011a; *Camporese et al*., 2010) have been unable to identify and quantify the individual contributions of various catchment processes to streamflow generation processes. Although *Vivoni et al*. (2007) quantified the contributing processes of streamflow generation at the catchment scale, their model was based on a number of simplifying assumptions that did not necessitate the distinction between active and contributing processes. In particular, they assumed that surface water flows to the catchment outlet without loss or impediment once it enters the surface domain (see *Ivanov et al*., 2004). This assumption is problematic in more complex systems where significant fractions of overland and in-stream flows are depleted (e.g. due to reinfiltration of overland flow on the hillslope, or losing sections along a stream) or retained in particular parts of the catchment (e.g. due to wetlands, weirs or other flow impediments and water storages).

In order to enable ISSHMs to be used for the identification of both active and contributing streamflow generating processes, it is necessary to first classify water as it enters the surface by the active flow generation mechanism, and then track that water on its journey through the catchment, to the point at which the hydrograph is being measured. *Partington et al*. (2011, 2012) and *Li et al*. (2013) achieved this by developing and applying a Hydraulic Mixing-Cell (HMC) method in order to identify the groundwater discharge components of hydrographs for a relatively flat synthetic catchment that exhibited dynamic gaining and losing reaches along the stream, and furthermore displayed clear time lags for flow from

upstream areas. However, this approach has not yet been applied to larger-scale catchments, or for the identification of overland flow generation mechanisms.

In this paper, the HMC method introduced by *Partington et al*. (2011) is modified to enable information about active and contributing processes to be obtained as outputs from ISSHMs. This enables the identification and quantification of contributing in-stream and overland flow generation mechanisms at larger (e.g. catchment) scales which informs the understanding of catchment functioning. This is particularly important as there are still difficulties in the capability to conduct or scale up the measurements of active processes that are required in order to gain an understanding of surface water-groundwater interactions and streamflow generation at the catchment scale (*Fleckenstein et al*., 2010). The Lehstenbach catchment is used as the basis for virtual experiments with the modified HMC method. Two models of contrasting scales are used to investigate both in-stream and overland flow generation mechanisms within the catchment. In-stream flow generation mechanisms are defined as those occurring on the boundaries of the stream, i.e. direct precipitation to the stream, direct groundwater discharge to the stream and overland flow into the stream. Overland flow generation is distinguished by rainfall runoff from the hillslope (without distinguishing infiltration-excess and saturation-excess) and groundwater discharge on the hillslope adjacent to the stream. Using the HMC method, this paper aims to demonstrate the value of quantifying in-stream and overland flow generation mechanisms to better understand processes at the catchment scale within the virtual experiments by:

1. Separating flow hydrographs into the constituent in-stream and overland flow generation mechanisms at the outlet and other select points;

2. Quantifying the spatial and temporal variability for in-stream and overland flow generation mechanisms at contrasting spatial (wetland 210 m^2 and catchment 4.2 km^2) and temporal (days vs. year) scales; and

3. Quantifying the differences between active and contributing processes within the catchment.

4.2. Case study: Lehstenbach catchment

The Lehstenbach catchment, (4.2 km^2) located in South-eastern Germany (50°8'35" N, 11°52'8" E, see Figure 4.1), has been the subject of a number of previous studies (*Lischeid et al*., 2002; *Lischeid et al*., 2007; *Frei et al*., 2010). Elevations within the catchment vary between 877 m above sea level in upslope areas and 690 m above sea level at the catchment's outlet. Average annual precipitation amounts to about 1150 mm/yr, the average annual evapotranspiration is approximately 600 mm/yr, and average annual runoff from the catchment is approximately 550 mm/yr (*Gerstberger*, 2001). The annual mean air temperature is approximately 5°C (*Gerstberger*, 2001).

The main regional aquifer in the Lehstenbach catchment is made of regolith material (around 40 m thick) originating from the weathering of the granitic bedrock (*Lischeid et al*., 2002). Nearly one-third of the catchment's total area can be classified as riparian wetlands, adjacent to the major streams. These wetlands are preferentially located in the centre of the bowl-shaped catchment, where subsurface flows converge. Within the wetland areas, groundwater levels typically fluctuate within the uppermost 0.5 m of the organic peat soil. In the upslope areas, which are mainly forested (*Picea abies*), groundwater levels are generally between 5 m and 10 m below the surface. Locally, the hydraulic connectivity between the groundwater in the riparian wetlands and the deeper regolith aquifer is restricted by an up to 2 m thick basal clay layer.

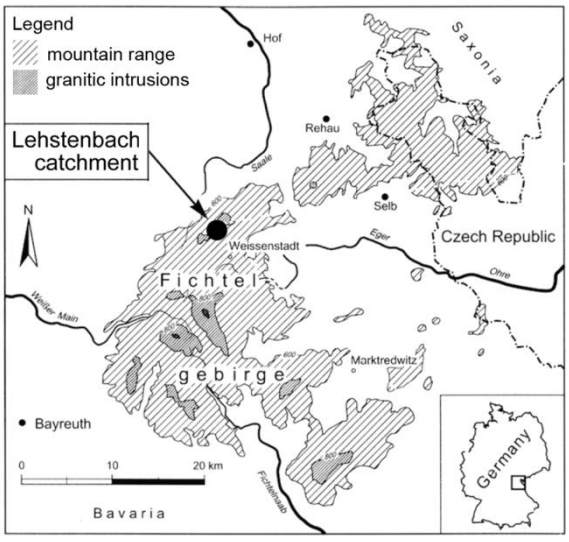

Figure 4.1: Location of the Lehstenbach catchment, after *Frei et al.* (2010).

Previous studies of the Lehstenbach catchment indicated that the dominant runoff generation processes (e.g. saturated overland flow and shallow subsurface flow) during rainfall events take place within the wetland areas (*Lischeid et al*., 2007; *Frei et al*., 2010). Large areas of these wetlands, predominantly located near the catchment's outlet, are characterised by a pronounced micro-topography, consisting of sequences of hollows and hummocks formed by the wetland's vegetation (*Knorr et al*. 2008). A conceptual hillslope plot depicting the in-stream and overland flow generation mechanisms in the Lehstenbach catchment is shown in Figure 4.2.

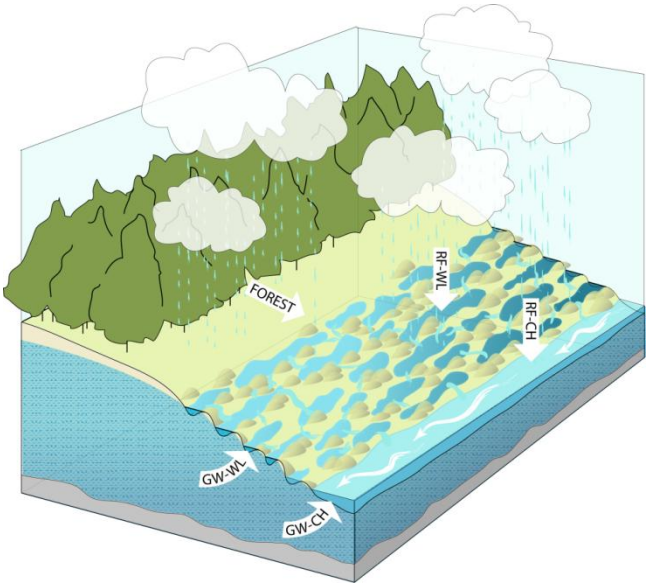

Figure 4.2: Conceptual diagram of in-stream and overland flow generation mechanisms typical of the Lehstenbach catchment during intense storm events. The in-stream and overland flow generation mechanisms shown are groundwater discharge to the channel (GW-CH) and wetland surfaces (GW-WL), direct rainfall to the channel (RF-CH) and wetland surfaces (RF-WL), and runoff from the forest.

Previous modelling by *Frei et al*. (2010, 2012) has been carried out for a synthetic riparian wetland typical of those within the Lehstenbach catchment. *Frei et al*. (2010) demonstrated a hysteretic relationship between wetland water storage and channel discharge. They concluded that enhanced mixing between surface and subsurface water had potential implications for the water quality within the catchment. However, *Frei et al*. (2010) did not explore mixing of rainfall and discharged groundwater at the wetland's surface, which necessitates quantifying the different overland surface flow and ponding generation mechanisms. These complex processes in the wetland suggest an analysis of only the active

mechanisms is insufficient to quantify the contributing overland flow generation mechanisms. In the present study, application of the HMC method to the wetland model expands on the work of *Frei et al*. (2010), and is used to quantify the fractions of overland flow that are generated from either rainfall running off the wetland or groundwater discharging to the wetland. However, their wetland model does not include the surrounding influences of adjacent wetlands, upslope forested areas and groundwater flows from upslope and deeper aquifers within the catchment. To investigate the catchment-scale processes, a model of the entire Lehstenbach catchment is developed, allowing analysis of in-stream and overland flow generation across the entire stream network and catchment, as well as accounting for contributions to the wetlands from deeper groundwater that originated from upslope areas.

4.3. Methodology

The modelling investigation within the study area is carried out at two different scales, as mentioned previously. Firstly, the model of a synthetic wetland typical of those in the Lehstenbach catchment is revisited, following *Frei et al*. (2010) (Section 4.3.2.1). Secondly, a model of the entire Lehstenbach catchment is developed (Section 4.3.2.2). In-stream and overland flow generation is analysed using an improved HMC method detailed in Section 4.3.3.

4.3.1. The fully integrated modelling platform

Numerical modelling in this study uses the ISSHM HydroGeoSphere (HGS). HGS is a fully integrated surface-subsurface flow model that incorporates 3D variably saturated subsurface flow using a modified form of the Richard's equation and 2D surface flow using the diffusion wave approximation to the St Venant equations. Further details of the numerical formulation of HGS can be found in *Therrien et al*. (2009) and *Brunner and Simmons* (2012). The surface and subsurface are coupled using a first-order exchange coefficient (*Liggett et al*., 2012). An important characteristic of fully integrated models such as HGS is that there is no requirement for a priori assumptions of specific streamflow generation mechanisms (*Mirus et al*., 2011a). Consequently, it is necessary to interrogate the model outputs to characterise the streamflow generation processes that are predicted by the model.

4.3.2. Development of case study models

4.3.2.1. Wetland model setup

The wetland model setup is described by *Frei et al*. (2010), and so only a brief description is presented here. The wetland model (Figure 4.3) is at the plot scale (21 m x 10 m), representing a relatively flat hillslope (average slope of 0.03 m/m) made up of a sequence of hummocks and hollows. The spatial structure of the micro-topography is represented using geostatistical indicator simulations based on a Markov Chain model of transitional probabilities (*Carle and Fogg*, 1996). The model domain is made up of 10 layers, with a total of 410,832 elements and 210,000 nodes, providing a fine discretisation of 0.1 m in the X, Y and Z directions. The organic peat is represented as homogeneous and isotropic with a saturated hydraulic conductivity of 0.2 m/d, a value that is based on a previous

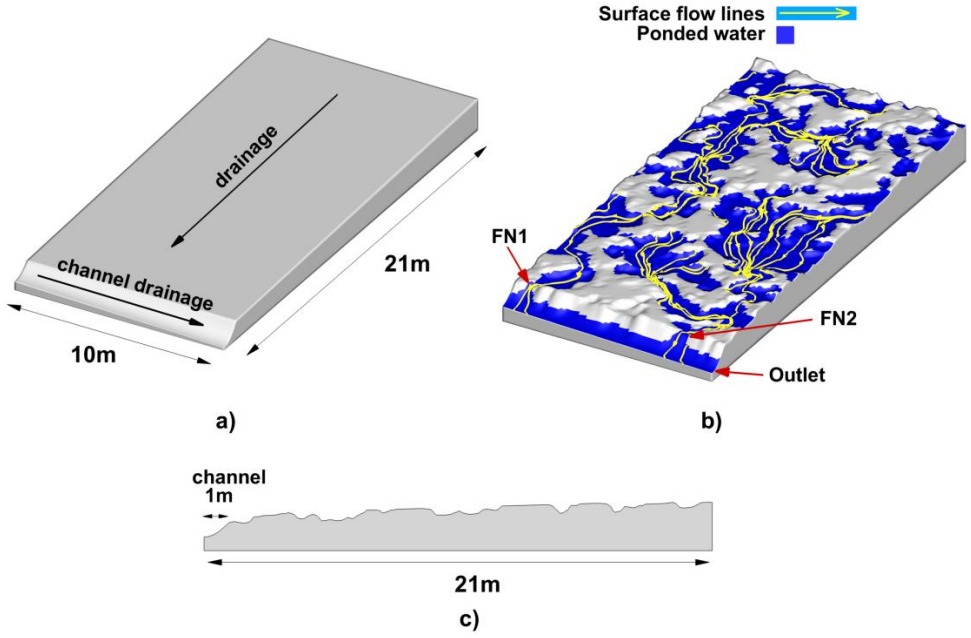

Figure 4.3: Geometry of the wetland segment: a) planar reference model showing the main drainage direction and channel location; b) smoothed realisation of the wetlands' hummocky micro-topography, with simulation results of developed overland flow in the wetland (after *Frei et al.* (2010)); c) cross section (Y = 5 m) of the micro-topography model (after Frei *et al.* (2010)). The division of overland flow into two distinct flow networks (denoted as FN1 and FN2) is shown by the surface flow lines. The model observation points for flow in this study are denoted by the red arrows, which correspond to surface water discharge from the wetlands to the channel from FN1 and FN2, and channel discharge at the outlet of the model.

modelling study from the field site (*Hauck*, 1999) and which is in line with values reported for similar wetlands (*Kruse et al*., 2008; *Schlotzauer and Price*, 1999). Constitutive relationships for unsaturated flow are assumed to follow the van Genuchten model of the soil-water retention and relative permeability functions (*van Genuchten*, 1980). The parameterisation of the van Genuchten model is based on field measurements from similar wetlands located in Alberta, Canada (*Price et al*., 2010). *Frei et al*. (2010) showed that the pronounced micro-topography resulted in distinct flow networks in the wetland model as shown in Figure 3b. The division of two flow networks (denoted as FN1 and FN2) and their discharge points to the channel are shown in Figure 4.3b.

The simulation period in this study focuses on a large storm event (13th - 21st July, 2001) from the 2000-2001 hydrological year (1/11/2000 – 31/10/2001). The simulation starts with a recession period (i.e. no rain) lasting 14 days. After day 14, an extended rainfall event occurs. The rainfall event persists for 8 days leading to the depressions on the slope filling until they spill to the adjacent down-slope depressions. Details of this 'fill and spill' mechanism (after *Tromp van-Meerveld and McDonnell*, 2006) and its influence on overland flow are described in *Frei et al*. (2010).

4.3.2.2. Catchment model setup

A digital elevation model (DEM) with a spatial resolution of 5 m x 5 m is used to represent the bowl-shaped topography of the catchment. Vertically, the model is discretised into two main geological units of variable thickness to represent the major soil types and subsurface geology of the Lehstenbach catchment. Within the wetland areas, the upper surface unit (1 m thick) represents the organic peat soils. This upper unit is represented in the grid by 10 sub-layers of uniform vertical thickness equal to 0.1 m (see Table 4.1).

For the ten sub-layers, the saturated hydraulic conductivity (K_{sat}) decays exponentially with depth to account for effects related to the transmissivity feedback mechanism, which has been described for peat forming wetlands [*Bishop et al*., 2004; *Jacks and Norrström*, 2004). Values for K_{sat} for the different sub-layers ranged between 20 m/d for the uppermost layer (representing fresh and less compacted organic material) and 8.6×10^{-3} m/d for the basal clay layer, which

separates the wetlands from the deeper aquifer (Table 4.1). The values for K_{sat} for the wetland areas are within the range reported by *Jacks and Norrstöm* (2001) who performed slug tests for similar wetlands located in the Luntoma catchment in South-western Sweden. The lower model unit (20-40 m thick) is represented in the grid by 10 sub-layers and is used to represent the main regolith aquifer. Similar to the wetland model, parameters for the soil-water retention functions are applied uniformly to the upper wetland layers based on field measurements from similar wetlands in Alberta, Canada (*Price et al*., 2010). Uniform parameters for the van Genuchten model as well as for K_{sat} (0.24 m/d) of the main regolith aquifer are obtained from a previous calibration of the model to field observations of aquifer heads and stream discharge at the catchment outlet for the 2000-2001 hydrological year (1/11/2000 – 31/10/2001) (see *Werb*, 2009).

Horizontally, the model uses a triangular mesh with variable node spacing (Figure 4.4). Nodal spacing in the mesh varies between 10 m in the direct vicinity of the streams, 30 m within riparian wetlands and 100 m for upslope areas. Within HGS, the locations of streams develop from flow between the surface and subsurface and tend to occur at topographical lows. However, the DEM used is too coarse to resolve differences in elevation between stream channels and the surrounding areas. Therefore, the elevations of surface nodes which coincide with stream locations are manually lowered by 1 m to correct for the smoothing of topography in the coarse DEM. For the subsurface flow domain, the bottom and lateral model boundaries are set to no flow to represent the contact with the low-permeability granitic bedrock and because it can be assumed that there is no exchange of groundwater with areas located outside of the Lehstenbach catchment. For the surface flow domain, a combination of variable rainfall, interception and evapotranspiration is applied over the catchment. Interception and evapotranspiration (*Panday and Huyakon*, 2004), within HGS, are simulated as mechanistic processes governed by plant and climatic conditions, as described by *Kristensen and Jensen* (1975) and *Wigmosta et al*. (1994). At the edges of the surface flow domain, a critical depth boundary is used to simulate surface water outflow from the model. Manning's roughness coefficient for the forested upslope areas are assigned uniformly to 1.9×10^{-6} $d/m^{1/3}$, representing areas of minor

ground vegetation (*Shen and Julien*, 1993). Friction slope for the wetlands are set to 8.1 x 10^{-5} d/$m^{1/3}$, typical for high grass (*Shen and Julien*, 1993).

Topography and land use for the Lehstenbach catchment are shown in Figure 4.4. The elemental type distribution shown in Figure 4.4 is used to delineate the stream, wetlands and forest areas. The detailed micro-topography of the wetland model cannot be included explicitly at the catchment scale due to computational constraints. Instead, the rill storage concept is used (see *Therrien et al*., 2009), whereby a ponding depth is specified at surface nodes which must be reached before surface flow is induced. Spatially distributed rill storage height zones are used to represent the micro-topographically induced threshold-type behaviour of runoff generation from the wetlands. These storage zones mimic the depression-storage characteristics and the typical fill and spill mechanisms of the wetlands' micro-topography. However, the behaviour of the wetlands in the catchment-scale model (as opposed to the wetland model) is influenced additionally by variable groundwater heads at the upslope boundaries, which are driven largely by recharge originating from infiltration in the upslope forested areas. The simulation period is the hydrological year 2000 (11/1/2000 - 10/31/2001), although a focus is placed on the large July storm (13th - 21st July, 2001) simulated in the wetland

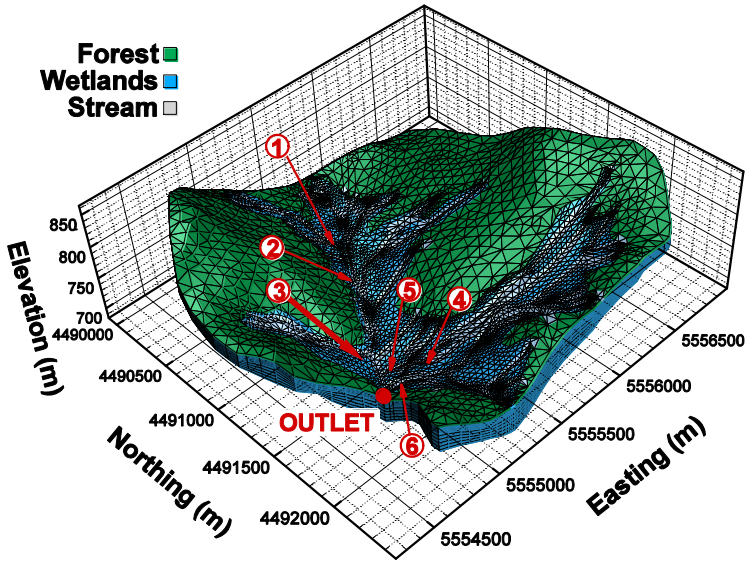

Figure 4.4: Model spatial discretisation of the Lehstenbach catchment and distribution of the stream, wetland and forest areas (the z-axis is exaggerated by a factor of 5). Model observation points are at locations 1 to 6 and the outlet.

Table 4.1: Surface and subsurface parameters used in the Lehstenbach catchment model. For a detailed description of all model parameters used in HGS, see *Therrien et al*. (2009).

model. Note that because the whole year is simulated in the catchment model, day 0 in the wetland model is the same as day 200 in the catchment model. Evaluation of simulated stream discharge to the observed discharge for the 2001-2005 hydrologic years yields a Nash-Sutcliffe efficiency of 0.51, which is deemed reasonable for this study.

4.3.3. HMC method

The HMC method developed by *Partington et al*. (2011) allows separation of the streamflow hydrograph by the in-stream flow generation mechanisms (i.e. groundwater discharge to the stream, direct rainfall to the stream, and overland flow to the stream). The HMC method works by utilising the spatiotemporal information of active in-stream flow generation mechanisms to obtain the contributing flow generation mechanisms. The HMC method treats each stream node in the surface domain of the model as a mixing cell. The method utilises the nodal fluid mass balance from the ISSHM at each model time-step, to calculate the fraction of water in each cell that derives from different in-stream flow generation mechanisms. For example, if a cell has a water volume of 0 units at the start of the time step and 2 units at the end of the time step, and during that time-step 1 unit of groundwater discharged into the cell and 1 unit of rainfall fell on the cell, then the fraction of groundwater discharge and direct rainfall in the cell would be 0.5. This becomes more complex if there is also outflow from the cell, because a mixing rule must be chosen for the mixing-cells, which dictates how the fractions are calculated at the end of each time step. The HMC method uses the "modified mixing rule", which simulates a mixing regime between perfect mixing and piston-flow (see *Campana and Simpson*, 1984).

Each in-stream flow generation mechanism is assigned a unique fraction *f*. Over each time-step of the model simulation, inflowing water into a cell from either the subsurface (e.g. groundwater discharge) or surface boundary conditions (e.g. rainfall) is classified by the corresponding unique fraction. The sum of all fractions in each cell, for an error-free fluid mass balance, is equal to 1. Inflow from adjacent cells is assigned the fractions from the upstream cell. *Partington et al*. (2011) derived an equation for the fraction *f* for each in-stream flow generation mechanism *k* at time *N* in cell *i* as:

$$f_{i(k)}^{N} = \left(\frac{V_i^{N-1}}{V_i^{N}} - \frac{\sum_{j=1}^{m} V_{ij}\Big|_{N-1}^{N}}{V_i^{N}} \right) f_{i(k)}^{N-1} + \frac{\sum_{j=1}^{n} V_{ji}\Big|_{N-1}^{N} f_{j(k)}^{N-1}}{V_i^{N}} \quad \textbf{(4.1)}$$

Where there are n sources and m sinks for cell i; $f_{j(k)}^{N-1}$ denotes fraction k at time N-1 in the neighbouring cell j, V denotes the volume with the superscript denoting time state and subscript i denoting the cell, ij denoting volume into cell j from cell i over the time-step from N-1 to N, and ji denoting volume from neighbour j into i.

To achieve the aims of the current study, some limitations from previous implementations of the HMC method must be addressed. Firstly, *Partington et al*. (2011, 2012) does consider the contributing mechanisms for overland flow, as groundwater discharge adjacent to the stream was negligible. Secondly, *Partington et al*. (2011) notes that the HMC method was only numerically stable if the ratio of outflow to storage was less than 1, and the fluid mass balance convergence criterion was very small ($<10^{-10}$ m^3/s). These stability conditions require very low convergence criterion ($<10^{-10}$ m^3/s) for the solution of the fluid mass balance equation, and very small time-steps (<100 s), thus increasing simulation time significantly. Use of the HMC method in this study expands on previous implementations by: (1) accounting for overland flow generation mechanisms in the HMC method, (2) modifying the HMC scheme to allow operation at sub-time-steps of the ISSHM flow solution time-step, and (3) developing stability handling criteria for HMCs to prevent instabilities from occurring. Addressing these limitations enables the quantification of contributing in-stream and overland flow generation mechanisms for the more complex virtual experiment considered in this current study.

4.3.3.1. Capturing in-stream and overland flow generation mechanisms

Overland flow generation mechanisms are considered by using additional HMC fractions to those used in *Partington et al*. (2011, 2012). All in-stream and overland flow generation mechanisms are delineated by surface node definition: e.g. ‘stream’ or ‘overland’. Surface nodes may also be defined as ‘other’ nodes, which could be lakes, reservoirs, upstream inflow boundaries or areas for which internal flow generation may not be of interest or are not known. In this study, forested areas are treated as ‘other’ nodes. With respect to groundwater discharge

and rainfall, flow generation at 'other' nodes is not captured explicitly. Instead, any water flowing from 'other' nodes to a stream or overland node is assigned an 'other' fraction of 1 (i.e. f_{other} = 1), i.e. without delineation of this water into components of groundwater discharge and rainfall. Unless water in the surface domain at the start of a simulation is assigned stream, overland or 'other' fractions from a previous simulation, then it is not possible to know which flow generation processes were responsible for initial surface water. Therefore, an "initial" fraction is also included; initial conditions for existing surface water in each cell default to the "initial" fraction (i.e. $f_{initial}$ = 1, and all other fractions are set to zero) unless predefined otherwise.

4.3.3.2. Sub-timed HMC algorithm to ensure stability

The stability of Eq. 4.1 in the HMC method is dependent on the ratio of outflow to storage (*Partington et al.*, 2011).]. Stability requires that the volume of water leaving a cell over a given time step is less than the volume in storage. The volume leaving a cell is calculated using the fluid mass balance, accounting for small errors in the water balance (i.e. $\sum f_{i(k)}^{N} \neq 1$) within each cell (for outflow and storage). Absolute error (ϵ) within cells is calculated as $\epsilon = |1-\sum f_{i(k)}^{N}|$. The HMC ratio for each cell *i* is defined as:

$$HMC\ ratio\,(i) = \frac{\sum_{j=1}^{m} V_{ij}\Big|_{N-1}^{N} f_{i(k)}^{N-1}}{V_i^{N-1} \sum_{\forall k} f_{i(k)}^{N-1}} \qquad \textbf{(4.2)}$$

Instability in the HMC method results when the cell ratio is greater than 1 in any HMC. For small HMCs, the storage volume may be quite small relative to the outflow. Maintaining the HMC ratio below 1 can necessitate very small time-steps when the cell's storage is small relative to the flow. This is problematic for long term transient simulations requiring large time-steps in the flow solution. As part of the improved HMC method, a sub-timed HMC method is implemented to prevent relatively small time-steps. This implementation removes the stability restriction (i.e. Eq. 4.2) imposed by the HMC method on the maximum time-step for the HGS flow solution. The sub-timed HMC method is applied when the maximum HMC ratio at any of the cells is greater than 1. It works by subdividing the fluxes and storage changes within a time-step. This subdivision between time-

steps *N*-1 and *N*, and calculation of fractions at each sub-time step *n* is done in the following way:

(1) Calculate the number of sub-time steps (*s*) required to ensure stability based on maximum HMC ratio:

$$s = [max.\ HMC\ ratio| + 1 \quad \textbf{(4.3)}$$

Where *max. HMC ratio* is the maximum HMC ratio.

(2) Calculate the sub-timed-ratios (t_{sub}) for adjusting inflows, outflows and storage changes at each *n*:

$$t_{sub}{}^{n} = \begin{Bmatrix} 1/(s-1) \ ; 1 \le n < s \\ 1 - t_{sub}{}^{1} * (s-1) \ ; \ n = s \end{Bmatrix} \quad \textbf{(4.4)}$$

(3) Calculate the changes in storage for the cells over the whole time-step:

$$dS_i = V_i^N - V_i^{N-1} \quad \textbf{(4.5)}$$

(4) Calculate the sub-timed HMC fractions, updating for all cells *i* at each sub-step *n* as follows:

$$f_{i(k)}^n = \left(\frac{V_i^{n-1}}{V_i^n} - \frac{\sum_{j=1}^{m} V_{ij}\big|_{N-1}^{N} * t_{sub}{}^{n}}{V_i^n} \right) f_{i(k)}^{n-1} + \frac{\sum_{j=1}^{n} V_{ji}\big|_{N-1}^{N} f_{j(k)}^{n-1} * t_{sub}{}^{n}}{V_i^n}, \ n = 1,...,s \quad \textbf{(4.6)}$$

Subject to

$$V_i^0 = V_i^{N-1} \ and \ f_{a(k)}^0 = f_{a(k)}^{N-1}, \ a = i, j \quad \textbf{(4.7)}$$

$$V_i^n = V_i^{N-1} + n * t_{sub}{}^{n} * dS_i \ for 1 \le n < s \quad \textbf{(4.8)}$$

$$V_i^s = V_i^N \quad \textbf{(4.9)}$$

4.3.3.3. Stability constraints for efficient execution of the HMC method

The sub-timed HMC scheme allows time-steps in the flow solution to be as large as convergence criteria allow. However, a very large HMC ratio (> 10000), results in a large number of sub-time steps. In terms of computational efficiency, a very large HMC ratio is not desirable, particularly for cells that only have very small volumes of water storage. In near dry cells, large HMC ratios will often arise at the onset of rainfall, groundwater discharge or overland flow, as the outflow can be significantly larger than storage. The large HMC ratio problem tends to occur in simulating ephemeral reaches of streams whereby particular stream cells become dry. Similarly, this problem occurs in simulating overland flow whereby the overland cells are often dry (due to overland flow only normally occurring in rainfall events). In these cases of a large HMC ratio, particular cells can become numerically unstable due to propagation of errors from the fluid mass balance. Fortunately, this occurs at cells that are of little interest in a physical sense (i.e. where active processes take place but with relatively insignificant volumes of water).

To address these problems and ensure stability and computational efficiency, criteria are added to the method and used to determine if each cell should be evaluated. If any of the above criteria are met, then the cell being evaluated is reset, which means that all fractions f in the reset cell are set equal to zero, and that the cell is assigned the reset fraction ($f_{\text{Reset}} = 1$). The criteria (a-e) for a reset cell are checked at each time-step allowing it to become active if the reset criteria are no longer met. The reset fraction allows the tracking of the fraction of water for which the flow generation is unknown (due to the cell being reset), which quantifies the effect of the reset fraction. Tracking of the reset fraction highlights through inspection of calculated HMC fractions if this unknown flow generation is significant. If the reset fraction of flow in the streamflow hydrograph is high (>1%) then each criterion can be modified to bring this to a satisfactory level (<1%).The reset criteria are as follows:

a) *Minimum volume*. Cells with relatively small water storages are reset unless surface flow is greater than zero (10^{-10} in this study).

b) *Ponding only*. Cells with no surface flow are reset if the inflow or outflow is greater than the volume of ponded water.

c) *Maximum HMC ratio*. Cells with a large HMC ratio (Eq. 4.2) are reset (10^4 in this study).

d) *Relative volume error too high*. Cells in which the ratio of the 'absolute volume error' to storage is large are reset, where the absolute volume error denotes the absolute value of the error in the volumetric cell balance (2.5 in this study).

e) *Error in HMC excessive*. Cells with a large absolute error (ϵ) are reset after updating the fractions in the cell at each time-step or sub-time-step (0.5 in this study).

4.4. Flow generation analyses conducted using the HMC method

The in-stream and overland flow generation mechanisms analysed for the case study (see Figure 4.2) are: (1) groundwater discharge to the stream channel (GW-CH), (2) direct rainfall to the stream channel (RF-CH) and overland flow to the stream channel. The overland flow generation mechanisms analysed are: (3) groundwater discharge to wetland surface areas (GW-WL), (4) direct rainfall on wetlands surface (RF-WL) and (5) overland flow from forested areas (Forest).

The unique fractions *f* used in this HMC analysis are: (1) GW-CH, (2) RF-CH, (3) GW-WL, (4) RF-WL, (5) Forest, and also (6) initial water (Initial) and (7) reset water (Reset). In-stream and overland flow generation mechanisms are determined based on surface cell type: i.e. stream, wetland or forest cells. Each analysis outlined below corresponds directly to aims 1 to 3. To aid the reader through the following sections, Table 4.2 below summarises the flow generation mechanisms analysed, and the corresponding unique HMC fractions and fraction types.

Table 4.2: Considered flow generation mechanisms, HMC unique fractions, and HMC fraction types.

Flow generation mechanism	Unique fraction	Fraction type
Groundwater discharge to the stream channel	GW-CH	In-stream
Direct rainfall to the stream channel	RF-CH	In-stream
Groundwater discharge to the wetlands	GW-WL	Overland
Direct rainfall to the wetlands	RF-WL	Overland
Surface flow from the forest area	Forest	Other
Unknown	Initial	Initial
-	Reset	Stability

4.4.1. Separating flow hydrographs by in-stream and overland flow generation mechanisms

The main output from the HMC method is the values of the unique fractions f at each cell, which are used to separate the flow hydrographs by multiplying the total flow at each time step by each of the unique fractions at the corresponding time step. Each flow hydrograph at the outlet and selected model observation points (see Figure 4.3 and Figure 4.4) is made up of a collection of cells. At each cell, the surface outflow is separated by the unique fractions into the corresponding flow generation mechanisms, and then these are summed for each collection of cells.

4.4.2. Analysing spatiotemporal variability of in-stream and overland flow generation

Spatial variability of in-stream and overland flow in both models is demonstrated in three ways. Firstly, visualisation of the HMC fractions across the model surface domain is shown in each model at different points in time. Secondly, flow hydrographs are shown at select observation points within each of the models. Lastly, the different flow generation mechanisms driving total flow at each of the locations are summarised. The summarising of the flow components is achieved by integrating over the flow curves for each of the flow generation mechanisms, at each selected observation point.

4.4.3. Analysing active and contributing processes

The analysis of active and contributing processes is carried out over the entire year long simulation for the catchment scale model. In particular, the components analysed are GW-CH, RF-CH and wetlands surface discharge to the stream channel (WL-CH = GW-WL + RF-WL). Runoff from the forested areas to the stream channel is also considered (Forest-CH). The active flow generation processes are determined by summing the inflowing fluxes to the surface domain (GW-CH, RF-CH, WL-CH, Forest-CH) at each time-step, and the contributing processes (taken at the outlet) are determined from the HMC analysis. A long-term ratio of contributing to active flow generation mechanisms is calculated to quantify the cumulative difference between these two.

4.5. Results and discussion

4.5.1. Wetland model

4.5.1.1. In-stream and overland flow generation mechanisms driving flow

The applied rainfall and the resultant outflow and corresponding flow generation components are shown in Figure 4.5a-b. From the time rainfall starts, streamflow increases slightly until day 17, at which point the rainfall rate increases significantly. The rain falling directly on the channel contributes to runoff immediately. The infiltration across the overland area increases the subsurface head, which in turn increases the groundwater discharge to the channel. The rapid response of rainfall directly on the channel (RF-CH) is clearly seen to follow the pattern of the rainfall input. During the highest rainfall period, over day 17, the groundwater discharge to the channel rises to an apparent quasi-steady-state. In the four days that follow, the GW-CH component only changes slightly in relation to the total streamflow. All major changes in streamflow between days 17 to 22 are attributed to changes in overland flow to the stream. It can be seen in Figure 4.5c that at approximately 17.6 days, overland flow from FN1 reaches the channel and causes a rapid increase in streamflow.

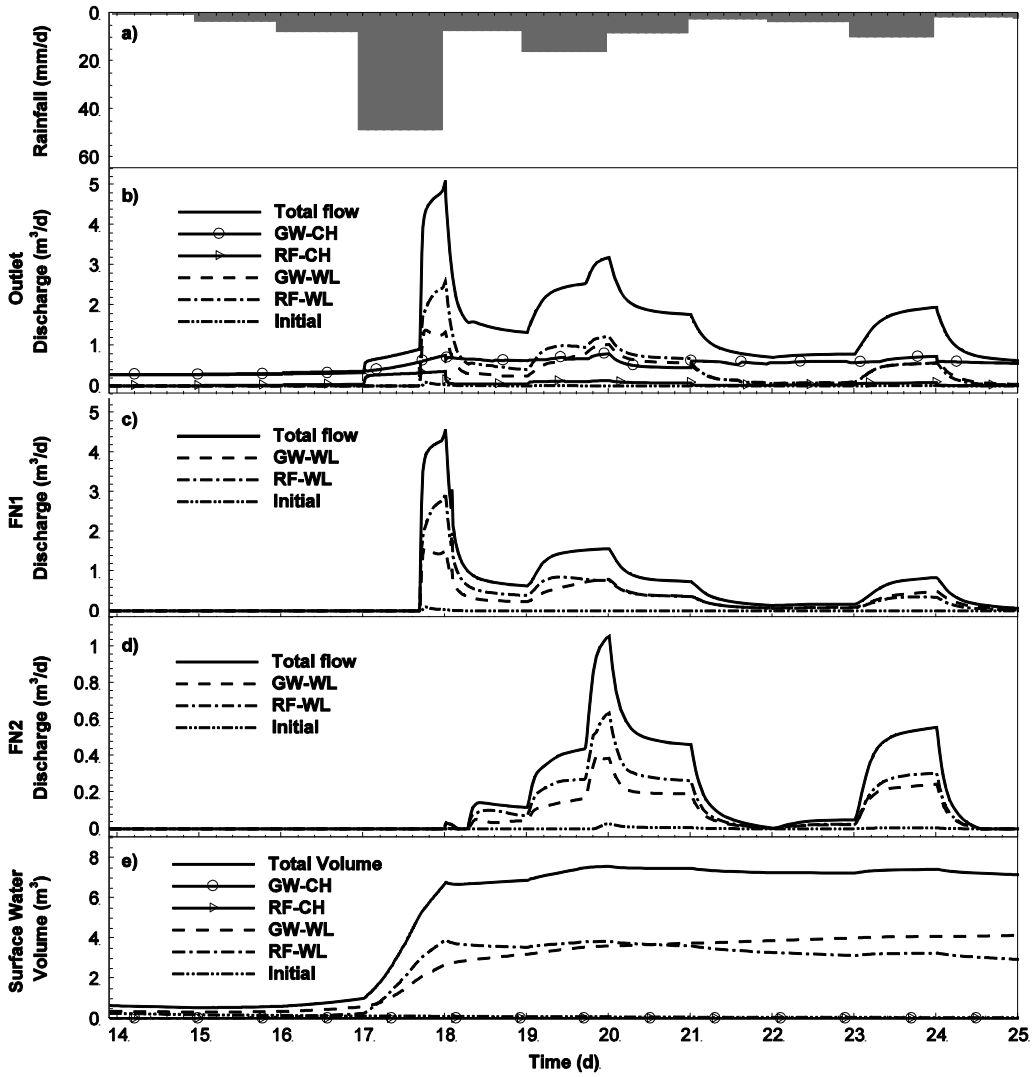

Figure 4.5: Hyetograph, simulated outlet hydrograph, simulated FN1 hydrograph, simulated FN2 hydrograph and simulated surface water storage graph for the wetland model during a large storm event. GW-CH and RF-CH are direct groundwater discharge and rainfall to the channel. GW-WL and RF-WL represent groundwater discharge and rainfall to the surface of the wetland area respectively. Initial represents the initial water in the surface domain at the beginning of the simulation. The reset fraction of flow was negligible and hence is not shown.

Figure 4.5d shows that almost half a day after FN1 starts discharging to the channel, at approximately day 18, FN2 starts contributing to streamflow. Whilst a greater proportion of rainfall to the wetland surface area (RF-WL) is evident, there is also a large component of groundwater that discharged to the wetland surface (GW-WL). This large component of GW-WL in the outflow hydrograph appears not only to be an increase in this overland flow generation mechanism at this particular time, but also a result of the mobilisation of the ponded water generated

from GW-WL. The total surface water storage across the model and also the flow generation mechanisms that created the storage are shown in Figure 4.5e. The ponding of water in the hollows makes up almost 100% of the surface storage (with the GW-CH and RF-CH water being relatively insignificant). There is only a relatively small variation in the total storage after day 18. A small component of initial water is contributing to streamflow at the outlet at day 18. The initial water was mobilised after the hollows fill and then spill toward the stream. This shows a slow rate of turnover (>18 d) of ponded surface water due to the time taken for the hollows to 'fill and spill', i.e. prior to the activation of the flow networks.

4.5.1.2. Spatiotemporal variability of in-stream and overland flow generation

Two snapshots of in-stream and overland flow generation are shown for the wetland model, just before the rainfall event at the start of day14 (Figure 4.6), and 6 days into the storm event at day 20 (Figure 4.7). The distributions of (1) GW-WL water in the hollows, and (2) GW-CH water, are shown in Figure 4.6 and Figure 4.7. After 14 days, the rainfall event begins and therefore there is no RF-CH or RF-WL fraction of surface water (not shown in Figure 4.6). The reason that the fraction of GW-WL water is not equal to 1 across the hummocks and hollows is because of the persistence of initial water, of which a small volume resides on the surface.

The development of overland flow in the wetlands is well established at day 20. An increase in the GW-WL component of streamflow is explained by the increased subsurface heads leading to a more developed seepage face along the bank. Close examination of the two flow networks (FN1 and FN2) highlights variations in the overland flow generation across the wetland. The overland flow network on the left (FN1) has a slightly higher component of groundwater discharge, whereas the flow network on the right (FN2) has a slightly higher component of rainfall, with clear spatial variation in each. The flow network FN2 has a higher rainfall driven component because of the larger surface area of the stored water, which receives more rainfall. The reset of cells at the top of the hummocks and the upper part of the stream bank is due to the fact that these cells have no surface flow to other cells and also the inflow from rainfall at these cells is much greater than the ponded water volume.

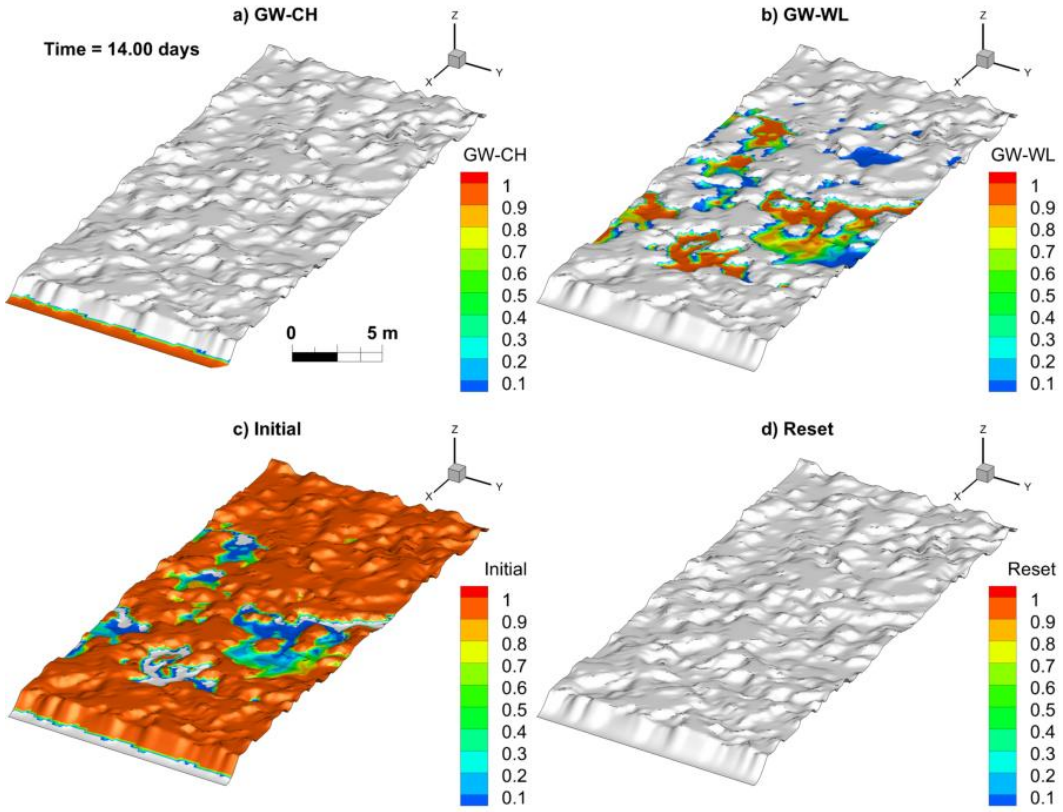

Figure 4.6: Wetland HMC fractions at day 14 (pre-storm event). The in-stream and overland flow generating mechanisms shown are: a) groundwater discharge to the channel (GW-CH), b) groundwater discharge to the wetland surface (GW-WL). The initial and reset fractions are also shown in c) and d) respectively. A GW-WL fraction of 0.5 denotes that 50% of the water at that cell was generated from groundwater discharging to the wetland surface.

Figure 4.8 shows a summary of the percentage of total volume of water derived from different in-stream and overland flow generation mechanisms. This summary is provided at the outlet and for each of the flow networks (FN1 and FN2). All volumes were determined by integrating over the flow hydrographs in Figure 4.5 (b-d). The contributions towards total flow from the two overland flow networks were calculated to be 34% and 10% for FN1 and FN2, respectively, making a total overland flow contribution of 44% over the simulation period. The components of initial water and reset water, are insignificant (<1%). The volume attributed to cumulative error was extremely small at the outlet (4×10^{-16}%).

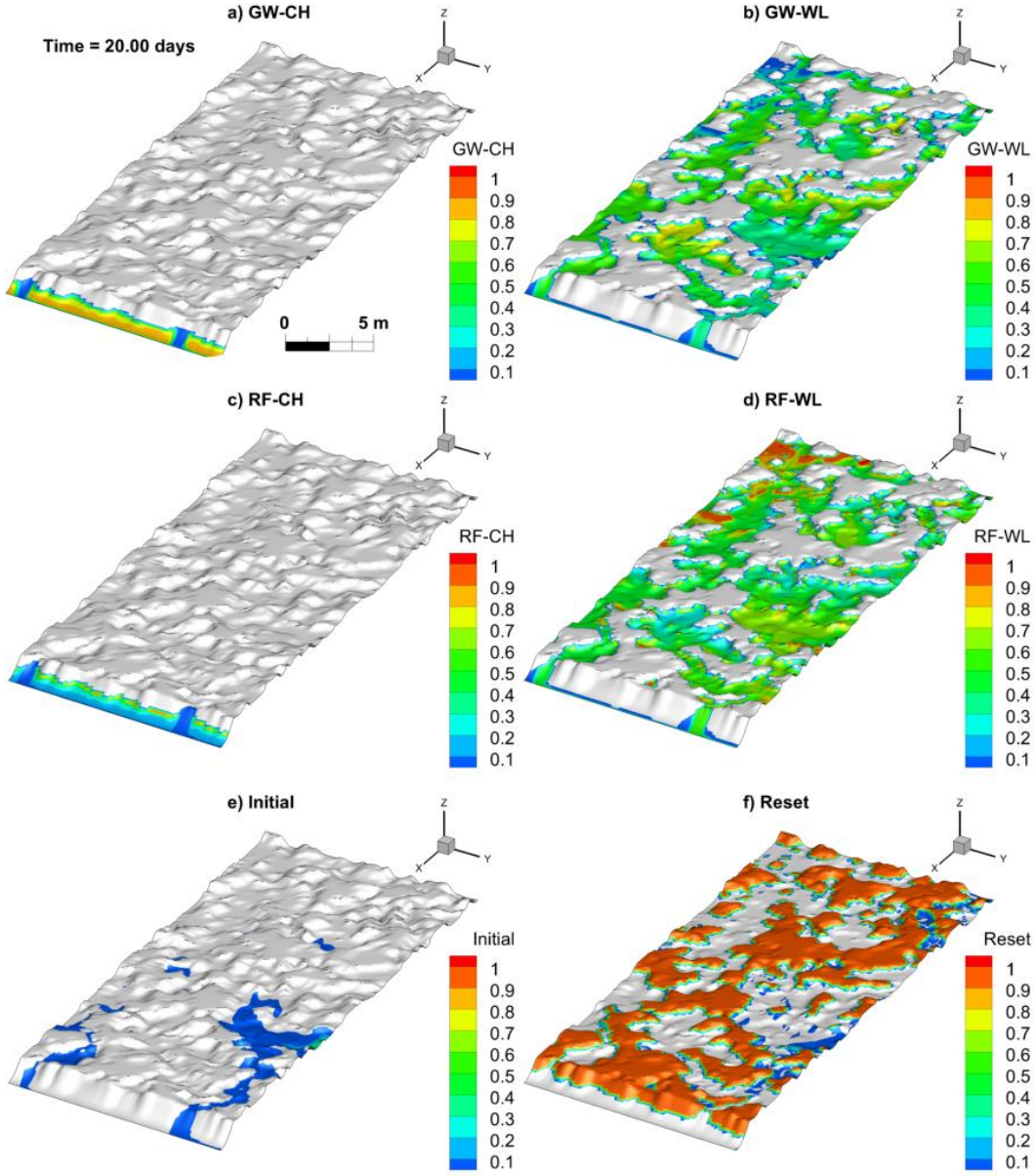

Figure 4.7: Wetland HMC fractions at day 20 (during the storm event). In-stream and overland flow generating mechanisms shown are: a) groundwater discharge to the channel, b) groundwater discharge to the wetland surface, c) rainfall to the channel, d) rainfall to the wetland. The remaining initial water (e) and the reset fraction (f) for reset cells are also shown.

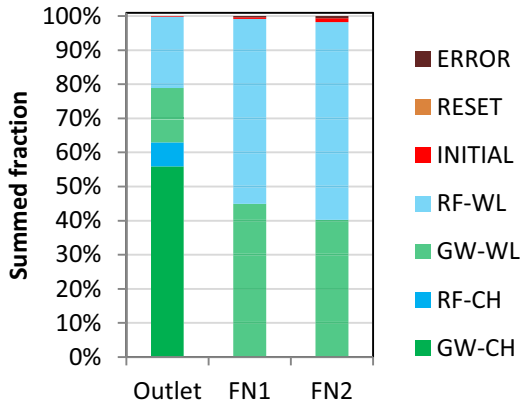

Figure 4.8: Comparison of different streamflow generation mechanism contributions at the outlet, FN1 and FN2. The initial and reset fractions and the cumulative error in the cells were insignificant, as can be seen at the top of the stacked columns.

To summarise, HMC analysis of the wetland model demonstrates clear spatial variability in overland flow generation, as depicted in Figure 4.6 and Figure 4.7. This variability is clear in the discharge hydrographs of the two flow networks (Figure 4.5), highlighting a complex relationship between rainfall input and runoff from the wetlands into the stream. However, despite this spatial variability, the flow networks have similar compositions of overland flow generation components at the point of discharge into the stream, with both FN1 and FN2 being dominated by RF-WL flow generation (Figure 4.8). The HMC analysis showed that the RF-WL component of flow is larger by about 5% over the GW-WL component in driving the overland flow contribution at the outlet (Figure 4.8). As evidenced in the Figure 4.5 discharge hydrographs, the storage across the overland area shows that the relationship between overland storage and overland flow contributions to streamflow at the outlet is non-linear. As noted in *Frei et al*. (2010) this non-linear relationship is caused by the complex nature of the 'fill and spill' mechanism. As expected, the direct RF-CH component of in-stream flow generation followed the rainfall input. This is because there are no significant time lags or losses along the stream to the subsurface. Similarly, the response to rainfall of groundwater discharge in the channel (GW-CH) is also as expected, although it has a slower response than the RF-CH component.

4.5.2. Catchment model

Three snapshots from the model simulation for the large storm in July 2001 are examined for surface water distribution and surface-subsurface exchanges. These snapshots are taken just prior to the storm (day 216), at the peak of the storm (day 218), and 2 days after the peak (day 220). Figure 4.9 shows standard HGS outputs of surface saturation, exchange flux and depth distribution across the catchment at each of these times. Figure 4.9a shows that saturation at the surface boundary increases across the catchment as the storm event progresses.

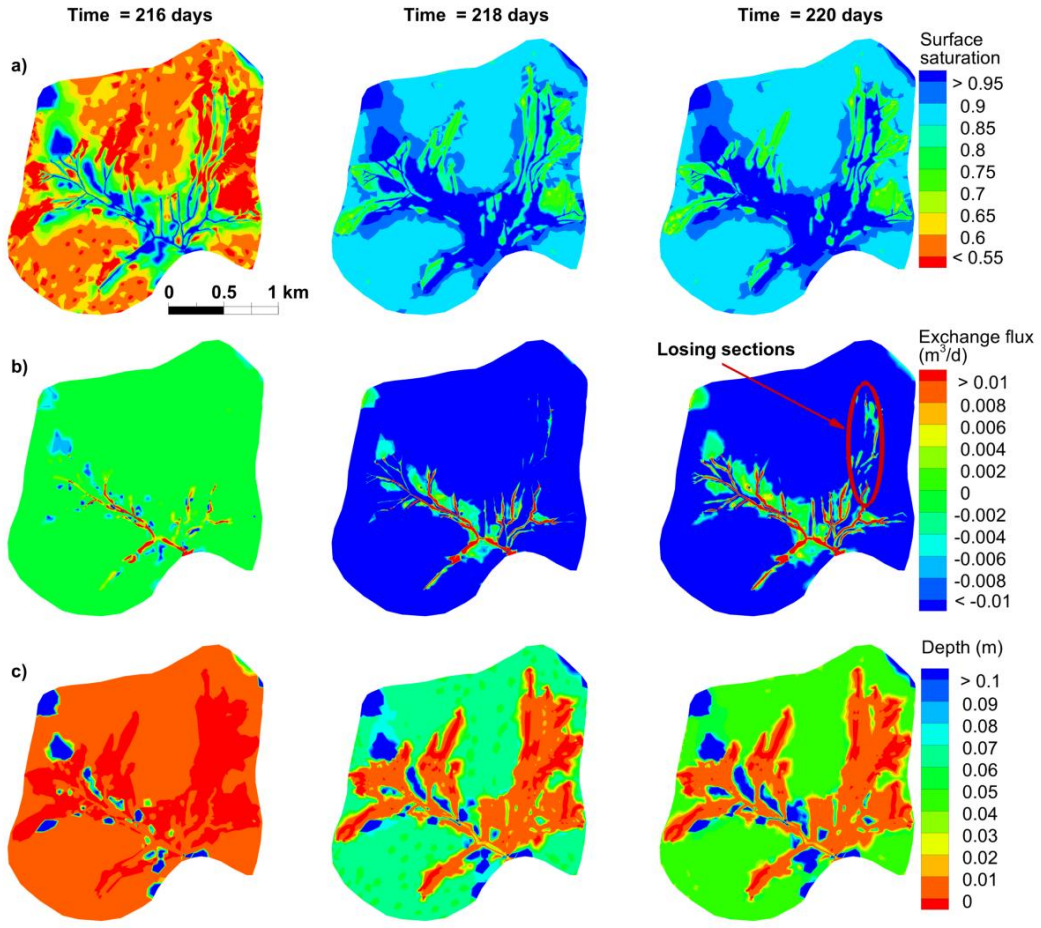

Figure 4.9: Simulated surface saturation (a), exchange flux (b) and surface water depth (c), prior to the storm, at the storm peak and 2 days after the storm peak. A losing section on the right arm of the stream is highlighted in the third frame of row b). Positive values of exchange flux indicate groundwater discharge to the surface and negative values indicate infiltration of surface water to the subsurface.

The exchange flux (Figure 4.9b) across the catchment shows where water is exfiltrating from the subsurface to the surface (positive values) and where water is

infiltrating into the subsurface from the surface (negative numbers). Prior to the storm event, there is no exchange across the forested areas, water is being lost from the wetlands to the subsurface, and groundwater is discharging to the stream. At the peak of the storm, the infiltration rate peaks in the forested areas, but the infiltration from the wetlands decreases. The area of groundwater discharging to the stream is slightly increased, but not significantly. At the cessation of the storm event, the infiltration rate is varied across the forested area. In Figure 4.9b at day 220, about two thirds of the reach on the right arm of the stream is losing (highlighted by a red ellipse).

The surface water depth distribution (Figure 4.9c) across the catchment highlights the wetland areas, where most surface ponding occurs. Excluding the stream, these wetland areas lie at the lowest elevation in the catchment. It is these ponded wetlands that provide the overland runoff during the storm event. There is discharge of groundwater at the upper part of the right arm of the stream, however, this water is returned to the subsurface across the losing stretch of this reach of the stream (highlighted in Figure 4.9b).

4.5.2.1. In-stream and overland flow generation mechanisms driving flow

The separated streamflow hydrograph at the outlet is shown in Figure 4.10. In Figure 4.10b, the GW-CH component of streamflow is seen to respond immediately to rainfall events with no clear lag, possibly due to propagation of a pressure wave. As rainfall ponds on the hydraulically connected wetlands, this in turn increases the head in the underlying aquifers. The GW-CH component of streamflow is seen to make up ~97% of the flow in dry periods – the GW-WL component of streamflow contributes a very small amount to streamflow during dry periods (~3%). The RF-WL and GW-WL components of the outlet hydrograph (Figure 4.10b) show that the wetlands only provide a significant component to streamflow during the larger storm events (e.g. at the storm peak, day 218). After the large storm event from day 221, the streamflow is supported mainly by GW-CH discharge to the stream. Overland flow from the forested areas had a negligible contribution to overland flow in the wetlands and hence also to streamflow, and for this reason is not shown in the hydrographs.

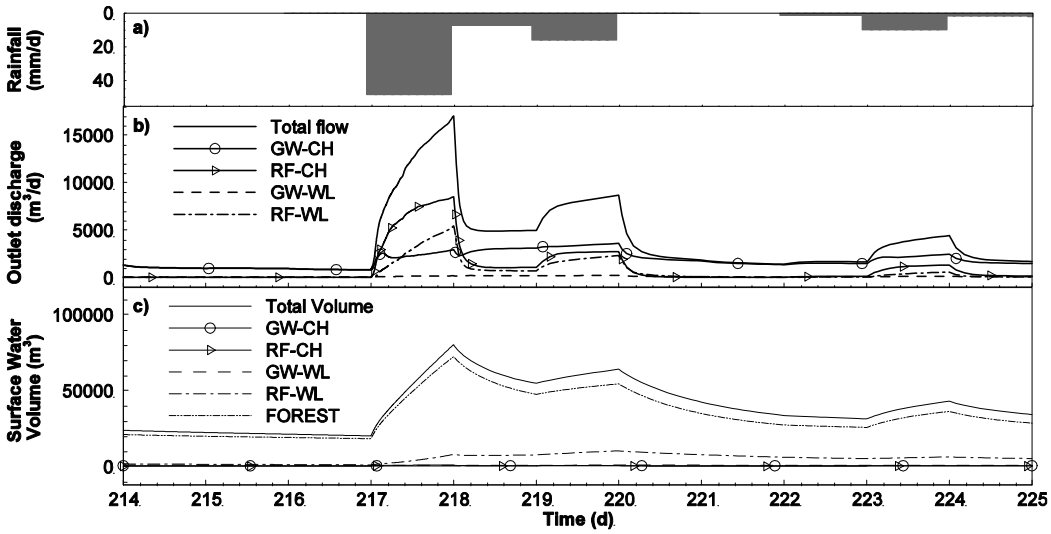

Figure 4.10: Hyetograph (a), separated discharge hydrographs at the outlet (b), as well as the HMC fractions in surface-storage across the catchment (c). Note that overland flow from the forest was negligible (< 0.2%) in contributing to streamflow and so is not shown in (b).

The total surface water storage across the Lehstenbach catchment and the storage of water from different flow generation mechanisms, i.e. the mechanism by which the water came into storage are depicted in Figure 4.10c. This figure shows that much of the storage in the surface is ponded water in the forested areas. The second largest component of storage is rainfall stored in the wetlands. Notably, the GW-CH and RF-CH generated surface storages are relatively insignificant with respect to total storage, yet provide the largest contribution to streamflow. The surface water volumes of initial, reset and cumulative error are relatively insignificant (i.e. appear as horizontal lines along y = 0 in the graphs) to the flow generation mechanisms and are therefore not shown.

4.5.2.2. Spatiotemporal variability of in-stream and overland flow generation

The in-stream and overland flow generation calculated by the HMC method (at the same snapshot times as in Figure 4.9) for the large July storm are shown in Figure 4.11. Prior to the storm, at day 216, the GW-CH component of streamflow over the entire stream is high and dominating. At this time, there are small patches of RF-CH generated stream water in places where little to no groundwater is discharging and where there is no upstream flow passing through. A portion of the wetland areas prior to the storm show GW-WL generated surface storage, a small

portion of which is feeding into the stream, which is more clearly apparent in the hydrograph of Figure 4.10. The speckled RF-WL water existing prior to the storm highlights areas where some ponding from rainfall has occurred that is yet to either runoff, infiltrate or evaporate. The source of this rain is attributed to smaller recent rainfall events (not shown). The bottom row of Figure 4.11 shows the amount of reset (or unknown) fraction across the catchment during the storm. Areas where the reset fraction is high correspond to areas where either no surface flow is occurring or ponding is insignificant (as defined in Section 4.3.3.3). This highlights areas where ponding processes take place, but in such small quantities of water that they are not of interest, particularly in relation to the streamflow hydrograph. As noted in Section 4.3.3.3, any reset cell is still tracked, which means that any surface flow out of a reset cell is also tracked so that the influence of these cells is accounted for.

At the peak of the large storm, at day 218, the fraction of GW-CH generation becomes diminished across the stream as rainfall generation mechanisms become dominant. The reduction of the fraction of GW-CH generation is matched by an increase in fractions of RF-CH, GW-WL and RF-WL generation. At day 218, an increase in the active part of the stream on the right arm (including upstream of the losing section) is shown in the RF-CH generation. The GW-WL generation on the wetlands at the peak of the storm is reduced. However, it is worth noting that the GW-WL water appears in the same area as where water has ponded, shown in the depth distribution in Figure 4.9.

As described in the stability criteria section 4.3.3.3, surface nodes containing less than 10^{-10} m^3 of water are excluded from analysis and are reset, which causes the 'speckled' effect that is seen adjacent to the upper reaches of the stream. This effect is attributed partly to the spatial variations in rill storage height across the wetlands. The small water storage at some wetland nodes relates to those wetland nodes not being saturated and water infiltrating quickly due to the high hydraulic conductivity near the surface.

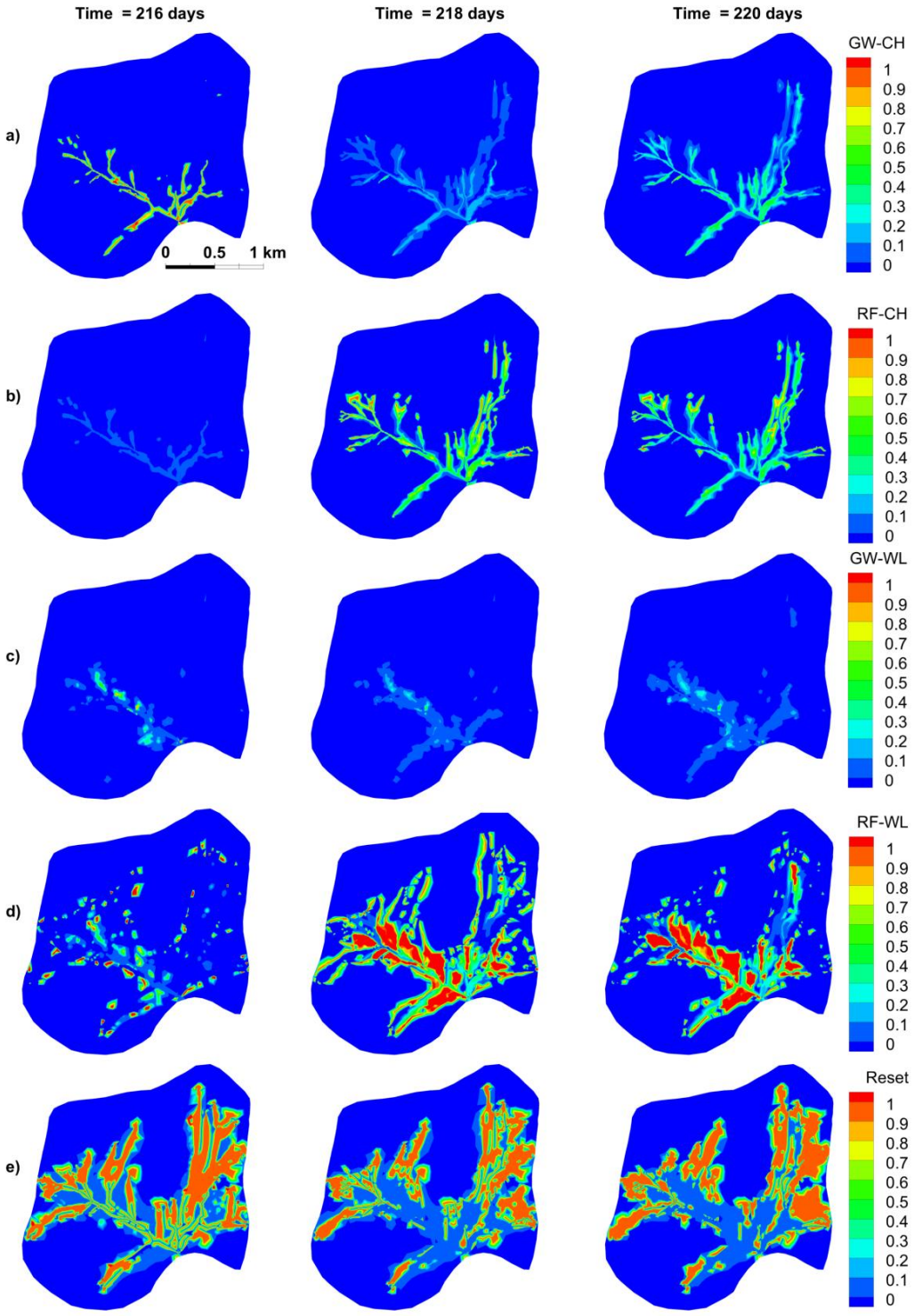

Figure 4.11: HMC calculated in-stream and overland flow generation for the Lehstenbach catchment – before peak (day 216), at peak (day 218) and after the peak (day 220). The flow generation components are: a) groundwater discharge to the channel (GW-CH), b) rainfall to the channel (RF-CH), c) groundwater discharge to the wetlands surfaces (GW-WL), and d) rainfall to the wetlands (RF-WL). The initial fractions are not shown as all initial water has been flushed from the catchment. The reset fractions are shown in row e).

After the peak of the storm event, at day 220, the GW-CH generation component starts to increase. This increase is most apparent in the lower reaches of the stream where the RF-CH generated streamflow has been mostly flushed from the stream. The RF-CH component is still strong in small isolated areas in upstream parts of the stream that are not flowing, and instead, are ponding. The wetlands receive more groundwater discharge after the storm, which is reflected in the extent of GW-WL generation across the catchment.

Analysis of the entire 2001 hydrological year allowed comparison of the longer term flow generation across the catchment to the July large storm event. Figure 4.12 shows box plots of the percent contribution of each of the flow generation mechanisms across the 7 model observation points depicted in Figure 4.4. The left plot shows the spread for the entire hydrological year and the right shows the spread for the large July storm (between days 17 and 20). The volume of water that passed through the outlet and locations 1-6 is determined by integrating over the streamflow hydrographs for each component of flow and dividing by the total volume of streamflow that passed through. Not shown are the fractions of 'forest' (maximum 0.3%), initial (maximum 0.05%) and reset (maximum 0.41%) and the cumulative error resulting from imperfect nodal fluid mass balances over the simulation (maximum -0.9%). These components are relatively insignificant in comparison to the four main flow generation mechanisms. This volumetric analysis indicates that the mechanisms for flow generation did not differ significantly across the Lehstenbach catchment, although greater variation can be seen across the focused period of the large July storm compared to the entire year. However, it is worth noting that the 'outliers' in the 'event' plot correspond to observation point 1, which contributes less than 1% of the flow over this event.

Comparison of the distribution of individual flow generation processes across the entire hydrological year showed surprising uniformity across the catchment. The similarities in flow generation processes over the year long time scale at the seven model observation locations are possibly due to the uniformly applied rainfall events and the simplified representation of the micro-topography across the wetlands.

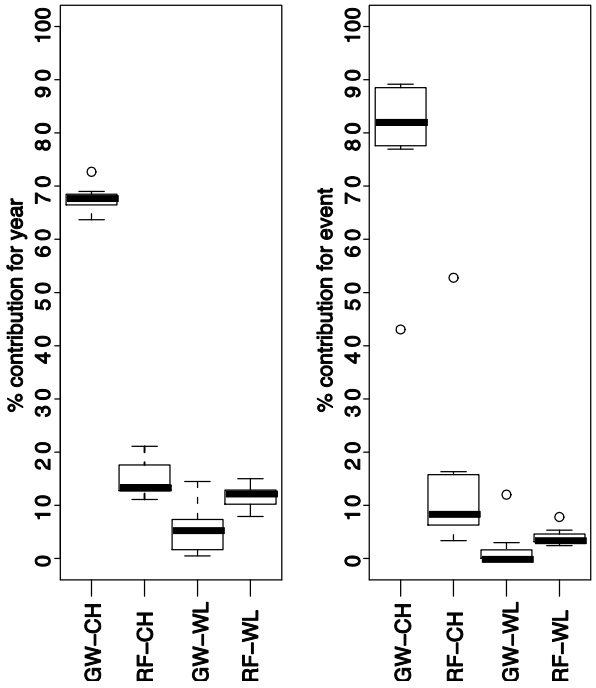

Figure 4.12: Box plots showing the spread of the average in-stream and overland flow generation mechanism contributions for the entire year and during the large storm event, across the 7 different model observation points. The thick black line represents the median; the box covers the inter quartile range (IQR) bounded by the lower and upper quartiles; the whiskers extend to the lowest and highest data point within the fences (where the fences are 1.5 x IQR above and below the upper and lower quartiles respectively); the circles represent data above and below the upper and lower fences respectively.

The distributions for the event scale show a larger spread across the seven model observation locations, which was also evident in the individual hydrographs. This difference in the drivers of streamflow across these observation points is possibly due to timing of the activation of WL-CH flow across different areas of wetlands, and the differences in head gradient at the stream interface driving GW-CH flow.

The catchment model shows a combination of simple processes varying in space and time, which leads to a complex culmination of in-stream and overland flow generation processes at the outlet. Rain falling in the forested areas mainly infiltrated and then recharged the underlying unconfined aquifer, which in turn fed the adjacent down-slope riparian wetlands and stream. Because of the 'rill storage' within the wetland areas, there is an aggregated 'fill and spill' mechanism that is averaged over the wetland areas. The rill storage provided a threshold to rainfall inducing runoff from the wetland areas. The GW-CH response to rainfall mimicked a dampened rainfall input. This GW-CH component appeared more

sensitive than the GW-WL component, which contributed very little to streamflow. The sensitivity of the GW-CH component is caused by the heads in the riparian wetlands controlling groundwater flow. As the wetlands and underlying unconfined aquifer are connected, increases in water levels in the wetlands from rainfall increases subsurface heads and hence increases the discharge of groundwater to the stream channel (i.e. GW-CH generation mechanism). Conversely, the slower, almost filtered response from the GW-WL generation mechanism is caused by: 1) the time delay in percolation recharging the unconfined aquifer from the forested areas; then 2) the slow flow of groundwater through the unconfined aquifers into the wetlands; then 3) the mobilisation of ponded water in the wetlands into the stream once the wetlands overtop into the stream.

4.5.2.3. Active versus contributing flow generation mechanisms

A comparison of the active and contributing flow generation processes for GW-CH, RF-CH and WL-CH is shown in Figure 4.13. In Figure 4.13a, the active component of GW-CH flow is clearly seen to be higher than the contributing processes which predominantly results from losing areas along the stream. It should be noted that the time lags in the stream also lead to a difference between the active and contributing components, although these are small in this catchment and hence do not play an obvious role. Similarly in Figure 4.13b and Figure 4.13c a much larger flux is evident of active RF-CH and WL-CH flow as opposed to the contributing portion at the outlet. This figure highlights the transient difference between the active and contributing processes in this catchment.

The long term ratio of contributing to active flow generation processes for WL-CH (0.78), RF-CH (0.34) and GW-CH (0.25) highlights the significant differences between active flow generation processes across the catchment and contributing flow generation processes driving outflow. Furthermore, the cumulative lines show how this dichotomy develops through time. This supports the need to differentiate between these active and contributing processes in interpreting streamflow hydrographs, and therefore, the need to separate the streamflow hydrograph properly.

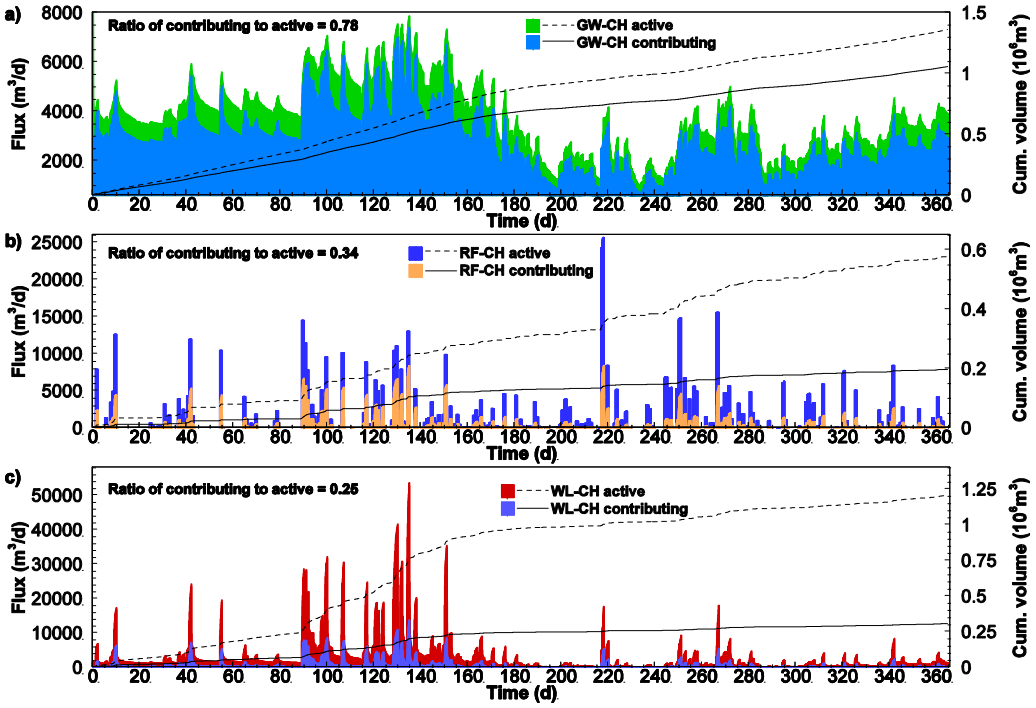

Figure 4.13: Comparison of active and contributing processes with respect to a) GW-CH, b) RF-CH, and c) WL-CH (where WL-CH = RF-WL + GW-WL). Note that the contributing component is superimposed on top of the active component in each of these graphs, i.e. they are not stacked. The long-term ratio of contributing to active processes is also noted in each of the plots, which highlights the average difference between the two. The dashed and dotted lines on each plot represent respectively the cumulative active and contributing components.

4.5.3. Comparison of wetland and catchment models

At the outlet of both models, GW-CH streamflow generation was fairly consistent across storms with only minor changes relative to the total streamflow hydrograph. The GW-CH component was seen to respond immediately to rainfall with no obvious lags in both models. Large changes in streamflow at the outlets for both models can be attributed to the overtopping of rills within the riparian wetlands driven by both RF-WL and GW-WL mechanisms. However, in the catchment model, the RF-CH component contributes significantly to total streamflow during the large storm event, which is attributable to the coarse model discretisation of the stream network. This discretisation does not capture the narrow nature of the actual channels, so that the channels in the model are wider than they are in reality. The surface area of the stream in the model captures additional rainfall that would not usually be attributed to the RF-CH flow

generation mechanism within the catchment. Overland flow from the wetlands in both models is dominated by RF-WL flow generation. The GW-WL component is almost as large as the RF-WL component in the wetland model; however, the GW-WL component is almost negligible at the outlet of the catchment model. The difference in the GW-WL component between the two models can be attributed to the discretisation of the wetlands. In the catchment model, the threshold behaviour to overland flow is captured, which is evident in the wetland model, but the catchment scale model does not capture the enhanced surface-subsurface mixing of the wetlands model, which results in a lot of the RF-WL water infiltrating and then discharging as GW-WL.

4.5.4. Limitations of wetland and catchment models

A number of assumptions were made within this modelling that limited the representation of reality, as well as any generalisations that can come from it. The main limitation of the wetland model is that it does not replicate a particular Lehstenbach wetland, hence there are no observed data to compare with, meaning the model can only be used for virtual experimentation.

For the catchment scale model, only outflow time series were available for calibration. As this was the only data used in evaluation of the model, there are likely to be multiple parameter sets that could yield the same Nash Sutcliffe efficiency, i.e. equifinality. Alternative parameter sets with equivalent model fits could potentially lead to significant differences in the spatiotemporal distribution of flow generation processes and hence influence the dynamics of contributing processes at the catchment outlet. The resulting non-uniqueness of processes elicited with the HMC method might not be representative of the actual processes occurring in the Lehstenbach catchment. This limitation could be addressed (at least in part) by using additional hydrometric data in model calibrations to further constrain the problem.

HMC analysis shows that the response of the wetlands in the catchment scale model seems to be consistent with the understanding of wetland runoff processes and the catchment behaviour in general; however, the effect of the mesh discretisation of the stream and wetlands in the catchment model mesh on the GW-CH response and WL-CH response still requires quantification. Refining the

coarse mesh would allow for better representation of the enhanced surface-subsurface mixing, as exhibited in the wetlands scale model, which is important in consideration of biogeochemical processes (*Frei et al*., 2012).

The subsurface response is affected by the subsurface boundary conditions, and no-flow boundaries in the subsurface prevent groundwater from flowing out through the subsurface, which leads to increased groundwater exfiltration near the outlet. Although this is generally consistent with the understanding of subsurface flows in the catchment based on previous studies (*Hauck*, 1999; *Lischeid et al*., 2002), a more thorough assessment of the effects of the subsurface boundary conditions on catchment outflow would be helpful to further refine our understanding of the system.

Model simulations would likely have been influenced by: (1) simplification of heterogeneity within soil types, (2) exclusion of preferential subsurface flow, and (3) spatiotemporal resolution of rainfall and evapotranspiration inputs (spatially uniform rather than distributed, daily rather than hourly rainfall and ET). It is expected that additional heterogeneity (e.g. within each soil layer) would lead to more complex stream-aquifer exchange patterns, although it is not expected that this would significantly alter the catchment response. Inclusion of shallow macropores in the forested areas of the catchment would allow rapid infiltration to the upper layer of the soil; however, this infiltrated water would be limited in recharging the aquifer due to the soils' saturated hydraulic conductivity below the extent of the macropores. The spatiotemporal resolution of the rainfall and ET could potentially have a large impact on the catchment response, particularly where short intense rainfall events lead to flashy streamflow responses, which would not be captured using the average daily rainfall. With respect to these assumptions, it is still expected that increased complexity of inputs would lead to at least the same or greater spatiotemporal variation in the different flow generation mechanisms. It is not expected that increased complexity would yield more homogeneous responses in in-stream and overland flow generation processes, although this is clearly yet to be tested. Furthermore, the influence of surface flow travel times, flow impediments and flow depletion processes are still important with respect to spatiotemporal variability of contributing flow generation processes.

4.5.5. Evaluation of HMC method implementation

The sub-timed scheme of the HMC method is an important improvement which allowed application to more complex problems than those studied in *Partington et al*. (2011, 2012) and *Li et al*. (2013). The sub-timed scheme was necessary in both of the models, significantly reducing the number of flow solution time-steps that would have been required with the previously developed HMC method (by 10^6 in the catchment year long simulation). The sub-timed scheme allowed the adaptive time-stepping scheme of the flow solution to perform as normal without tight restrictions on the maximum time-step. Complementary to this improvement, the stability constraints used in the improved HMC method were able to ensure stability of the cells in the simulations. The reset fractions resulting from cells that were reset when they met the criteria outlined in Section 4.3.3.3, highlighted areas that were of little interest with respect to overland flow generation processes. The reduction of active cells allowed faster computation and highlighted areas of little activity with respect to flow generation processes, which is reflected in the spatial distribution of the reset fraction (Figure 4.6, Figure 4.7 and Figure 4.11) and in the actual contributing fraction of flow from reset cells.

4.6. Conclusions

In this paper, an improved Hydraulic Mixing-Cell (HMC) method was developed that enables both active and contributing processes to be obtained from the outputs of Integrated Surface-Subsurface Hydrological Models (ISSHM), thereby enabling streamflow generation processes to be identified for catchments that include significant storage, travel times and losses. Specifically, the following improvements to the HMC method were made: (1) accounting for overland flow generation mechanisms, (2) implementing a sub-timed scheme, and (3) implementing HMC stability constraints.

This improved HMC approach was applied to two virtual experiments based on the Lestenbach catchment and a wetland typical of the catchment, which enabled (i) separation of simulated streamflow hydrographs into their constituent in-stream and overland flow generation mechanisms, (ii) quantification of the spatial and temporal variability for in-stream and overland flow generation mechanisms at contrasting spatial and temporal scales, and (iii) quantification of the degree to

which the active and contributing processes differ within the catchment model, leading to an improved understanding of simulated streamflow generation processes. The application of the HMC method in this study is a promising first step in the refinement of the method; however, as discussed in the model limitations, the catchment model would benefit from some improvements. Further development of the catchment model by further calibration using additional hydrometric data will serve to improve the veracity of the model for quantifying spatiotemporal variability within the Lehstenbach catchment. Furthermore, investigation into the influence of the no flow subsurface boundary conditions used and the areal mesh discretisation would also help to make the catchment model more representative of the Lehstenbach catchment.

Further development of the HMC method is recommended by greater subdivision of the rainfall driven overland flow generation mechanisms into saturation-excess and infiltration-excess. It would be extremely useful to also develop an automatic definition of the stream based on flow depth, velocity and direction. In addition, the HMC method should be further expanded to track flow in the subsurface, which would allow tracking of other flow domains, for example, from macropores and fractures. Extension to the subsurface would also allow identification of the source areas of groundwater discharging to the surface. The inclusion of time stamps to the HMC fractions would also improve the HMC method, and allow analysis into event and pre-event water contributions.

The composition of streamflow with respect to the different surface runoff generating processes entails important information on runoff processes and mechanisms during large rainfall events and during dry periods. The methodology presented here provides a tool to decipher and deconvolute the integrated streamflow signal using numerical models. This improves assessment of catchment functioning within the 'hypothetical reality' of the model. This is an important aspect of the HMC method when applied to physically distributed models that have no a priori assumption of flow generation processes. Use of the HMC method provides a necessary assessment of whether or not a catchment model behaves in the way desired, or more importantly, the way the catchment processes are conceptualised. In that sense, it is useful for a 'soft calibration' based on understanding of catchment functioning from field observations. This

can only serve to strengthen the relatively small arsenal of tools currently available for analysing catchment models.

Acknowledgements

The authors gratefully acknowledge Pascal Goderniaux and two anonymous reviewers whose reviews greatly improved the manuscript. The authors also gratefully acknowledge the assistance of Grace Lin in developing figures for the manuscript. This work is supported by the Australian Research Council through its Linkage scheme and the South Australian Department for Water as the industry partner under grant number LP0668808. Parts of this research were funded by the Swiss National Foundation, Ambizione grant PZ00P2_126415. The views expressed in this paper are solely those of the authors.

Chapter 5

5 Thesis Conclusions

The streamflow hydrograph entails important information on flow generation processes during large rainfall events and during dry periods. The streamflow hydrograph is one of the most important hydrological descriptors available, containing the pertinent information of flow maxima and the total volume of water flowing out of a catchment over time. This information is critical for management of flooding and water resources. The understanding of where stream water originates from in the hydrosphere and the processes by which it reaches the stream underpins catchment hydrology. Research to understand these processes is being increasingly carried out utilising physics-based fully Integrated Surface-Subsurface Hydrological Models (ISSHM). In the absence of required field data, such models are necessary for improving our understanding of catchment hydrological response. To understand the response, it is critical to understand the nature in which the processes of flow generation across a catchment and at different periods in time express themselves in the streamflow hydrograph, whilst accounting for the processes of flow depletion. However, even though detailed spatiotemporal outputs from ISSHMs have provided some insight into catchment functioning, the interpretation of all of this information into an understanding of how all of the flow generation processes across a catchment express themselves in the streamflow hydrograph has yet to be realised. In a modelling framework, this research has achieved this through the development and application of a new method which identifies and quantifies streamflow generation contributions allowing full deconvolution of the streamflow hydrograph into its constituent components of streamflow generation.

5.1. Research contributions

The overall contribution of this thesis was in improving the interpretation of in-stream and overland flow generation mechanisms from ISSHMs (Objective 1), and the applications this allowed (Objectives 2 to 4). The improvements in this thesis were achieved through development of a new method that enables identification and quantification of the active and contributing processes from the outputs of ISSHMs, thereby enabling streamflow generation processes to be analysed for catchments that include significant storage, travel times and losses.

Use of the HMC method provides a necessary assessment of whether or not a catchment model behaves in the way desired, or more importantly, the way the catchment processes are conceptualised. The method can be used for a 'soft calibration' based on understanding of catchment functioning from real observations. This can only serve to strengthen the relatively small arsenal of tools currently available for analysing catchment models.

Specifically, in meeting the objectives of this research laid out in the introduction, the following research contributions were made:

1. A Hydraulic Mixing-Cell method was developed to quantify the contribution of flow generation mechanisms to streamflow, allowing separation of the streamflow hydrograph into its constituent flow generation components (i.e. groundwater discharge and direct rainfall to the stream, and groundwater discharge and direct rainfall to overland areas). Because the HMC method tracks the streamflow generation mechanisms along the stream, temporal and spatial components that affect these mechanisms can be accounted for. The HMC method correctly handles dynamic complex flow regimes (rapid changes of gaining stream to losing stream and vice versa), accounts for storage effects, flow impediments and the travel times that occur within a catchment. The method easily handles the dynamic nature of varying flow regimes in large and complex systems (e.g. the Lehstenbach catchment). The only data requirements for the HMC method are the fluxes at each cell and surface water depths, which are part of the flow solution. By using this method, contributing processes can be identified and quantified. Improved knowledge of catchment processes as simulated by HydroGeoSphere was

obtained through Hydraulic Mixing-Cell analysis, with meaningful separation of the streamflow hydrograph indicating how overland and in-stream flow generation processes drive streamflow.

2. A benchmark against which baseflow separation methods can be tested was developed by simulating flow in a hypothetical V-catchment in HGS and using the HMC method to provide the baseflow contribution to total streamflow at the outlet of the catchment. This benchmark was used to determine the potential error in commonly used automated methods for estimation of in-stream groundwater contributions to streamflow. The numerical experiments in this showed that even in the "simple" hypothetical V-catchment, baseflow dynamics are complex. This complexity in baseflow dynamics affected the performance of the commonly used automated separation methods, which resulted in unsatisfactory performance of each method examined in at least one of the events and scenarios considered. The potential error was found to be significant in automated methods for estimating groundwater contributions to streamflow, and this warrants caution in overvaluing their outputs. It is perhaps the case that the uncertainty associated with simple automated methods precludes their use for providing anything more than very rough estimates of baseflow.
3. The first investigation – using an ISSHM – was conducted into the spatiotemporal variability in both overland and in-stream flow generation mechanisms. This was done using two models of a wetland and catchment, from a case study of a real catchment. The spatiotemporal variability was analysed through snapshots in time during a large storm event, and through hydrographs at a number of points within each of the models. Both models exhibited significant spatial variability in flow generation processes. In the catchment model, temporal variability of streamflow generation at a number of locations was seen to be significant over a large storm, but similarities increased using a longer term annual average of flow in-stream and overland flow generation processes.
4. The first investigation – using an ISSHM – was conducted into the dichotomy that exists between 'active' and 'contributing' streamflow generation mechanisms within a modelling framework. Differences

between the active and contributing processes were quantified by the long term ratio between active and contributing processes. It was found that accounting for in-stream and overland losses and in-stream and overland flow travel time is necessary in accurately quantifying the constituent in-stream and overland flow generation components of streamflow. It is therefore recommended to employ the HMC method in ISSHM studies of various flow generation processes.

5. The HMC method developed in this research was implemented in the HGS code. This implementation means that all of the analyses conducted in this research can be carried out in models built in HGS using simple instructions in the HGS pre-processor.

5.2. Research limitations

Limitations of this research were due to current modelling limitations, scope of research and time-constraints. The limitations that arose are detailed as follows:

1. *Modelling limitations:* A main limitation of this research lay within the ability to run a large number of (tens and hundreds of simulations) or long term models scenarios (years). This is due to the lengthy model run-times (of the order of weeks for each simulation in each of the research papers) that result from solving the highly non-linear partial differential equations describing flow. A parallel version of HGS has now been developed which should reduce the model run-times and allow a greater number of scenarios to be explored in future research. Another limitation associated with the run-times relates to the accuracy required in the HGS flow solution in order to ensure stability in the HMC method and also ensure an acceptable level of error. Despite this being highlighted as a limitation, it should be noted that it is good modelling practice to ensure tight convergence criteria, resulting in minimal nodal fluid mass balance errors as opposed to global mass balance errors.
2. *Limitations in investigation of automated baseflow separation methods:* The investigation of commonly used automated baseflow separation methods was limited by the number of scenarios run and scenario time-length in the hypothetical catchment used. The shape of the catchment considered was rectangular, however, effects of convergent and divergent

catchment shapes were not considered. The characterisation of physical parameters within the catchment was relatively simple, without consideration of multilayered soils or heterogeneous soil properties. The hydrological forcing was applied in a spatially uniform manner and at a coarse temporal scale (daily) in these simulations, although these effects may be important in the catchment response of baseflow generation. This research focused on commonly used automated methods that rely only on the streamflow hydrograph for the baseflow separation, however there has been an emergence of physically based filters (e.g. *Furey and Gupta*, 2001, 2003; *Huyck et al.*, 2005) which were not considered.

3. *Limitations of streamflow generation analysis:* The HMC method developed in this research was used to delineate the direct groundwater discharge and rainfall to streams and overland areas. A common consideration of overland flow generation mechanisms not considered in this research was the rainfall runoff mechanisms of infiltration excess (Hortonian) and saturation excess (Dunne). These processes were not considered in the case study of this research, although in most other catchments, these mechanisms will be of interest. The use of ISSHMs in building intuition of catchment functioning is highly valuable, although it is also dependent on the assumptions in the model (even if these are deemed reasonable). In consideration of streamflow generation mechanisms, real observation will always be the most important driver for advancing the science. However, as highlighted throughout this thesis, the conceptual understanding of streamflow generation processes can be built from ISSHMs.

5.3. Recommendations for future work

This research has opened up a new way of analysing and interpreting flow processes using ISSHMs. There are still further applications of the HMC method that would benefit research utilising ISSHMs and address the limitations identified above. It is recommended that the HMC method be expanded to improve analysis and interpretation of subsurface flow processes including flow through: saturated and unsaturated dual continuum media, fractures, and macro-pores. Further development of the HMC method is recommended by greater subdivision of the rainfall driven overland flow generation mechanisms into

saturation-excess and infiltration-excess. Extension to the subsurface would also allow identification of the source areas of groundwater discharging to the surface. Furthermore, the inclusion of time stamps to the HMC fractions would serve to improve the HMC method, and allow analysis into event and pre-event water contributions. Application of the HMC method encompassing all of the above recommendations would provide a highly comprehensive analysis of catchment functioning and provide complete analysis of the different aspects of streamflow generation as shown in Figure 5.1 (adapted from *Sklash and Farvolden*, 1979). This research considered the flow generation delivery mechanisms without distinction of the overland flow generation mechanisms, i.e. infiltration excess and saturation excess overland flow.

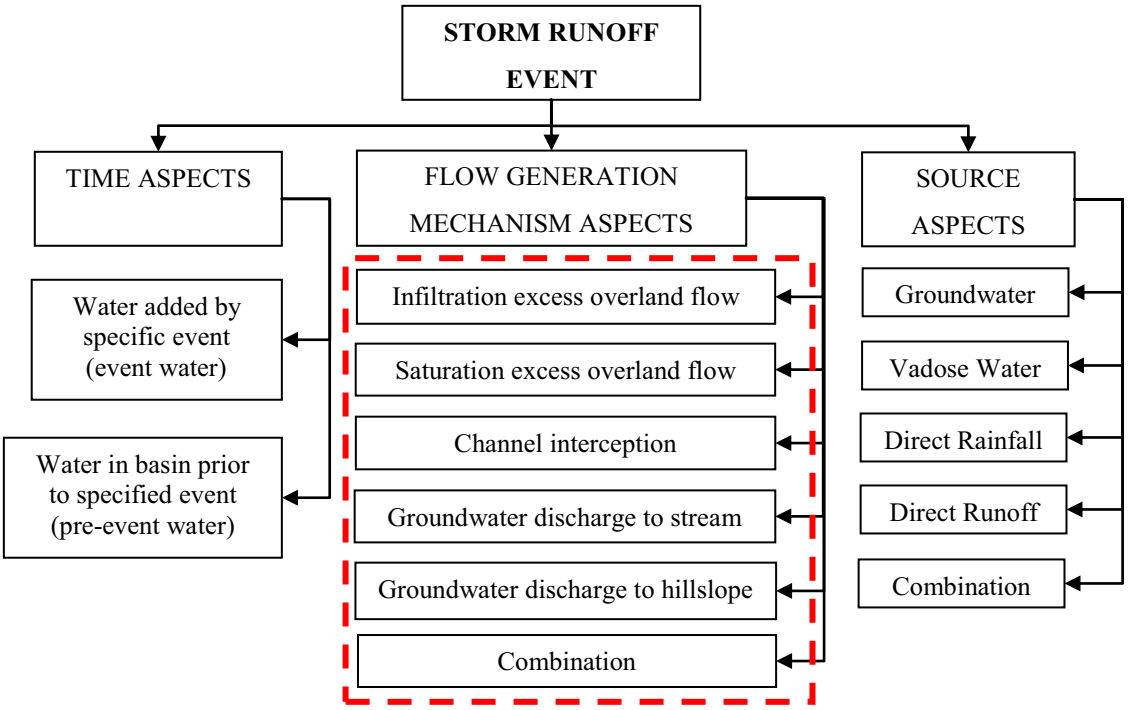

Figure 5.1: Comprehensive conceptualisation of catchment response to rainfall (adapted from *Sklash and Farvolden*, 1979). The dashed red line indicates the aspects considered in this research, although without distinction of overland rainfall driven mechanisms (i.e. infiltration excess (Hortonian) or saturation excess (Dunne)).

The HMC method presented in this thesis can be applied within any ISSHM, and as part of this research has been coded into the HGS code to allow other HGS users the ability to easily utilise it. For example, this HGS implementation has already been used outside of this research in *Sebben* (2011) and *Li et al.* (2012) and is currently being used in a number of other research projects. It is recommended that the HMC method be employed in future versions of other

ISSHM codes. This is relatively simple as the coding of the HMC method requires only that all components of the nodal fluid mass balance (inflows, outflows, and changes in storage) and nodal neighbour relations be output or passable within the code. The HMC method could be very beneficial in future model inter-comparison studies to compare the constituent components of the streamflow hydrograph and spatiotemporal flow generation.

With respect to the application of the HMC method in investigating potential errors in commonly used automated baseflow separation methods, further work is required to understand the appropriate use of baseflow separation methods. More complex baseflow separation methods than those considered in this study should be tested in future studies. Physically based filters (e.g. *Furey and Gupta, 2001*, 2003; *Huyck et al.*, 2005) could prove to be more robust. This is because they provide a physically based relation of rainfall and ET (and other physical parameters) to baseflow.

In all of the simulations carried out in this research, the characterisation of hydrological forcing and distribution of catchment characteristics could be improved. Future studies should aim to elucidate the spatial and temporal scale dependence of flow generation mechanisms. In the studies using hypothetical catchments for numerical experimentation, the impact of variations in geology, topography and vegetation, should be investigated by incrementally adding layers of complexity to similar models in order to try and understand flow generation dynamics.

References

Adar, E.M., S.P. Neuman, and D.A. Woolhiser (1988), Estimation of Spatial Recharge Distribution Using Environmental Isotopes and Hydrochemical Data .1. Mathematical-Model and Application to Synthetic Data, *Journal of Hydrology*, 97:251-277.

Ambroise, B. (2004), Variable 'active' versus 'contributing' areas or periods: a necessary distinction, *Hydrological Processes*, 18: 1149–1155, doi:10.1002/hyp.5536.

Arnold, J.G., P.M. Allen, R. Muttiah, and G. Bernhardt (1995), Automated Base-Flow Separation and Recession Analysis Techniques, *Ground Water*, 33: 1010-1018.

Arnold, J.G., and P.M. Allen. (1999), Automated methods for estimating baseflow and ground water recharge from streamflow records, *Journal of the American Water Resources Association*, 35: 411-424.

Barnes, B. (1939), The structure of discharge-recession curves, *Transaction of the American Geophysical Union*, 20: 721-725.

Becker, M.W., T. Gerogian, H. Ambrose, J. Siniscalchi, K. Frederick (2004), Estimating flow and flux of ground water discharge using water temperature and velocity, *Journal of Hydrology*, 296: 221-233.

Bishop, K., J. Seibert, S. Köhler, and H. Laudon (2004), Resolving the double paradox of rapidly mobilized old water with highly variable responses in runoff chemistry, *Hydrological Processes*, 18: 185–189, doi: 10.1002/hyp.5209.

Brunner, P., P.G. Cook, and C.T. Simmons (2009a), Hydrogeologic controls on disconnection between surface water and groundwater, *Water Resources Research*, 45, W01422, doi:10.1029/2008WR006953.

Brunner, P., C.T. Simmons, and P.G. Cook (2009b), Spatial and temporal aspects of the transition from connection to disconnection between rivers, lakes and groundwater, *Journal of Hydrology*, 376:159-169. doi:10.1016/j.jhydrol.2009.07.023.

Brunner, P., and C.T. Simmons (2011), HydeoGeoSphere: A fully integrated physically based hydrological model, *Ground Water*, doi:10.1111/j.1745-6584.2011.00882.x.

Boughton, W.C. (1993), A hydrograph-based model for estimating the water yield of ungauged catchments, Paper presented at *Hydrology and Water Resources Symposium*, Inst. of Eng. Aust., Newcastle, N.S.W.

Brutsaert, W., and J.L. Nieber (1977), Regionalized Drought Flow Hydrographs from a Mature Glaciated Plateau, *Water Resources Research*, 13: 637-644.

Campana, M.E., and E.S. Simpson (1984), Groundwater Residence Times and Recharge Rates Using a Discrete-State Compartment Model and C-14 Data. *Journal of Hydrology*, 72:171-185.

Camporese, M., C. Paniconi, M. Putti, and S. Orlandini (2010), Surface-subsurface flow modeling with path-based runoff routing, boundary condition-based coupling, and assimilation of multisource observation data, *Water Resources Research*, 46, W02512, doi:10.1029/2008WR007536.

Carle, S.F. and G.E. Fogg (1996), Transition Probability-Based Indicator Geostatistics, *Mathematical Geology*, 28(4): 453–476, doi:10.1007/BF02083656.

Carsel, R. F., and R.S. Parrish (1988), Developing Joint Probability-Distributions of Soil-Water Retention Characteristics, *Water Resources Research*, 24:755-769.

Chapman, T. (1991), Evaluation of Automated Techniques for Base-Flow and Recession Analyses – Comment, *Water Resources Research*, 27: 1783-1784.

Chapman, T. (1999), A comparison of algorithms for stream flow recession and baseflow separation, *Hydrological Processes*, 13: 701-714.

Chapman, T.G. (2003), Modelling stream recession flows, *Environmental Modelling and Software*, 18:683-692.

Chow, V.T. (1959), *Open channel hydraulics*, McGraw-Hill, New York.

Cook, P.G., G. Favreau, J.C. Dighton and S. Tickell (2003), Determining natural groundwater influx to a tropical river using radon, chlorofluorocarbons and ionic environmental tracers, *Journal of Hydrology*, 277: 74-88.

Cook, P.G., C. Wood, T. White, C.T. Simmons, T. Fass and P. Brunner (2008), Groundwater inflow to a shallow, poorly-mixed wetland estimated from a mass blance of radon, *Journal of Hydrology*, 354: 213-226.

Croton, J.T., and D.A. Barry (2001), WEC-C: a distributed, deterministic catchment model - theory, formulation and testing, *Environmental Modelling and Software*, 16:583-599.

Ebel, B.A. and K. Loague (2006), Physics-based hydrologic-response simulation: Seeing through the fog of equifinality, *Hydrological Processes*, 20(13): 2887-2900, doi:10.1002/hyp.6388.

Ebel, B.A., K. Loague, D.R. Montgomery, and W.E. Dietrich (2008), Physics-based continuous simulation of long-term near-surface hydrologic response for the Coos Bay experimental catchment, *Water Resources Research*, 44, W07417, doi:10.1029/2007WR006442.

Ebel, B.A., B.B. Mirus, C.S. Heppner, J. E. VanderKwaak, and K. Loague (2009), First-order exchange coefficient coupling for simulating surface water-groundwater interactions: parameter sensitivity and consistency with a physics-based approach, *Hydrological Processes*, 23:1949-1959.

Eckhardt, K. (2005), How to construct recursive digital filters for baseflow separation, *Hydrological Processes*, 19: 507-515.

Eckhardt, K. (2008), A comparison of baseflow indices, which were calculated with seven different baseflow separation methods, *Journal of Hydrology*, 352:168-173.

Facchi, A., B. Ortuani, D. Maggi, and C. Gandolfi. (2004), Coupled SVAT-groundwater model for water resources simulation in irrigated alluvial plains, *Environmental Modelling and Software*, 19:1053-1063.

Fenicia, F., H.H.G. Savenije, P. Matgen, and L. Pfister (2006), Is the groundwater reservoir linear? Learning from data in hydrological modelling, *Hydrology and Earth Systems Science*, 10: 139-150.

Ferket, B.V.A., B. Samain, and V.R.N. Pauwels (2010), Internal validation of conceptual rainfall-runoff models using baseflow separation, *Journal of Hydrology*, 381: 158-173.

Fleckenstein, J.H., S. Krause, D.M. Hannah, and F. Boano (2010), Groundwater-surface water interactions: New methods and models to improve understanding of processes and dynamics, *Advances in Water Resources*, 33(11): 1291-1295. doi:10.1016/j.advwatres.2010.09.011.

Freeze, R.A. and R.L. Harlan (1969), Blueprint for a physically-based, digitally-simulated hydrologic response model, *Journal of Hydrology*, 9:237-258.

Freeze, R.A. (1972), Role of Subsurface Flow in Generating Surface Runoff 1. Base Flow Contributions to Channel Flow, *Water Resources Research*, 8: 609-623.

Frei, S., G. Lischeid, and J.H. Fleckenstein (2010), Effects of micro-topography on surface-subsurface exchange and runoff generation in a virtual riparian wetland - A modeling study, *Advances in Water Resources*, 33(11): 1388-1401, doi:10.1016/j.advwatres.2010.07.006.

Frei, S., K.H. Knorr, S. Peiffer, and J.H. Fleckenstein (2012), Surface micro-topography causes hot spots of biogeochemical activity in wetland systems: A virtual modeling experiment, *Journal of Geophysical Research*, 117, G00N12, doi:10.1029/2012JG002012.

Furey, P.R., and V.K. Gupta (2001), A physically based filter for separating base flow from streamflow time series, *Water Resources Research*, 37(11): 2709-2722.

Furey, P.R., and V.K. Gupta (2003), Tests of two physically based filters for base flow separation, *Water Resources Research*, 39(10): 1297.

Gaukroger, A.M., and A.D. Werner (2011), On the Panday and Huyakorn surface-subsurface hydrology test case: analysis of internal flow dynamics, *Hydrological Processes*, 25: 2085-2093.

Gerstberger, P. (2001), Waldökosystemforschung in Nordbayern, Die Bitök-Untersuchungsflächen im Fichtelgebirge und Steigerwald, in: Bayreuther Forum Ökologie, edited by: BITÖ K, B. I. f. T. Ö ., BITÖK, Bayreuther Institut für Terrestrische Ökosystemforschung, Bayreuth, 193 pages.

Gilfedder, M., G.R. Walker, W.R. Dawes, and M.P. Stenson (2009), Prioritisation approach for estimating the biophysical impacts of land-use change on stream flow and salt export at a catchment scale, *Environmental Modelling and Software*, 24:262-269.

Goderniaux, P., S. Brouyere, H. J. Fowler, S. Blekinsop, R. Therrien, P. Orban, and A. Dassargues (2009), Large scale surface-subsurface hydrological model to assess climate change impacts on groundwater reserves, *Journal of Hydrology*, 373: 122-138, doi:10.1016/j.jhydrol.2009.04.017.

Goderniaux, P., S. Brouyère, S. Blenkinsop, A. Burton, H. J. Fowler, P. Orban, and A. Dassargues (2011), Modeling climate change impacts on groundwater resources using transient stochastic climatic scenarios, *Water Resources Research*, 47, W12516, doi:10.1029/2010WR010082.

Gupta, H.V., S. Sorooshian, and P.O. Yapo (1999), Status of automatic calibration for hydrologic models: Comparison with multilevel expert calibration, *Journal of Hydrologic Engineering*, 4: 135-143.

Halford K.J., and G.C. Mayer (2000), Problems Associated with Estimating Ground Water Discharge and Recharge from Stream-Discharge Records, *Ground Water,* 38: 331-342.

Hall, F.R. (1968), Base-Flow Recessions-a Review, *Water Resources Research*, 4: 973-983.

Hattermann, F., V. Krysanova, F. Wechsung, and M. Wattenbach (2004), Integrating groundwater dynamics in regional hydrological modelling, *Environmental Modelling and Software*, 19:1039-1051.

Hauck, A. (1999), Hydrological Charakterization of the Lehstenbach Catchment. Unpublished Diploma Thesis, Department of Ecological Modelling, University of Bayreuth, Bayreuth, Germany.

Hewlett, J. D., and C. A. Troendle (1975), Non-point and diffuse water sources: A variable source area problem, Pages 21-46 in Watershed Management, *American Society of Civil Engineering*, New York.

Huyck, A.A.O., V.R.N. Pauwels, and N.E.C. Verhoest (2005), A base flow separation algorithm based on the linearized Boussinesq equation for complex hillslopes, *Water Resources Research*, 41.

HydroGeoLogic Inc. (2006), *MODHMS: a comprehensive MODFLOW based hydrologic modeling system, Version 3.0, Code documentation and user's guide*, HydroGeoLogic Inc., Herndon, VA.

Ivanov, V.Y., E.R. Vivoni, R.L. Bras, and D. Entekhabi (2004), Catchment hydrologic response with a fully distributed triangulated irregular network model, *Water Resources Research*, 40, W11102, doi:10.1029/2004WR003218.

Jacks, G., and A.C. Norrström (2004), Hydrochemistry and hydrology of forest riparian wetlands, *Forest Ecology and Management*, 196(2-3): 187–197, doi: 10.1016/j.foreco.2004.01.055.

Jones, J.P., E.A. Sudicky, A.E. Brookfield, and Y.J. Park (2006), An assessment of the tracer-based approach to quantifying groundwater contributions to streamflow, *Water Resources Research*, 42.

Kampf, S. K., and S. J. Burges (2007), A framework for classifying and comparing distributed hillslope and catchment hydrologic models, *Water Resources Research*, 43, W05423, doi:10.1029/2006WR005370.

Kollet, S.J. and R.M. Maxwell (2006), Integrated surface-groundwater flow modeling: A free-surface overland flow boundary condition in a parallel groundwater flow model, *Advances in Water Resources*, 29(7): 945-958, doi:10.1016/j.advwatres.2005.08.006.

Knorr, K.H., B. Glaser, and C. Blodau (2008), Fluxes and C-13 isotopic composition of dissolved carbon and pathways of methanogenesis in a fen soil exposed to experimental drought, *Biogeosciences*, 5: 1457–1473.

Kristensen, K., and S. Jensen (1975), A model for estimating actual evapotranspiration from potential evapotranspiration, *Nordic Hydrology*, 6(3), 170–188, doi: 10.2166/nh.1975.011.

Kruse, J.,B. Lennartz, and P. Leinweber (2008), A modified method for measuring saturated hydraulic conductivity and anisotropy of fen peat samples, *Wetlands*, 28(2): 527–531, doi:10.1672/07-153.1.

Li, L., H.R. Maier, M.F. Lambert, C.T. Simmons, and D. Partington (2012), Framework for Assessing and Improving the Performance of Recursive Digital Filters for Baseflow Estimation with Application to the Lyne and Hollick Filter, Accepted article in *Environmental Modelling and Software*.

Li, Q., A.J.A. Unger, E.A. Sudicky, D. Kassenaar, E.J. Wexler, and S. Shikaze (2008), Simulating the multi-seasonal response of a large scale watershed with a 3D physically-based hydrologic model, *Journal of Hydrology*, 357: 317-336, doi:10.1016/j.jhydrol.2008.05.024.

Liggett, J. E., Werner, A. D. and Simmons, C. T. (2012), Influence of the first-order exchange coefficient on simulation of coupled surface-subsurface flow, *Journal of Hydrology*, 414-415, 503-515, doi:10.1016/j.jhydrol.2011.11.028.

Linsley, R.K., M.A. Kohler, J.L.H. Paulhus, and J.S. Wallace (1958), *Hydrology for Engineers*, McGraw Hill, New York.

Lischeid, G., A. Kolb, and C. Alewell (2002), Apparent translatory flow in groundwater recharge and runoff generation, *Journal of Hydrology*, 265(1-4): 195–211, doi:10.1016/S0022-1694(02)00108-7.

Loague, K., and J.E. Vanderkwaak, (2002), Simulating hydrological response for the R-5 catchment: comparison of two models and the impact of roads, *Hydrological Processes*, 16: 1015-1032, doi:10.1002/hyp.316.

Loague, K., C.S. Heppner, B.A. Ebel, and J.E. Vanderkwaak (2010), The quixotic search for a comprehensive understanding of hydrologic response at the surface: Horton, Dunne, Dunton, and the role of concept-development simulation, *Hydrological Processes*, 24: 2499-2505, doi:10.1002/hyp.7834.

Lyne, V., and M. Hollick, (1979), Stochastic time-variable rainfall-runoff modelling. *Hydrology and Water Resources Symposium*, Institution of Engineers, Australia, Perth, 89-92.

Maillet, E. (1905), *Essai d'Hydraulique Souterraine et Fluviale*, Hermann, Paris. 218.

Mau, D.P., and T.C. Winter. (1997), Estimating Ground-Water Recharge from Streamflow Hydrographs for a Small Mountain Watershed in a Temperate Humid Climate, New Hampshire, USA, *Ground Water*, 35: 291-304.

Maxwell, R.M., and S.J. Kollet (2008), Quantifying the effects of three-dimensional subsurface heterogeneity on Hortonian runoff processes using a coupled numerical, stochastic approach, *Advances in Water Resources*, 31: 807-817, doi:10.1016/j.advwatres.2008.01.020.

McCallum, J.L., P.G. Cook, P. Brunner, and D. Berhane (2010), Solute dynamics during bank storage flows and implications for chemical base flow separation, *Water Resources Research*, 46.

McCuen, R.H. (2005), *Hydrologic Analysis and Design*, Prentice Hall.

McGlynn, B.L., and J.J. McDonnell (2003), Quantifying the relative contributions of riparian and hillslope zones to catchment runoff, *Water Resources Research*, 39.

McGuire, K.J., and J. J. McDonnell (2006), A review and evaluation of catchment transit time modelling, *Journal of Hydrology*, 330:543-563.

McLaren, R.G., P.A. Forsyth, E.A. Sudicky, J.E. VanderKwaak, F.W. Schwartz, and J.H. Kessler (2000), Flow and transport in fractured tuff at Yucca Mountain: numerical experiments on fast preferential flow mechanisms, *Journal of Contaminant Hydrology*, 43:211-238.

Mirus, B.B., K. Loague, J.E. VanderKwaak, S.K. Kampf, and S.J. Burges (2009), A hypothetical reality of Tarrawarra-like hydrologic response, *Hydrological Processes*, 23:1093-1103.

Mirus, B. B., B. A. Ebel, C. S. Heppner, and K. Loague (2011a), Assessing the detail needed to capture rainfall-runoff dynamics with physics-based hydrologic response simulation, *Water Resources Research*, 47, W00H10, doi:10.1029/2010WR009906.

Mirus, B.B., K. Loague, N.C. Cristea, S.J. Burges, and S.K. Kampf (2011b), A synthetic-hydrologic response dataset, *Hydrological Processes*, 25(23): 3688-3692. doi:10.1002/hyp.8185.

Moriasi, D.N., Arnold, J.G., Van Liew, M.W., Bingner, R.L., Harmel, R.D., and T.L. Veith (2007), Model Evaluation Guidelines for Systematic Quantification of Accuracy in Watershed Simulations, *Transactions of the American Society of Agricultural and Biological Engineers*, 50: 885-900.

Nathan, R.J., and T.A. McMahon (1990), Evaluation of Automated Techniques for Base-Flow and Recession Analyses, *Water Resources Research*, 26: 1465-1473.

Panday, S., and P.S. Huyakorn (2004), A fully coupled physically-based spatially-distributed model for evaluating surface/subsurface flow, *Advance in Water Resources*, 27: 361-382, doi:10.1016/j.advwatres.2004.02.016.

Park, Y.J., E.A. Sudicky, S. Panday, and G. Matanga (2009), Implicit Subtime Stepping for Solving Nonlinear Flow Equations in an Integrated Surface-Subsurface System, *Vadose Zone Journal*, 8(4): 825-836, doi:10.2136/vzj2009.0013.

Park, Y.-J., E. A. Sudicky, A. E. Brookfield, and J. P. Jones (2011), Hydrologic response of catchments to precipitation: Quantification of mechanical carriers and origins of water, *Water Resources Research*, 47, W12515, doi:10.1029/2011WR010075.

Partington, D., P. Brunner, C.T. Simmons, R. Therrien, A.D. Werner, G.C. Dandy, H.R. Maier (2011), A hydraulic mixing-cell method to quantify the groundwater component of streamflow within spatially distributed fully integrated surface water - groundwater flow models, *Environmental Modelling and Software*, 26:886-898, doi:10.1016/j.envsoft.2011.02.007.

Partington, D., P. Brunner, C.T. Simmons, A.D. Werner, R. Therrien, H.R. Maier, G.C. Dandy (2012), Evaluation of outputs from automated baseflow separation methods against simulated baseflow from a physically based, surface water-groundwater flow model, *Journal of Hydrology*, 458-459: 28-39, doi:10.1016/j.jhydrol.2012.06.029.

Pettyjohn, W.A., and R. Henning (1979), Preliminary estimate of ground-water recharge rates, related streamflow and water quality in Ohio. Ohio State University Water Resources Center Project Completion Report Number 552.

Piggott, A.R., S. Moin, and C. Southam (2005), A revised approach to the UKIH method for the calculation of baseflow, *Hydrological Sciences Journal-Journal Des Sciences Hydrologiques*, 50: 911-920.

Price, J. S., R.G. McLaren, D.L. Rudolph (2010), Landscape restoration after oil sands mining: conceptual design and hydrological modelling for fen reconstruction, *International Journal of Mining, Reclamation and Environment*, 24(2):109–123, doi:10.1080/17480930902955724.

Rutledge, A.T. (1998), Computer programs for describing the recession of ground-water discharge and for estimating mean ground-water recharge and discharge from streamflow data, US Geological Survey Water-Resources Investigations Report, 98-4148.

Sayama, T., and J.J. McDonnell (2009), A new time-space accounting scheme to predict stream water residence time and hydrograph source components at the watershed scale, *Water Resources Research*, 45.

Schwartz, S.S. (2007), Automated algorithms for heuristic base-flow separation, *Journal of the American Water Resources Association*, 43: 1583-1594.

Schlotzhauer, S.M., and J.S. Price (1999), Soil water flow dynamics in a managed cutover peat field, Quebec: Field and laboratory investigations, *Water Resources Research*, 35(12): 3675–3683, doi:10.1029/1999WR900126.

Sebben, M.L. (2011), Evaluation and Inter-Code Comparison of Complex, Catchment-Scale Hydrological Models, Honours Thesis, Flinders University, Bedford Park, Adelaide, South Australia.

Sebben, M.L., A.D. Werner, J.E. Liggett, D. Partington, and C.T. Simmons (2012), On the testing of fully integrated, surface-subsurface hydrological models, *Hydrological Processes*, doi:10.1002/hyp.9630.

Singh, K.P., and J.B. Stall, (1971), Derivation of Base Flow Recession Curves and Parameters, *Water Resources Research*, 7: 292-303.

Singh, V.P., and D.A. Woolhiser (2002), Mathematical Modeling of Watershed Hydrology, *Journal of Hydrologic Engineering*, 7(4): 270–292, doi:10.1061/(ASCE)1084-0699(2002)7:4(270).

Shen, H. W., and P. Julien (1993), Erosion and sediment transport, in *Handbook of Hydrology*.12.1-12.61.

Shen, C., and M.S. Phanikumar (2010), A process-based, distributed hydrologic model based on a large-scale method for surface-subsurface coupling, *Advances in Water Resources*, 33: 1524-1541, doi:10.1016/j.advwatres.2010.09.002.

Sklash, M. G., and R. N. Farvolden (1979), Role of Groundwater in Storm Runoff, *Journal of Hydrology*, 43:45-65.

Sloto, R., and M. Crouse (1996), HYSEP: A computer program for streamflow hydrograph separation and analysis. US Geological Survey, Water Resources Investigations, Report 96-4040.

Smakhtin, V.U. (2001), Low flow hydrology: a review, *Journal of Hydrology*, 240: 147-186.

Sophocleous, M. (2002), Interactions between groundwater and surface water: The state of the science, *Hydrogeology Journal*, 10, 52– 67, doi:10.1007/s10040-001-0170-8.

Spongberg, M.E. (2000), Spectral analysis of base flow separation with digital filters, *Water Resources Research*, 36(3): 745-752.

Szilagyi, J. (2004), Heuristic continuous base flow separation, *Journal of Hydrologic Engineering*, 9:311-318.

Tallaksen, L.M. (1995), A review of baseflow recession analysis, *Journal of Hydrology*, 165: 349-370.

Therrien, R., R.G. McLarren, E.A. Sudicky, and S.M. Panday (2009), Hydro-GeoSphere, A Three-dimensional Numerical Model Describing Fully-integrated Subsurface and Surface Flow and Solute Transport Groundwater, Simul. Group, Univ. of Waterloo, Waterloo, Ont., Canada.

Tromp-van Meerveld, H. J., and J. J. McDonnell (2006), Threshold relations in subsurface stormflow: 2. The fill and spill hypothesis, *Water Resources Research*, 42(2): W02411, doi:10.1029/2004WR003800.

van Genuchten, M.T. (1980), A closed-form equation for predicting the hydraulic conductivity of unsaturated soils, *Soil Science Society American Journal*, 44, 892–898.

VanderKwaak, J.E., and K. Loague (2001), Hydrologic-response simulations for the R-5 catchment with a comprehensive physics-based model, *Water Resources Research*, 37(4): 999-1013, doi:10.1029/2000WR900272.

Vivoni, E.R., D. Entekhabi, R.L. Bras, V.Y. Ivanov (2007), Controls on runoff generation and scale-dependence in a distributed hydrological model, *Hydrology and Earth Systems Science*, 11: 1683-1701.

Weiler, M., and J. McDonnell (2004), Virtual experiments: a new approach for improving process conceptualization in hillslope hydrology, *Journal of Hydrology*, 285:3-18.

Werb, S. (2009), Simulation der hydrologischen Dynamik im Einzugsgebiet des Lehstenbachs mit dem physikalisch begründeten Modell HydroGeoSphere, Dip. thesis, University of Bayreuth, Bayreuth, Germany.

Werner, A.D., M.R. Gallagher, and S.W. Weeks (2006), Regional-scale, fully coupled modelling of stream-aquifer interaction in a tropical catchment, *Journal of Hydrology*, 328: 497-510.

Wigmosta, M.S., L.W. Vail, and D.P. Lettenmaier (1994), A distributed hydrology vegetation model for complex terrain, *Water Resources Research*, 30(6): 1665-1679, doi:10.1029/94WR00436.

Winter, T.C. (1999), Relation of streams, lakes, and wetlands to groundwater flow systems, *Hydrogeology Journal*, 7(1): 28-45, doi:10.1007/s100400050178.

Wittenberg, H. (1994), Nonlinear Analysis of Flow Recession Curves, Pages 61-67 in Friend: Flow Regimes from International Experimental and Network Data, International Association Hydrological Sciences, Wallingford.

Wittenberg, H., and M. Sivapalan (1999), Watershed groundwater balance estimation using streamflow recession analysis and baseflow separation, *Journal of Hydrology*, 219: 20-33.

Wittenberg, H. (2003), Effects of season and man-made changes on baseflow and flow recession: case studies, *Hydrological Processes*, 17: 2113-2123.

Appendix A
Copy of Paper from Chapter 2

Partington, D., P. Brunner, C. T. Simmons, R. Therrien, A. D. Werner, G. C. Dandy, and H. R. Maier. 2011. A hydraulic mixing-cell method to quantify the groundwater component of streamflow within spatially distributed fully integrated surface water - groundwater flow models. *Environmental Modelling and Software*, 26:886-898.

Partington, D., Brunner, P., Simmons, C.T., Therrien, R., Werner, A.D., Dandy, G.C. & Maier, H.R. (2011) A hydraulic mixing-cell method to quantify the groundwater component of streamflow within spatially distributed fully integrated surface water-groundwater flow models.
Environmental Modelling & Software, v. 26(7), pp. 886-898

Appendix B
Copy of Paper from Chapter 3

Partington, D., P. Brunner, C. T. Simmons, A. D. Werner, R. Therrien, G. C. Dandy, and H. R. Maier. 2012. Evaluation of outputs from automated baseflow separation methods against simulated baseflow from a physically based, surface water-groundwater flow model. *Journal of Hydrology*, 458-459: 28-39.

Partington, D., Brunner, P., Simmons, C.T., Werner, A.D., Therrien, R., Maier, H.R. & Dandy, G.C. (2012) Evaluation of outputs from automated baseflow separation methods against simulated baseflow from a physically based, surface water-groundwater flow model.
Journal of Hydrology, v. 458-459(August), pp. 28-39